

THE MECHANICAL BEHAVIOR OF FAULTED ROCK  
AT HIGH TEMPERATURE AND PRESSURE

by

ROBERT MICHAEL STESKY

B.Sc., University of Toronto  
1968

M.Sc., University of Toronto  
1970

SUBMITTED IN PARTIAL FULFILLMENT  
OF THE REQUIREMENTS FOR THE  
DEGREE OF DOCTOR OF  
PHILOSOPHY

at the

MASSACHUSETTS INSTITUTE OF  
TECHNOLOGY

July 1975

Signature of Author . . . . .

Department of Earth and Planetary  
Sciences, July 11, 1975

Certified by . . . . .

Thesis Supervisor

Accepted by . . . . .

Lindgren

Chairman, Departmental Committee  
on Graduate Students



## ABSTRACT

THE MECHANICAL BEHAVIOR OF FAULTED ROCK  
AT HIGH TEMPERATURE AND PRESSURE

by Robert Michael Stesky

Submitted to the Department of Earth and Planetary Sciences on July 11, 1975, in partial fulfillment of the requirements for the degree of Doctor of Philosophy.

Frictional sliding in faulted rock was studied at 2 to 6 kbar pressure, 25° to 700°C, and sliding rates of 10<sup>-5</sup> to 10<sup>-2</sup> cm/sec. Measurements were made in several different rock types, including two granites, gabbro, peridotite, dunite, anorthosite, and quartzite.

Sliding occurred in two ways: by sudden, rapid, and audible slips, called stick-slip, or by smooth sliding, called stable sliding. Stick-slip prevailed at low temperature and high pressure but gave way to stable sliding at high temperature. The transition temperature was somewhat different for different rocks, but generally was near 200° to 300°C at 3 to 4 kbar pressure. Two exceptions were a quartzite, which showed stick-slip up to 450°C, and a peridotite, which did not show stick-slip at all, even down to 25°C.

The friction stress for all these rocks was very similar, within ± 10 to 15%, and decreased only slowly as temperature increased. The sliding stress increased markedly with pressure, and at low temperatures it closely followed the relationship:  $\tau = a + b\sigma_n$ , where  $\tau$  is the shear stress on the fault,  $\sigma_n$  is the normal stress, and a and b are parameters which slowly vary with temperature. At high temperatures and pressures, the shear stress increased less markedly with normal stress.

At low temperatures the sliding stress was nearly independent of sliding rate, increasing 2 to 3% for three decades increase in sliding rate. The effect of rate is more marked at high temperatures, the stress increasing about 15% for three decades increase in rate. If the fault was held at reduced load for some period of time, the stress for the subsequent initial sliding increased with increasing holding time.

Acoustic emissions were detected during frictional sliding in granite at 1 and 2 kbar pressure and 25° to 700°C. Emissions occurred during sliding even at the highest temperature. The b-value, or amplitude distribution, was the same at all temperatures. The conclusion of this study was that brittle cracking occurred during stable sliding in granite at all temperatures to 700°C.

The deformation mechanisms during stable sliding in granite at high temperature were further studied by measuring the activation energy for sliding at different temperatures and by examination of deformed fault material with optical and transmission electron microscopy. The activation energy was about 30 kcal/mole below 500°C and increased to about 85 kcal/mole at higher temperature. The feldspars, microcline and

oligoclase, forming 65% of the rock, were brittle at all temperatures. Quartz (30% of the rock) was brittle below 500°, but deformed plastically at higher temperature. Its dislocation density increased markedly from about  $2 \times 10^8 \text{ cm}^{-2}$  initially to greater than  $10^{11} \text{ cm}^{-2}$ . The fine gouge grains (less than 1  $\mu\text{m}$ ) showed no similar increase in dislocation density. The micas, biotite and muscovite, deformed plastically at all temperatures down to 25°C, at least near the fault zone.

The laboratory measurements were used to estimate the friction stress on the San Andreas fault. The average shear stress was found to lie between 750 and 2000 bars, from 4 to 10 times larger than the upper limit calculated from heat flow measurements. This difference could be explained by low strength alteration materials in the fault zone or by pore pressure considerably in excess of hydrostatic.

Thesis Supervisor: William F. Brace  
Title: Professor of Geology

## TABLE OF CONTENTS

ABSTRACT . . . . .	11
TABLE OF CONTENTS . . . . .	iv
ACKNOWLEDGMENTS . . . . .	vii
INTRODUCTION . . . . .	1
CHAPTER I - FRICTION IN FAULTED ROCK AT HIGH TEMPERATURE AND PRESSURE	
Abstract . . . . .	5
Introduction . . . . .	6
Apparatus and Procedure . . . . .	8
Rocks Studied . . . . .	12
Observations	
Friction data . . . . .	12
Petrographic study . . . . .	12
Discussion	
Stick-slip to stable-sliding transition . . . . .	12
Effect of temperature on sliding stress	
Granite sawcuts . . . . .	17
Faulted granite and gabbro . . . . .	17
Other faulted rocks . . . . .	20
Effect of pore water pressure on friction in granite . . . . .	21
Conclusions . . . . .	22
Acknowledgments . . . . .	23
References . . . . .	24
Table I . . . . .	28
Figure Captions . . . . .	29
Figures . . . . .	31
CHAPTER II - TIME-DEPENDENCE OF FRICTION IN FAULTED ROCK AT HIGH TEMPERATURE AND PRESSURE	
Abstract . . . . .	46
Introduction . . . . .	47
Previous Work . . . . .	48
Present Investigation . . . . .	49
Experimental Procedure	
Apparatus and sample configuration . . . . .	50
Rocks studied . . . . .	51
Observations	
Rate experiment . . . . .	51
Relaxation experiment . . . . .	53
Holding experiment . . . . .	55
Discussion	
Effect of rate on steady-state sliding . . . . .	56
Analysis of relaxation measurements . . . . .	58
Transient frictional phenomena . . . . .	59

TABLE OF CONTENTS (continued)

CHAPTER II - TIME-DEPENDENCE OF FRICTION IN FAULTED ROCK AT  
HIGH TEMPERATURE AND PRESSURE

Discussion (continued)	
Stick-slip . . . . .	62
Episodic fault creep . . . . .	63
Relaxation on natural faults . . . . .	64
Conclusions . . . . .	65
References . . . . .	66
Figure Captions . . . . .	71
Figures . . . . .	73

CHAPTER III - ACOUSTIC EMISSION DURING HIGH-TEMPERATURE  
FRICTIONAL SLIDING

Abstract . . . . .	83
Introduction . . . . .	84
Experimental Technique . . . . .	85
Observations During Fracture . . . . .	88
Observations During Frictional Sliding . . . . .	89
Discussion . . . . .	92
Conclusions . . . . .	95
Acknowledgments . . . . .	96
References . . . . .	96
Figure Captions . . . . .	98
Figures . . . . .	100

CHAPTER IV - MECHANISMS OF HIGH TEMPERATURE FRICTIONAL  
SLIDING IN WESTERLY GRANITE

Abstract . . . . .	108
Introduction . . . . .	109
Present Study . . . . .	110
Experimental Procedure	
Activation energy measurement . . . . .	111
Microscopy . . . . .	112
Observations	
Experimental activation energy . . . . .	113
Optical microscopy . . . . .	114
Transmission electron microscopy	
Room-temperature fault . . . . .	117
High-temperature friction samples . . . . .	118
Discussion	
Deformation mechanisms during sliding . . . . .	121
Processes of frictional sliding in granite . . . . .	126
Flow law for stable sliding in granite at high temperature . . . . .	128
Conclusions . . . . .	130
References . . . . .	131
Figure Captions . . . . .	134
Figures . . . . .	138

## TABLE OF CONTENTS (continued)

CHAPTER V - ESTIMATION OF FRICTIONAL STRESS ON THE SAN ANDREAS FAULT FROM LABORATORY MEASUREMENTS	
Abstract . . . . .	158
Introduction . . . . .	158
Constraints of Heat Flow Data . . . . .	159
Experimental Observations . . . . .	160
Calculation of Shear Stresses on San Andreas Fault . . . . .	162
Conclusion . . . . .	167
Acknowledgments . . . . .	167
References . . . . .	168
Figure Captions . . . . .	170
Figures . . . . .	171
SUMMARY . . . . .	176
APPENDIX A - SUMMARY OF FRICTION STRESS MEASUREMENTS . . . . .	181
APPENDIX B - JACKET CONSTRAINTS . . . . .	190
BIOGRAPHY . . . . .	197

## ACKNOWLEDGMENTS

I wish to express my gratitude to Dr. William F. Brace, my thesis supervisor, for his guidance, encouragement and support without which this thesis would not have been completed, and for patiently waiting so long for the final draft. His laboratory on the seventh floor was a stimulating place to spend four years, where science was exciting and the atmosphere of work was very enjoyable. Many people have contributed to this atmosphere and to the success of this thesis. At the risk of forgetting someone, I will name a few:

Dr. W. F. Brace, for suggesting the problem, providing the equipment, and making key suggestions along the way.

Dr. C. Goetze, for giving many new insights into the problems of high temperature deformation.

Dr. D. L. Kohlstedt, for providing the expertise on transmission electron microscopy and for spending many valuable hours with me on the microscope looking at my samples.

Dr. P.-Y. F. Robin, for three years of enjoyable office-sharing and for many stimulating discussions that have contributed to my understanding of science.

Mr. D. (Jock) Hearst, for teaching me much about a machine shop, making all the necessary parts, and keeping the equipment in top shape so that almost no time was lost because of breakdowns.

Mrs. Madge Slavin, for her patient handling of office details, for her smile and her apple cake.

K. Hadley, W. Durham, and P. Tapponnier, for many hours of discussion on rock mechanics.

I also thank Erindale College and Dr. D. W. Strangway for hiring me before the thesis was done and for allowing me the time to complete it.

Lastly, and most importantly, I thank my wife, Christine. Without her this effort would have been pointless. She saw me through many rough spots, when I would have been quite willing to give up. She also was a willing partner in the often overwhelming task of putting this thesis together. She typed it, and retyped it, and typed it once again, under pressures of time brought about by my procrastination. For all this, I thank her, and for many more things than I'm willing to put down on paper.

## INTRODUCTION

Faults are one of the most ubiquitous structures of the earth's crust. They form under a wide variety of conditions and in almost all rock types. The importance of faults to the mechanical behavior of the crust is underscored by the recent realization that most, if not all, shallow earthquakes occur along pre-existing faults and that almost all lithospheric plate boundaries are faults or have faults associated with them. But our knowledge of the properties of faults under a wide variety of conditions is still rather rudimentary. Much work has been done near room temperature, but very little is known about fault behavior at the high temperatures expected at depth in the earth. Further, little attempt has been made to quantitatively apply laboratory measurements to geological fault problems. Clearly, this must be done in order to have any basis for accepting or rejecting field hypotheses.

The kinds of questions we would like to answer are many. Why do faults occur and what determines their location? What is the strength of a fault and how does it vary with depth? How does its strength depend on mineralogy, sliding rate, and the presence of aqueous fluids? Why do some faults produce earthquakes and others slowly creep? What determines the magnitude of earthquakes or the rate at which creep sliding occurs? Are seismic faults as strong as, or stronger than, creeping faults? Can we predict when an earthquake will occur, and where? Can a seismic fault be modified so that it slowly creeps, thus preventing a disastrous earthquake?

Recent work has gone a long way toward solving many of these problems. For example, field study has pointed out that the presence of fault creep may correlate with high fluid pressures or with the presence of minerals such as clays and serpentine. Many of the parameters that control the magnitude of an earthquake have been identified by seismologists. Heat flow studies have provided us with the first indication that the strength of an active fault may be relatively low, on the order of a few hundred bars. Further, it is clear now that earthquakes can be predicted under some circumstances by monitoring certain physical properties of the crust, such as seismic wave velocity, gravitational and magnetic field, and surface displacements, which change before an earthquake event.

The fundamental problem of why a fault behaves as it does remains largely unanswered. The most promising approach seems to be laboratory study. Here the physical conditions can be closely controlled and altered at will and the fault behavior and characteristics can be examined in some detail. However, the basic question of how to apply these results to the earth must always be considered. How can we hope to reproduce the long times and slow rates of natural deformation? The best approach is to make the measurements at high temperatures where the processes occur at higher rates. The results can then be extrapolated to the lower rates in the earth.

The pioneering work was done by Brace and Byerlee (1970), who developed the capability of measuring the strength and sliding behavior of faulted rock at high temperature and pressure. They found that two types of sliding behavior occurred at high pressure. At low temperature the sliding was jerky, with sudden audible slips and stress drops. This motion, called stick-slip, was postulated to be a possible earthquake mechanism. At high temperatures stick-slip gave way to steady creep sliding with no audible

stress drops. For the two rocks that they studied, granite and gabbro, stick slip occurred at low temperature and high pressure, stable sliding at high temperature and low pressure. Stable sliding tended to occur at lower temperatures in the gabbro than in the granite.

This thesis is a continuation of their work. The primary aim was to investigate the details of the sliding process and to discover, as much as possible, the deformation mechanisms. To this end, the study was restricted mainly to conditions under which the sliding was stable. I examined several aspects of the problem, each summarized in one of the first four chapters. First, the effect of pressure, temperature, rock type, and water on the fault strength and sliding behavior was studied. Included in the data are earlier measurements made by W.F. Brace, D.K. Riley, and P.-Y.F. Robin. Second, three rock types, granite, gabbro, and peridotite, were selected for an examination of the variation of fault strength with time or sliding rate. This is clearly an important step in being able to extrapolate our results to the earth. Then for a detailed study of the deformation mechanisms during frictional sliding, summarized in Chapters III and IV, I chose Westerly granite, for which we have the most friction data at high temperature. Firstly, I adapted the techniques of acoustic emission studies to the high temperature friction experiment. The aim was to monitor the extent of brittle cracking by means of the high frequency, stress wave pulses emitted. Secondly, I measured the experimental activation energy during frictional sliding to give some clues to the physical processes. Thirdly, I made a detailed petrographic study of the faulted samples deformed at different temperatures and pressures. The study made use of both transmitting and reflecting optical microscopes and the transmission electron microscope. The

purpose was to examine the character of the fault zone and determine how each mineral behaved under different conditions of pressure and temperature. Finally, I attempted to understand the mechanical properties of stable sliding in the light of knowledge of the microscopic processes.

In the final chapter, I apply my results quantitatively to the problem of the strength of the San Andreas fault. The laboratory data predict a strength much greater than the upper limit calculated from heat flow measurements. I then examine various ways in which the laboratory and field data can be brought into closer agreement and suggest some critical field observations to test the ideas.

In all, 162 experiments were performed: 76 by W.F. Brace, D.K. Riley, and P.-Y.F. Robin; 86 by myself. Of these, 18 were used to study the effect of rate, 10, acoustic emission, and 6, the activation energy for sliding.

#### REFERENCE

Brace, W.F. and Byerlee, J.D., 1970. California earthquakes: Why only shallow focus? *Science*, 168: 1573-1575.

## CHAPTER I

## FRICTION IN FAULTED ROCK AT HIGH TEMPERATURE AND PRESSURE

## ABSTRACT

Two hundred observations of frictional behavior of seven low-porosity silicate rocks were made at temperatures to 700°C and pressures from 2.5 to 6 kbars. For all rocks except one, peridotite, stick-slip occurred at low temperature and gave way to stable sliding at some high temperature, different for each rock. Up to some temperature, depending on rock type, the friction stress was relatively unaffected by temperature. The shear stress decreased at higher temperature, and in some cases such decrease was related to the coincidence of fracture and friction strength. While somewhat dependent on rock type, the friction stress for the seven rocks studied was about the same, within 10 to 15%. Up to 265°C, water had little effect on the frictional behavior of faulted granite at 3 kbars effective pressure.

## INTRODUCTION

Many observations of frictional behavior of rock have been made near room temperature. (For example, see Jaeger and Cook, 1969, Chapter 3). Frictional stress, fault stability and other characteristics depend upon factors such as pressure or normal stress, surface roughness, and thickness of gouge (Byerlee, 1967; Coulson, 1970; Handin et al., 1972; Engelder, 1973; and others). How significant are these parameters at temperatures encountered near active faults in the earth? Temperature tends to stabilize sliding for some rocks (Brace and Byerlee, 1970); to what extent does rock type affect sliding behavior at high temperature? Further, how does water, present in natural faults, affect frictional behavior of rocks at high temperatures?

Such questions need to be answered before experimental results can be applied to natural seismic faults. Previous studies offer little help. Apparently the effect of temperature depends in some poorly understood way on pressure or normal stress, rock type, and fault structure. For sawcuts in limestone and hornblende biotite schist at normal stresses less than 20 bars, Drennon and Handy (1972) observed an increase in shear stress with temperature up to 200°C. They attributed this result to the removal of adsorbed water above 100°C, presumably allowing asperity to asperity bonding. They also found that higher temperature promoted stick-slip behavior.

For sawcuts in sandstone at pressures to 5 kbars, Handin et al. (1973) and Logan et al. (1973a) found an increase in frictional strength

with temperature to 400°C, an increase related to the formation of glass on the surface during sliding. The presence of such glass presumably increased the contact area, and caused a corresponding increase in frictional force to maintain sliding. Since glass formed even in room temperature experiments, they attributed its formation to localized frictional heating. At the high normal stresses of these experiments, an increase of temperature promoted stable sliding rather than stick-slip.

For sawcuts in granite at pressures to 5 kbars (Brace and Byerlee, 1970), frictional strength decreased with temperature by about the same amount as fracture strength, relative to room temperature values. Also stick-slip, present at low temperatures and high pressure, gave way to stable sliding at high temperatures. Sawcuts in limestone at 2 kbars confining pressure (Handin et al., 1973) showed a similar decrease in frictional stress with temperature, although stable sliding occurred at all temperatures.

For faulted serpentinite, Raleigh and Paterson (1965) found that at 1 kbar confining pressure, the coefficient of sliding friction was approximately constant to 500°C. At higher pressure, the sliding stress decreased markedly with temperature. Similar results were obtained for sandstone (Handin and Hager, 1958) and for dunite, pyroxenite, and granite (Griggs et al., 1960). In all cases, the high temperature frictional sliding was stable.

Thus our understanding of the effects of temperature is somewhat spotty and questions such as those posed earlier appeared to warrant further study. We present here new results for a variety of low porosity silicate rocks, two of which, Westerly granite and San Marcos gabbro,

were singled out for more detailed study. Some of our observations were summarized by Brace (1972) and Stesky and Brace (1973) but are here given in more detail. We examined the effects of temperature, rock type, fault structure, and fault history on the stick-slip to stable sliding transition and on the sliding stress. In addition, we explored the effect of pore water pressure on sliding behavior at temperatures to 300°C.

#### APPARATUS AND PROCEDURE

The apparatus and sample configuration (Figure 1) were described briefly by Brace and Byerlee (1970). Cylindrical samples, 35 mm long and 16 mm in diameter, were placed in a 1.3 mm thick graphite sleeve which was in turn inserted into a 0.32 mm thick annealed copper tube. Tungsten carbide spacers minimized the temperature gradient across the sample. Polycrystalline alumina (Lucalox, General Electric) prevented excess heat loss through the ends of the column. A thermocouple reached the base of the sample through a hollow plug and an axial hole in the carbide and alumina spacers. The hole also allowed the pore pressure in the sample to be controlled.

The graphite-copper jacket combination allowed considerable fault displacement without rupturing. Thin copper alone tore after only a small amount of sliding at high pressures. The graphite "blunted" the edges of the fault. To test whether the graphite-copper jacket affected the strength and behavior of the faulted rock, we compared a series of room temperature measurements, using a polyurethane rubber jacket (wall thickness, 3.2 mm). Both fracture and friction data are shown in Figure 2. Different symbols distinguish stable from unstable behavior. Unstable faulting involved a rapid, audible stress drop; during stable

faulting, the stress decreased more slowly with no audible noise. Similar criteria distinguished stick-slip from stable sliding, although the latter did not involve a decrease in stress. The transitional behavior, indicated as STA/STK, was characterized by small stress drops (less than 200 bars), with or without intervening periods of stable sliding.

Fracture or friction strength were evidently not affected by the type of jacket used (Figure 2). However, at confining pressures below 2.5 to 3 kbars, the faulting was stable with the copper-graphite jacket, whereas it was unstable with the rubber. Many subsequent fracture runs with the copper-graphite jacket at 500 bars did not substantiate this distinction (22 out of 32 samples fractured unstably). It was nevertheless felt that a confining effect of the copper could be important at low confining pressures. We thus decided to limit our runs to pressures greater than 2.5 kbars where the results for the two series were nearly identical behavior, under the assumption that jacket constraint was then negligible. The stabilizing effects of the copper-graphite jacket were likely to be less important at higher temperatures because of the increased ductility of the copper and graphite.

The sample was heated by an internally-wound furnace which surrounded the copper jacket (Figure 1). To minimize convection in the argon pressure medium, powdered boron nitride (a good thermal and poor electrical conductor) was placed between the copper jacket and the furnace wall. Repeated measurement of sliding strength after both a small and a large amount of displacement showed that the powder in no way constrained the sample. The geometry of the apparatus and the strain of the graphite-copper jacket imposed a maximum sliding displacement of about 2.5 to

3.0 mm. The temperature along the axis of a hollow dummy sample (fired aluminum silicate, American Lava Corp.) is shown in Figure 3. Assuming that the faulted rocks behaved as the dummy sample, the temperature difference over the fault was approximately  $25^{\circ}$  at  $700^{\circ}\text{C}$  and less at lower temperatures. About 75% of the fault area was within  $10^{\circ}$  of the peak value. The temperatures quoted for the experiments are the average along the fault and are probably correct to within  $10^{\circ}\text{C}$ .

Pressure in the argon was measured with a Heise gauge and was maintained constant to within 10 bars. In so-called "dry" experiments, the bottom end of the sample was vented to the atmosphere, so the pore pressure was close to zero.

The axial force was provided by a piston driven at a constant rate by a ball screw mechanism. The stiffness of the machine was about  $10^5$  kg/cm. The load was measured externally with a conventional strain gauge load cell, with a probable error of about 2%. The axial stress and the resolved stresses on the fault surface, corrected for the actual area of fault contact, were accurate to about 6 to 8%. Included in this error is that for the fault angle, the angle between the fault plane and the maximum principal compressive stress; it could be reasonably well measured to within  $1^{\circ}$  or  $2^{\circ}$ .

Most runs were done at a constant piston-displacement rate of  $9.4 \times 10^{-5}$  cm/sec. The displacement was measured outside the pressure vessel with a differential transformer mounted between the moving piston and the fixed lower platen. These measurements were accurate to within 1%.

To explore possible effects of small amounts of moisture, samples were heated at pressure for 1 to 25 hours, with and without vacuum

( $10^{-2}$  torr), and were heated and then run at room temperature (Brace and Byerlee, 1970). In all cases, the sliding motion was unaffected by the procedure and the frictional stress agreed to within the experimental reproducibility.

We studied three types of faults: ground surfaces cut at  $30^\circ$  to the axis (sawcut series), faults formed at room temperature and 500 bars (fault series), and faults formed at high temperature and pressure (fracture series). Because we wished to learn about natural, gouge-filled faults, the most extensive work was done with the fault series. An advantage of the fault over the fracture series was the reproducibility of the fault in the former; faults in the fracture series varied so in gouge thickness or orientation that comparison between runs was more uncertain.

A typical fault series run is illustrated in Figure 4 for San Marcos gabbro. The rock was fractured at 500 bars and  $25^\circ\text{C}$ . The pressure was sufficient to give a well-defined fault in most cases, yet was not so high as to cause too large an initial displacement. The pressure and temperature were then increased to the conditions for study. The temperatures ranged from  $25^\circ$  to  $700^\circ\text{C}$ , although most were above  $200^\circ\text{C}$ ; the pressures were 2.5 to 6 kbars. Most runs were of the incremental type, as in Figure 4. Once sliding was attained, the load was removed and the pressure or temperature changed to make a new measurement with the same sample. The effect of displacement was checked by repeating the first measurement at the end of the experiment. In most cases, the stresses agreed to within 2 to 3% after area correction.

For the sawcut and fracture series, high temperature and pressure were attained initially and, in almost all runs of these types, were

held constant throughout the entire experiment. In the fracture series runs, the fault was formed and deformation was continued until sliding occurred.

#### ROCKS STUDIED

Typical crustal igneous and metamorphic rocks were selected for study. In Table 1 their modal analysis, density, porosity, and average grain size are given. Most of these rocks have been used in previous studies. The anorthosite was collected specially for this work. The location was a roadcut 5.2 miles southwest of Indian Lake on New York State highway 10.

#### OBSERVATIONS

##### Friction data

Our measurements of the frictional strength and behavior of these rocks are summarized in Appendix A.

##### Petrographic study

We examined optically thin sections of a number of faulted samples, in an attempt to answer two questions: (1) are stick-slip and stable sliding associated with different fault characteristics, and (2) have any new mineral phases been produced during sliding? We chose samples from both the fault (gabbro, anorthosite, Pigeon Cove granite, and quartzite) and fracture (Westerly granite and dunite) series.

There were very few differences between STA and STK samples in the fault series. Each had a narrow, moderately well-defined fault zone, probably the result of the uniform conditions of formation (500 bars, 25°C). The gouge consisted of a few fractured remnant grains in a

fine-grained matrix. The region adjacent to the gouge zone was usually highly fractured, the cracks tending to be axially oriented. No detailed crack orientation study has been made. We observed many grains in the gouge which appeared to have been plucked from the fault wall during sliding: a particularly striking example is shown in Figure 5. Since we would expect the number of plucked grains to increase as sliding continued, plucking is a possible mechanism for the increase in gouge thickness with total displacement (Engelder, 1973).

One difference was noted, however, between stick-slip and stable sliding runs. In room temperature, stick-slip samples of gabbro and anorthosite (both at 4 kbars), mica and amphibole were abruptly truncated at the fault and the fragments offset (Figure 6a). In high temperature stable sliding runs (gabbro at 400°C and anorthosite at 250°C, both at 4 kbars), mafic grains appeared to be drawn out along the fault surface (Figure 6b). This observation seems to contrast with that of Borg and Handin (1966) who found no evidence of ductility in amphibole up to 500°C and 5 kbars.

For fracture series, where the fault is formed at the temperature of sliding, the only obvious new feature was that the fault zone width increased with the temperature of deformation. This observation has been noted by others (Griggs et al., 1960) and seems to be a characteristic of the fracture process itself. In a dunite sample deformed at 365°C the finely-crushed olivine gouge was oxidized and discolored, suggesting the ease with which olivine fault gouge, at least, can be altered.

A preliminary x-ray and optical study was made of the fault gouge powders of four gabbro samples deformed at 4 kbars and temperatures of

100°C (STK), 138°C (STK), 395°C (STA), and 500°C (STA). Observations with a binocular microscope (15 to 40 X) indicated that smaller grain sizes were produced at higher temperature. Because of the large gap in temperature between the stick-slip and the stable sliding runs chosen, it was not possible to assign this trend to the differences in either temperature or type of motion. No attempt was made to quantify the grain size distribution.

X-ray diffraction patterns of the gouge powders for the 100°C and 500°C runs were compared with that of ground undeformed San Marcos gabbro. Compared to virgin material, both gouges showed a significant depression of the biotite and amphibole peaks relative to the quartz and plagioclase peaks. Furthermore, quartz peaks were depressed relative to the plagioclase peaks in the 500°C sample. The significance of these differences is unclear; they may be explained by differences in fault paths (and thus in sampling) as well as by intrinsic differences in grinding or straining of the various mineral types in the gouge.

When examined under a polarizing microscope, all fault gouge grains exhibited birefringence. Although not identified, the possibility that glass was present cannot be excluded, since intensely deformed glass may not be isotropic. In the x-ray diffraction study, no new peaks appeared for the gouges, although small amounts of a new phase could remain undetected by this method. In fact, no pyroxene peaks were seen in any of the patterns, in spite of reported modal analyses indicating 8 volume percent of calcium-rich clinopyroxene in the rock.

Our petrographic study, then, has been rather unsuccessful. Differences in fault characteristics could be explained simply by differences in temperature, independent of sliding behavior. We could have missed

new mineral phases or small amounts of glass. Some of our observations are suggestive, but more detailed work is necessary.

## DISCUSSION

### Stick-slip to stable-sliding transition

All the data on the sliding behavior of Westerly granite are shown in Figure 7, with runs from the different series distinguished by different symbols. The points labelled HOL refer to the pore pressure study discussed below. As has been noted previously (Brace and Byerlee, 1970), stick-slip behavior was restricted to low temperatures and high pressures. It is possible to delineate a region of pressure and temperature in which stick-slip occurs, although the boundary cannot be defined to better than about 100°C (Brace and Byerlee, 1970). This is not surprising since there are likely to be many factors which influence this change in behavior besides pressure and temperature, including precise location of fault relative to pistons, sample variations, and variation in fault curvature. The data of the gabbro (not plotted) gave similar results, although the transition occurred at a lower temperature.

Rock type is also known to affect the sliding behavior of faults. Low porosity quartz-rich rocks tend to exhibit stick-slip at room temperature and high pressure, while rocks containing calcite, dolomite, serpentine, and mica slide stably (Byerlee and Brace, 1968; Coulson, 1970; Brace, 1972; Logan *et al.*, 1973b; Jackson and Dunn, 1973; and others). We have made a series of reconnaissance friction measurements of several rock types at 3 and 4 kbars. These rocks included two granites, a quartzite, an anorthosite, a gabbro, a peridotite, and a dunite.

We can characterize the frictional behavior of the rocks by the temperature at which the sliding changed from stick-slip to stable sliding.

Figure 8 shows for each rock the range of temperature within which the transition occurred. While it is clear that the transition temperature varied with rock type, the reason for this behavior is not as clear. A possible cause may be the particular composition, amount, and distribution of the minerals in the rock. Byerlee and Brace (1968) have shown that about 3% serpentine distributed homogeneously along grain boundaries in a dunite can cause stable sliding at room temperature and high pressure, whereas an essentially similar dunite without serpentine slides with stick-slip motion. The presence of clays or other platy silicates along grain boundaries might be expected to have a similar effect. The presence of serpentine could explain the room-temperature stable sliding of the peridotite, compared to the stick-slip motion of the dunite. Serpentine was concentrated in veins in the peridotite; such veins tended to influence the formation of faults, resulting in a greater concentration of serpentine in the fault zone than in the bulk of the rock.

The occurrence of other specific minerals may also affect the sliding behavior. As noted earlier, amphibole seemed to undergo a brittle to ductile transition between 25° and 250°C at 4 kbar. The gabbro and anorthosite, both containing amphibole, showed a sliding transition within the same range of temperature. The transition temperature of Westerly granite, containing 5% biotite but no amphibole, was about 50°C higher than that of gabbro and anorthosite, while that of the quartzite, containing neither amphibole nor mica, was at least 200°C higher. The results of Jackson and Dunn (1973) at 140 bars pressure and 25°C similarly suggest that the sliding transition in foliated gneiss was affected by the relative amounts of quartz and micaceous minerals.

Other rock properties similarly could influence the sliding behavior. The effect of grain size and thickness of gouge and the effect of roughness

of the fault surface have been studied (e.g., Jaeger, 1959; Byerlee, 1967; Jaeger and Rosengren, 1969; Brace and Byerlee, 1970; Handin *et al.*, 1972; Engelder, 1973), but little is known about the importance of these properties at high temperature. Judging from our Westerly granite data in Figure 7, there could be as much as a 100°C difference in transition temperature between sawcuts (almost no gouge) and faults (with a 0.5 mm thick layer of gouge) at 5 kbar. Indeed, for a sample composed entirely of crushed Westerly granite, sliding was stable at room temperature and 4 kbar confining pressure (Byerlee and Brace, 1969).

#### Effect of temperature on sliding stress

Granite sawcuts. Figure 9 gives our high temperature Westerly granite sawcut data recalculated for the resolved stresses on the fault surface. We also include data for laboratory-dry Westerly granite sawcuts from Byerlee (1967). Our values up to 300°C agree very well with the earlier results and follow the approximate relationship,  $\tau = 0.5 + 0.6\sigma_n$ . Frictional sliding on sawcuts thus seems to be relatively unaffected by temperature up to 300°C, with a suggestion of a slight decrease in the shear stress above 300°C.

Faulted granite and gabbro. Figures 10 and 11 show the resolved frictional stress for Westerly granite and San Marcos gabbro, respectively. Friction in Westerly granite (Figure 10) was remarkably unaffected by temperature up to 600°C. The data scatter about the line,  $\tau = 0.8 + 0.6\sigma_n$ . These stresses are comparable to those of the sawcut samples, although the faulted rock was slightly stronger. Handin *et al.* (1973) observed a similar difference for Tennessee sandstone at room temperature and attributed the higher strength of faults to surface irregularities. Above 600°C, the shear stress in faulted granite decreased slightly, indicating a change in behavior.

Similar but more marked effects were observed for the gabbro (Figure 11). Up to 400°C, the data fall about the line,  $\tau = 0.7 + 0.6\sigma_n$ . Thus, at low temperatures the frictional strength of faulted granite and gabbro were about the same. Such was not true at higher temperatures; for example, at 700°C, the shear stress for the gabbro was about 30% less than that for the granite.

What is the cause of this sudden change in behavior above 500° to 600°C? We get some insight into this problem if we examine a series of measurements made at constant pressure. The differential stress for sliding is plotted for granite and gabbro (Figure 12) at a constant confining pressure of 4 kbar and a range of temperatures. Also plotted are measurements of the fracture strength of intact rock at 4 kbar (our data) and at 5 kbar (Griggs *et al.*, 1960).

Apparently at some temperature the frictional and fracture strengths became equal. Fracture had a greater temperature dependence than had friction in the case of our fault series runs. Also, at high temperatures, the fracture stress was independent of pressure as shown by the 4 kbar and 5 kbar measurements. This fact suggests that the frictional stress was constant with normal stress at high pressures and similar temperatures. That this seems to be the case can be seen in Figures 10 and 11. The 700°C friction curves show a marked decrease in slope at higher normal stresses.

Thus it seems that for our fault series experiments the frictional process was little affected by temperature, provided that frictional strength was less than fracture strength. At high temperatures where the fracture strength was less than the low temperature frictional strength, deformation in prefaulted rocks may have been accompanied by alteration of fault structure or by re-faulting of the rock.

Evidence for such structural changes is shown in Figure 13. Here we plot in more detail the data for three incremental runs with the gabbro. Similar, though less marked, effects were also observed with the granite. At 300°C (S5), cycling between 2.5 and 3.5 kbars produced no change in sliding stress at a given normal stress, within the measurement uncertainty. Even at 600°C (S9), cycling to 5 kbars caused no change in frictional stress, although the level of stress was less than that at lower temperature. At 700°C (S16), however, cycling to 3.5 and 5 kbars caused a progressive decrease in the sliding stress at 2.5 kbars. Evidently, permanent changes in fault structure, such as smoothing of irregularities or widening of the fault zone, occurred in the region of pressure and temperature where fracture and frictional strengths are the same. A further cycling below 5 kbars produced no further change in sliding, suggesting that such permanent changes were not the result of displacement alone, but also the pressure and temperature conditions of sliding.

That this is not the whole story is evident from the 600°C run. Sliding at 5 kbars and 600°C was well within the region where fracture and friction stresses are the same, but no permanent change in stress occurred after cycling. A further run (S3), made at about 650°C but not plotted in Figure 13, showed stress changes comparable to that of the 700°C run. The rock was cycled between 2.5 and 5.0 kbars and a significant decrease in sliding stress occurred on repeating the 2.5 kbars measurement. Thus, a temperature of 650°C at 5 kbars seemed to be necessary for permanent changes of fault structure in San Marcos gabbro with the displacements used in our runs.

The permanent changes of friction stress and, by inference, of fault structure associated with sliding at high temperature and pressure seem to be relatively minor. This result contrasts markedly with that of a fracture series run on Westerly granite at 4 kbars and 630°C (Sample A12). The fault was formed at these conditions and displacement was continued until a constant friction stress was obtained. The resulting sliding stress was about one-third of that for a fault series run at the same pressure and temperature. As we have discussed previously, the fault formed under these conditions tended to have a much wider gouge zone and the fracturing was more extensive than that formed at low temperature. It seems then that fault width and perhaps other characteristics of the gouge zone may play a very dominant role in determining the frictional strength of faults at these high temperatures.

Note also that in the 700°C run (S16) with the gabbro, the friction values at D, E, F, and G (Figure 13) fall on the straight line,  $\tau = 0.45\sigma_n$ . There is now no "cohesion" term, and the coefficient of friction is lower.

Other faulted rocks. Our measurements of the frictional strength of other rocks, all made at a constant confining pressure, are shown in Figure 14. The results are compatible with those of Westerly granite and San Marcos gabbro, although the temperature at which friction began to decrease markedly was different for different rocks.

Byerlee (1968) suggested that room-temperature friction stress is nearly independent of rock type; his results are supported by the low pressure data of Dieterich (1970) and Jackson and Dunn (1973). Our data indicate that frictional stress may be somewhat more dependent on rock type than they suggest. For example, the frictional strength of the quartzite (92% quartz) was greater than that of Pigeon Cove granite (47% quartz), which in turn was greater than that of Westerly granite (28%

quartz), (Table 4). The difference in friction stress between dunite and peridotite may be explained, as with sliding behavior, by the presence of serpentine along the fault surface in peridotite; the sliding stress of the peridotite was comparable to that of serpentinite (Raleigh and Paterson, 1965). In any case, except possibly for the quartzite, the variation among the different rocks (Figure 14) is fairly insignificant in geophysical terms, say  $\pm 10$  to 15%.

Effect of pore water pressure on friction in granite.

Application of our laboratory data to the earth is complicated by the possibility that geologic faults contain water under pressure. How would our results and conclusions change under such conditions? Many experiments have been performed at room temperature (Byerlee, 1967; Handin et al., 1972; Byerlee and Brace, 1972; Handin et al., 1973; Engelder, 1973), but to our knowledge none have been done at high temperature.

We explored the effects of pore fluids at high temperature using faulted Westerly granite. Our procedure was the same as for the fault series runs, but as much as five hours were allowed for equilibration of pore pressure. Water was introduced through the hole in the bottom plug and through a similar hole drilled for three-quarters of the length of the sample. The hole was necessary to keep the pore pressure constant during the run. Tests with dry rock at room temperature (HOL-1 and HOL-2) indicated that while the hole caused the fracture strength to decrease by about 10% the frictional stress was unaffected, within the scatter of the data.

Figure 15 shows our HOL series data, as well as the "dry" friction data from Tables 3 and 4. We have assumed that the effective pressure is given by the confining minus the pore pressure; Byerlee (1967) has shown

that such a law is valid for friction in sawcuts in Westerly granite. It would seem to be valid also in the case of HOL series faults at high temperature, judging from our results, although a much higher pore pressure would be necessary to establish this law conclusively. The frictional strength was little affected by the presence of pore water pressure up to 265°C, assuming this effective pressure law. We do not seem to observe the slight weakening found by Byerlee (1967) for sliding on wet surfaces at zero pore pressure. In his case, shear stress decreased by about 400 bars when water was introduced into the rock, a decrease that could be masked by scatter in our data.

We also found that introducing water under pressure did not change dramatically the temperature for the stick-slip to stable sliding transition. The transition, shown in Figure 14 and also in Figure 7, occurred between 140° and 265°C at an effective pressure of 3 kbars. This is in reasonable agreement with that found for dry granite, although they could differ by as much as 50 to 100°C. Byerlee and Brace (1972) showed that the transition was unaffected by pore water pressure at room temperature for a constant effective pressure; our results suggest that the same is true up to 265°C.

#### CONCLUSIONS

1. As suggested earlier (Brace and Byerlee, 1970), stick-slip in gabbro and granite and probably most silicate rocks occurs at low temperatures and high pressures.
2. The temperature of transition between stick-slip and stable sliding behavior is dependent on rock type; the transition temperature for quartzite is at least 150°C above that for gabbro, anorthosite, and

dunite. These differences may be related to the presence or absence of minerals such as amphibole, mica, or serpentine.

3. Petrographic study of faulted samples revealed no significant differences between stick-slip and stable sliding samples. A possible brittle-ductile transition of amphibole may correlate with the stick-slip to stable sliding transition in gabbro and anorthosite. The search for new mineral phases or glass was not successful.

4. Up to 300°C for Westerly granite sawcuts, 600°C for Westerly granite faults, and 400°C for San Marcos gabbro, frictional stress is unaffected by temperature at a sliding rate of  $10^{-4}$  cm/sec and 4 kbar confining pressure.

5. The friction stress of seven silicate rocks is the same within about 10 to 15% at 4 kbar pressure, 25° to 700°C, and  $10^{-4}$  cm/sec sliding rate. The variations, while somewhat dependent on rock type, are small in geophysical terms, in agreement with the suggestion of Byerlee (1968).

6. Up to 265°C, water has little effect on the frictional behavior of faulted Westerly granite at 3 kbars effective pressure and  $10^{-4}$  cm/sec sliding rate.

#### ACKNOWLEDGMENTS

Our studies were supported by the U.S. Geological Survey under Contract No. 14-08-0001-13229. J.D. Byerlee carried out several of the early experiments with us and made a number of key suggestions during the course of the work. M.S. Paterson, C. Goetze, A. Arzi, H. Heard, and C.B. Raleigh helped us particularly with high temperature procedure.

## REFERENCES

- Borg, I., and Handin, J., 1966. Experimental deformation of crystalline rocks. Tectonophysics, 3: 249-368.
- Brace, W.F., 1972. Laboratory studies of stick-slip and their application to earthquakes. Tectonophysics, 14(3/4): 189-200.
- Brace, W.F., and Byerlee, J.D., 1970. California earthquakes: Why only shallow focus? Science, 168: 1573-1575.
- Brace, W.F. and Orange, A.S., 1968. Further studies of the effects of pressure on electrical resistivity of rocks. J. Geophys. Res., 73(16): 5407-5420.
- Brace, W.F. and Stesky, R.M., 1973. Time-dependence of frictional sliding in gabbro at high temperature and pressure (Abstract). Am. Geophys. Union, Trans., 54(4): 466.
- Brace, W.F., Orange, A.S. and Madden, T.R., 1965. The effect of pressure on the electrical resistivity of water-saturated crystalline rocks. J. Geophys. Res., 70(22): 5669-5678.
- Byerlee, J.D., 1967. Frictional characteristics of granite under high confining pressure. J. Geophys. Res., 72(14): 3639.
- Byerlee, J.D., 1968. Brittle-ductile transition in rocks. J. Geophys. Res., 73(14): 4741-4750.
- Byerlee, J.D. and Brace, W.F., 1968. Stick-slip, stable sliding, and earthquakes - effect of rock type, pressure, strain rate, and stiffness. J. Geophys. Res., 73: 6031-6037.
- Byerlee, J.D. and Brace, W.F., 1969. High-pressure mechanical instability in rocks. Science, 164: 713-715.
- Byerlee, J.D. and Brace, W.F., 1972. Fault stability and pore pressure. Bull. Seism. Soc. Am., 62(2): 657-660.

- Christensen, N.I., 1966. Elasticity of ultrabasic rocks. J. Geophys. Res., 71(24): 5921-5931.
- Coulson, J.H., 1970. The effects of surface roughness on the shear strength of joints in rock. Tech. Rept. MRD-2-70, Missouri River Div., Corps of Engineers, Omaha, Nebr., 283 pp.
- Dieterich, J.H., 1972. Time dependent friction in rocks. J. Geophys. Res., 77(20): 3690-3697.
- Drennon, C.B. and Handy, R.L., 1972. Stick-slip of lightly loaded limestone. Int. J. Rock Mech. Min. Sci., 9: 603-615.
- Engelder, J.T., 1973. Quartz fault-gouge: Its generation and effect on the frictional properties of sandstone. Ph.D. Dissertation: Texas A & M Univ., College Station, Tex., 153 pp.
- Goodman, R.E., 1973. Pore pressure in intact and jointed rocks induced by deformation (Abstract). Int. Colloquium Seismic Effects of Reservoir Impounding, Royal Soc. London.
- Griggs, D.T., Turner, F.J. and Heard, H.C., 1960. Deformation of rocks at 500° to 800°C. In: D.T. Griggs and J. Handin (Editors), Rock Deformation (A Symposium), Geol. Soc. Am., Mem. 79, 39-104.
- Handin, J. and Hager, R.V., 1958. Experimental deformation of sedimentary rocks under confining pressure: tests at high temperature. Am. Ass. Petrol. Geol. Bull. 42(12): 2892-2934.
- Handin, J., Friedman, M., Logan, J., Sowers, G.M. and Stearns, D.W., 1972. Mechanical properties of rocks affecting earthquakes generation. Annual Progress Rept. No 1, ARPA Contract No. 14-08-001-12723, Office of Earthquake Research, U.S. Geol. Survey, Menlo Park, Calif., 147 pp.
- Handin, J., Friedman, M., Logan, J., Sowers, G.M. and Stearns, D.W., 1973. Mechanical properties of rocks affecting earthquakes generation.

Semi-annual Progress Rept. No. 2, ARPA Contract No. 14-08-0001-12723,  
Office of Earthquake Research, U.S. Geol. Survey, Menlo Park, Calif.  
 72 pp.

- Jackson, R.E. and Dunn, D.E., 1973. Sliding friction and stick-slip related to foliation, grain size and composition (Abstract). Am. Geophys. Union, Trans., 54(4): 464.
- Jaeger, J.C., 1959. The frictional properties of joints in rocks. Geofis. Pura Appl. 43: 148-158.
- Jaeger, J.C. and Cook, N.G.W., 1969. Fundamentals of Rock Mechanics. Methuen, London, 513 pp.
- Jaeger, J.C. and Cook, N.G.W., 1970. Friction in granular materials. Proc. Int. Conf. Struct. and Solid Mech. Civ. Eng., Southampton, U.K., Paper 20: 257-266.
- Jaeger, J.C. and Rosengren, K.J., 1969. Friction and sliding of joints. Proc. Aust. Inst. Min. Met., 229: 93-104.
- Logan, J.M., Friedman, M. and Rigert, J.A., 1973a. Partial melting of sandstone during frictional sliding in triaxial experiments (Abstract). Am. Geophys. Union., Trans., 54(4): 465.
- Logan, J.M., Iwasaki, T., Friedman, M. and Kling, S., 1973b. Experimental investigation of sliding friction in multi-lithologic specimens. Geological Factors in Rapid Excavation, Pincus (Editor), Engineering Geology Case Histories No. 9, Geol. Soc. Am.: 55-67.
- Raleigh, C.B. and Paterson, M.S., 1965. Experimental deformation of serpentine and its tectonic implications. J. Geophys. Res., 70(16): 3965-3985.
- Stesky, R.M. and Brace, W.F., 1973. Estimation of frictional stress on the San Andreas fault from laboratory measurements. Proc. Conf. on Tectonic

Problems of the San Andreas Fault System, R.L. Kovach and A. Nur  
(Editors), Geological Sciences Vol. XIII, School of Earth Sciences,  
Stanford University, Stanford, Calif., 206-214.

TABLE I

## Description of rocks

Name	Density (g/cm <sup>3</sup> )	Porosity (%)	Average grain size (mm)	Modal analysis	Location and references
Westerly granite	2.646	1.1	0.75	28 qtz 35 micr 32 an <sub>17</sub> 5 mica	Westerly, R.I. (Brace et al., 1965)
San Marcos gabbro	2.819	0.2	2.0	65 an <sub>42</sub> 12 biot 8 cpx 7 amph 5 qtz 3 oxide	San Marcos, Calif. (Brace and Orange, 1968)
Mount Albert periodotite	3.307	0.2	1.0	89 fo <sub>93</sub> 7 opx 2 cpx 1 oxide < 1 serp	Gaspe, Quebec (Brace and Orange, 1968)
Pigeon Cove	2.627	0.6	6.0	47 qtz 51 orth 2 amph	Lanesville, Mass. (Brace and Orange, 1968)
Rutland quartzite	2.643	0.5	0.3	91 qtz 7 orth 2 micr	Rutland, Vt. (Brace et al., 1965)
Snowy Mountain anorthosite	2.855	0.4	0.5	69 an <sub>40-45</sub> 2 garnet 17 amph 6 chlor, mica 6 oxide	Snowy Mountain N.Y.
Twin Sisters dunite	3.320	0.1%	10.0	99 fo <sub>90</sub> 1 oxide	Twin Sisters Mt., Wash. (Christen- sen, 1966)

qtz = quartz  
 micr = microcline  
 orth = orthoclase  
 an<sub>17</sub> = plagioclase (with anorthite content)  
 biot = biotite  
 cpx = clinopyroxene  
 opx = orthopyroxene

amph = amphibole (hornblende)  
 fo<sub>99</sub> = olivine (with forsterite content)  
 chlor = chlorite  
 serp = undifferentiated serpentine  
 mica = undifferentiated mica  
 oxide = undifferentiated opaque minerals  
 garnet = undifferentiated garnet

## FIGURE CAPTIONS

- Figure 1. Sample configuration.
- Figure 2. The effect of the copper-graphite jacket on fracture and friction of San Marcos gabbro at room temperature.
- Figure 3. Temperature along the axis of the sample.
- Figure 4. Typical fault-series run (San Marcos gabbro, run S2). The curves have not been corrected for change in fault area. (Adapted from Stesky and Brace, 1972).
- Figure 5. Fault gouge zone and adjacent fractured region in Rutland quartzite (run A33, 3 kbar, 440°C; STK). Fragments of the grain at the center of the photograph are caught up in the fault zone, adding to the gouge. The arrows lie along the boundaries of the gouge zone and indicate the direction of fault motion. (Crossed polars.)
- Figure 6A. Fractured amphibole grains (dark) offset along the fault zone in Snowy Mt. anorthosite (run A31, 4 kbar, 22°C; STK). The arrows indicate the direction of fault motion. (Plane light.)
- Figure 6B. Apparent ductility of amphibole (dark) in Snowy Mt. anorthosite (run A35, 4 kbar, 256°C; STA). The fault was formed under the same conditions as that of Figure 6A. The arrows indicate the direction of fault motion. (Plane light.)
- Figure 7. Sliding behavior of Westerly granite. The stipled region indicates an approximate boundary between stick-slip and stable sliding.
- Figure 8. Temperature of transition from stick-slip to stable-sliding behavior for seven rocks. The length of the bar is determined by the minimum difference in temperature between runs of different sliding behavior. In all cases, stable sliding occurs at the higher temperature.

- Figure 9. Frictional stress of Westerly granite sawcuts at temperatures to 500°C. Some of the room-temperature data, as well as the line,  $\tau = 0.5 + 0.6\sigma_n$ , are from Byerlee (1967).
- Figure 10. Frictional stress of faulted Westerly granite (fault series) at temperatures to 700°C.
- Figure 11. Frictional stress of faulted San Marcos gabbro (fault series) at temperatures to 700°C. The dashed lines are fitted to all the data within each temperature range regardless of sliding history (compare with Figure 13).
- Figure 12. Fracture and fault-series frictional strength of Westerly granite and San Marcos gabbro at constant pressure and at temperatures to 800°C. For the 4 kbar fracture strength data of both rocks, the strain rate was about  $2.7 \cdot 10^{-5} \text{ sec}^{-1}$ . The 5 kbar granite fracture data are from Griggs *et al.* (1960), run at a strain-rate of about  $5 \cdot 10^{-3} \text{ sec}^{-1}$ . Note the shift in scale on the stress axis. The error in differential stress is indicated for each group of measurements.
- Figure 13. Three incremental fault-series runs of San Marcos gabbro. The order of the measurements for each run is indicated by a letter at each data point.
- Figure 14. Frictional strength of various rocks at constant pressure and at temperatures to 700°C (all are fault series, except dunite). The Westerly granite (WG) and San Marcos gabbro (SMG) trends (both at 4 kbar) are from Figure 12.
- Figure 15. Frictional strength and sliding behavior of wet and dry Westerly granite at 3 kbar effective pressure and temperatures to 500°C. The two wet samples contained a pore-water pressure of about 200 bar.

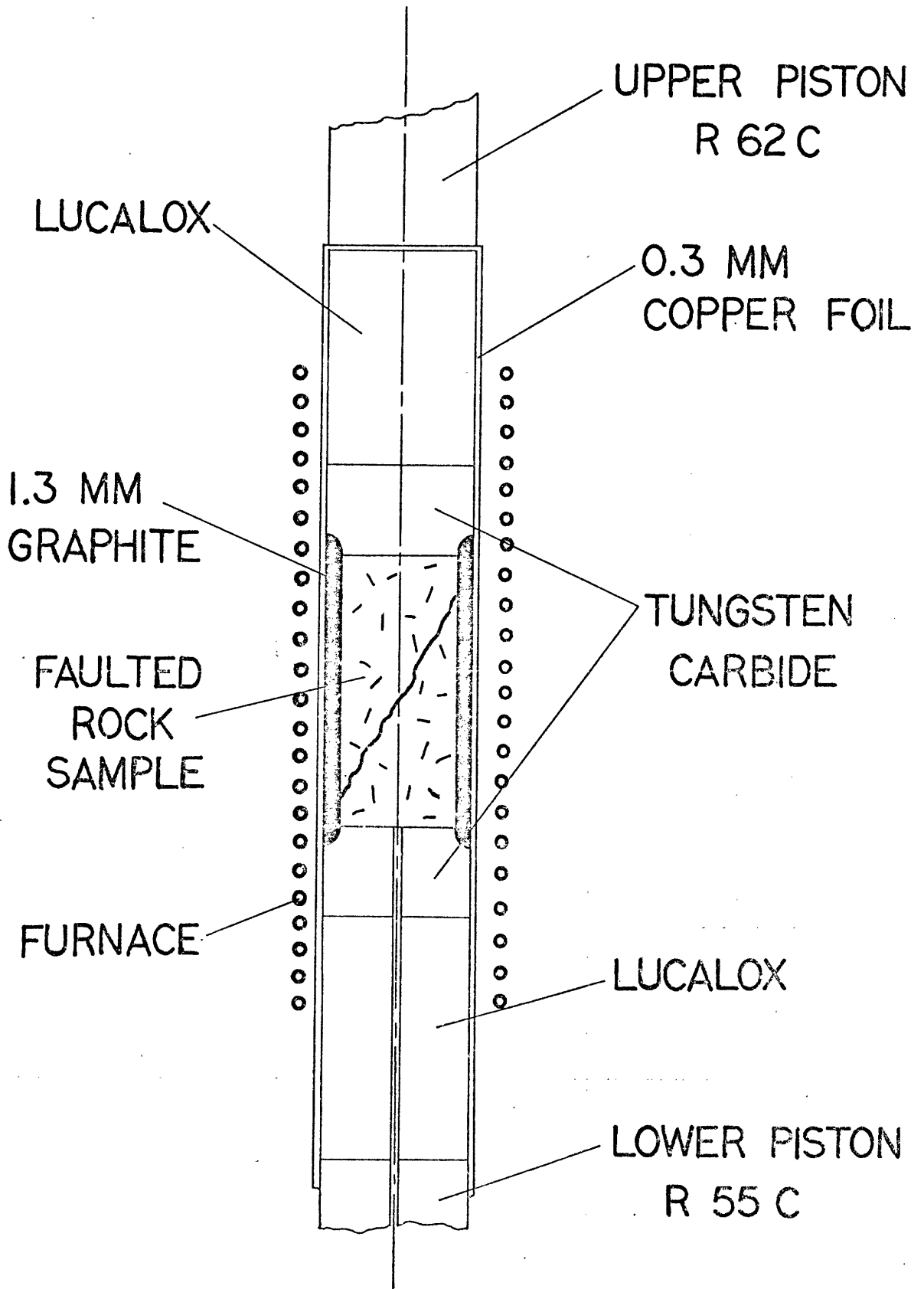
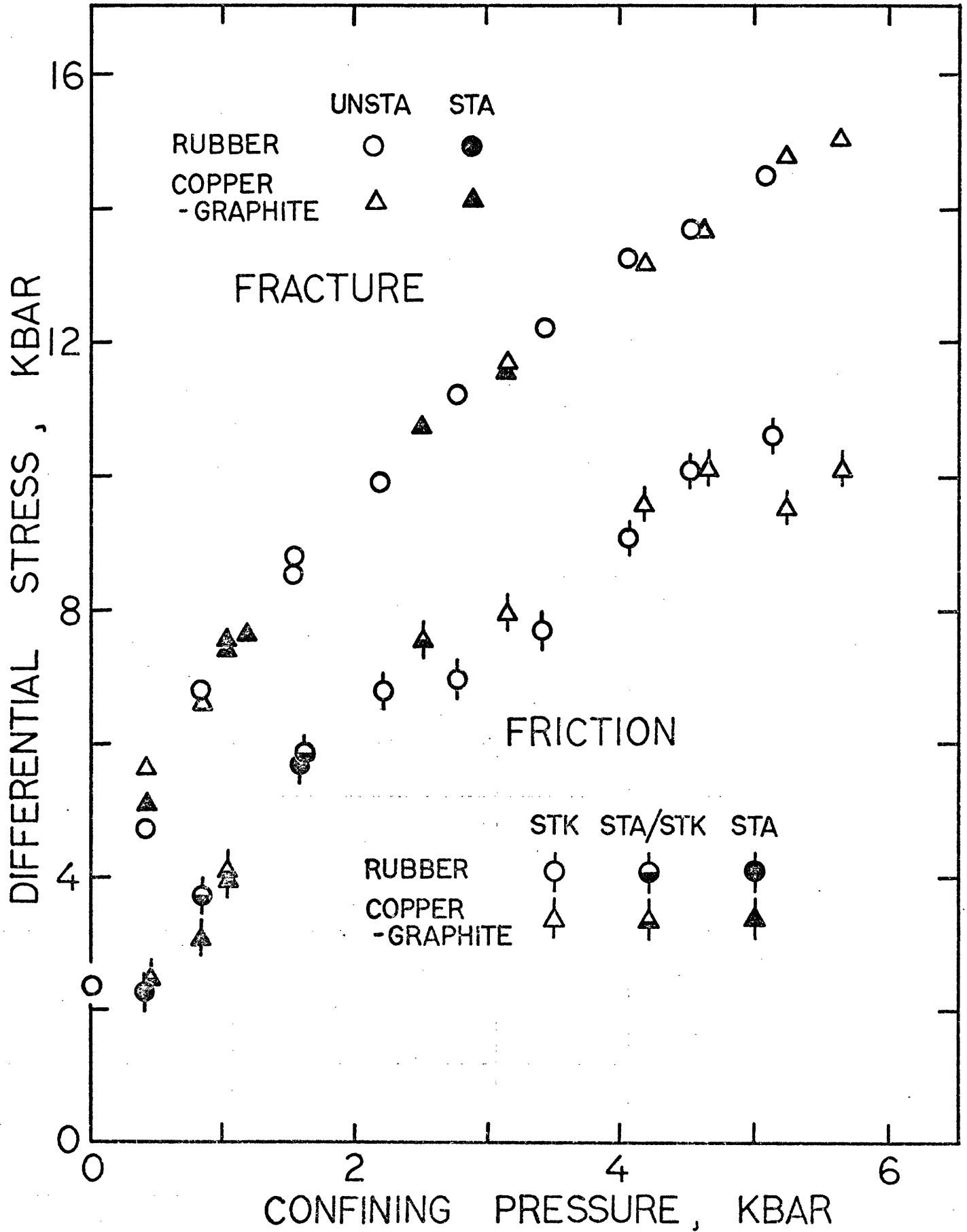


FIG. 1

5/5



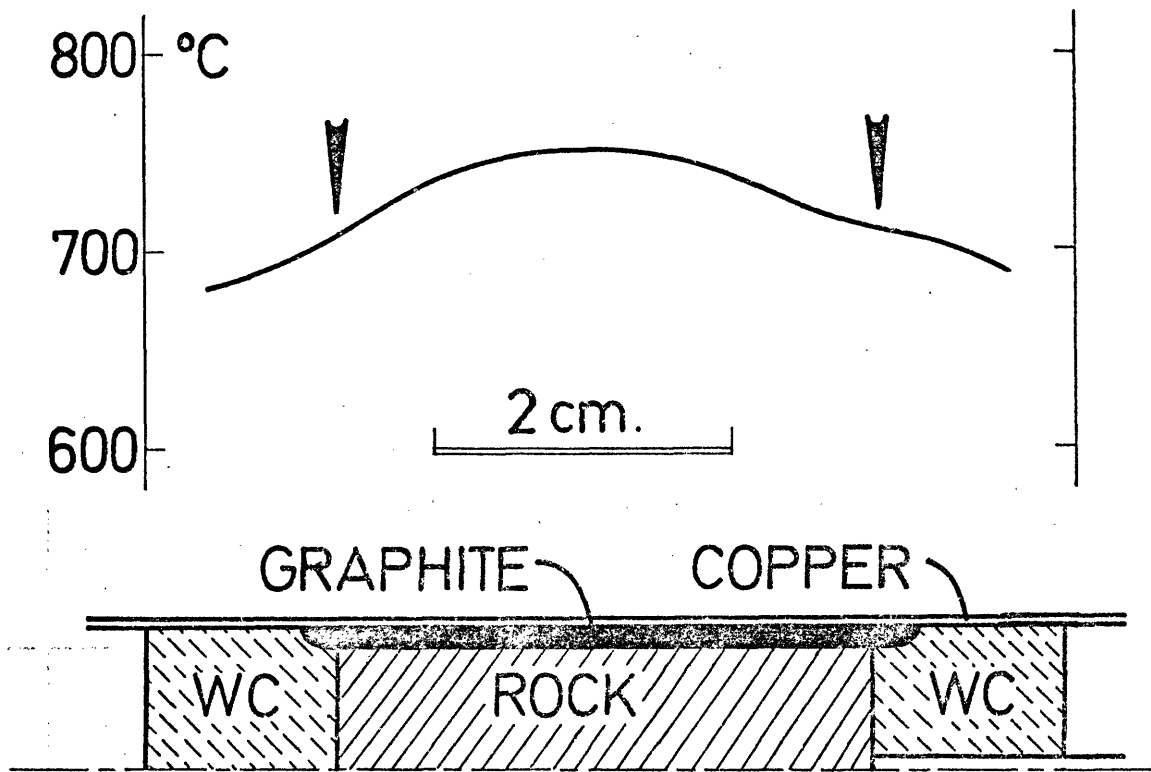
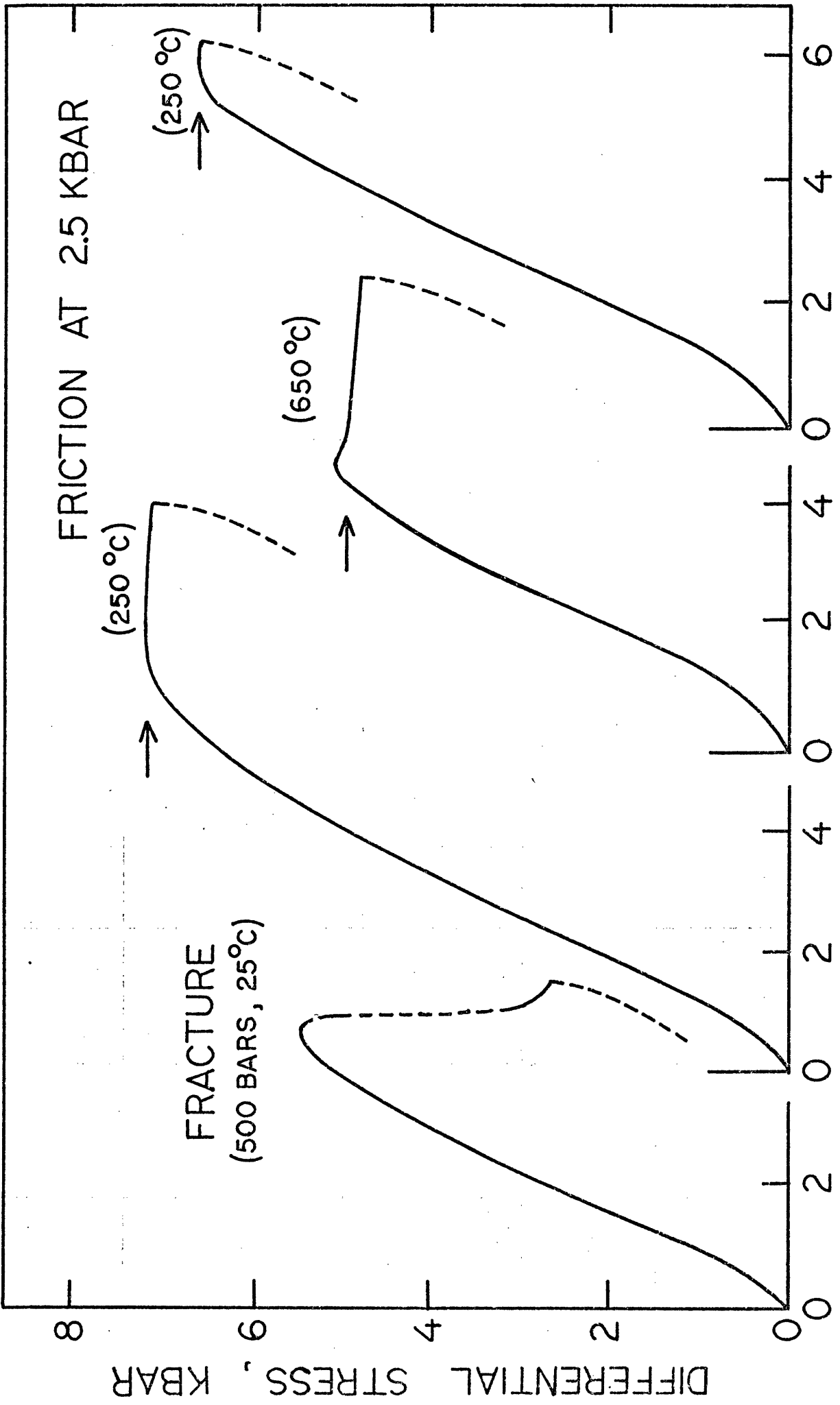


FIG. 3

5/5



DIFFERENTIAL STRESS, KBAR

FRICITION AT 2.5 KBAR

(250 °C)

(650 °C)

FRACTURE (500 BARS, 25°C)

APPARENT AXIAL SHORTENING, %

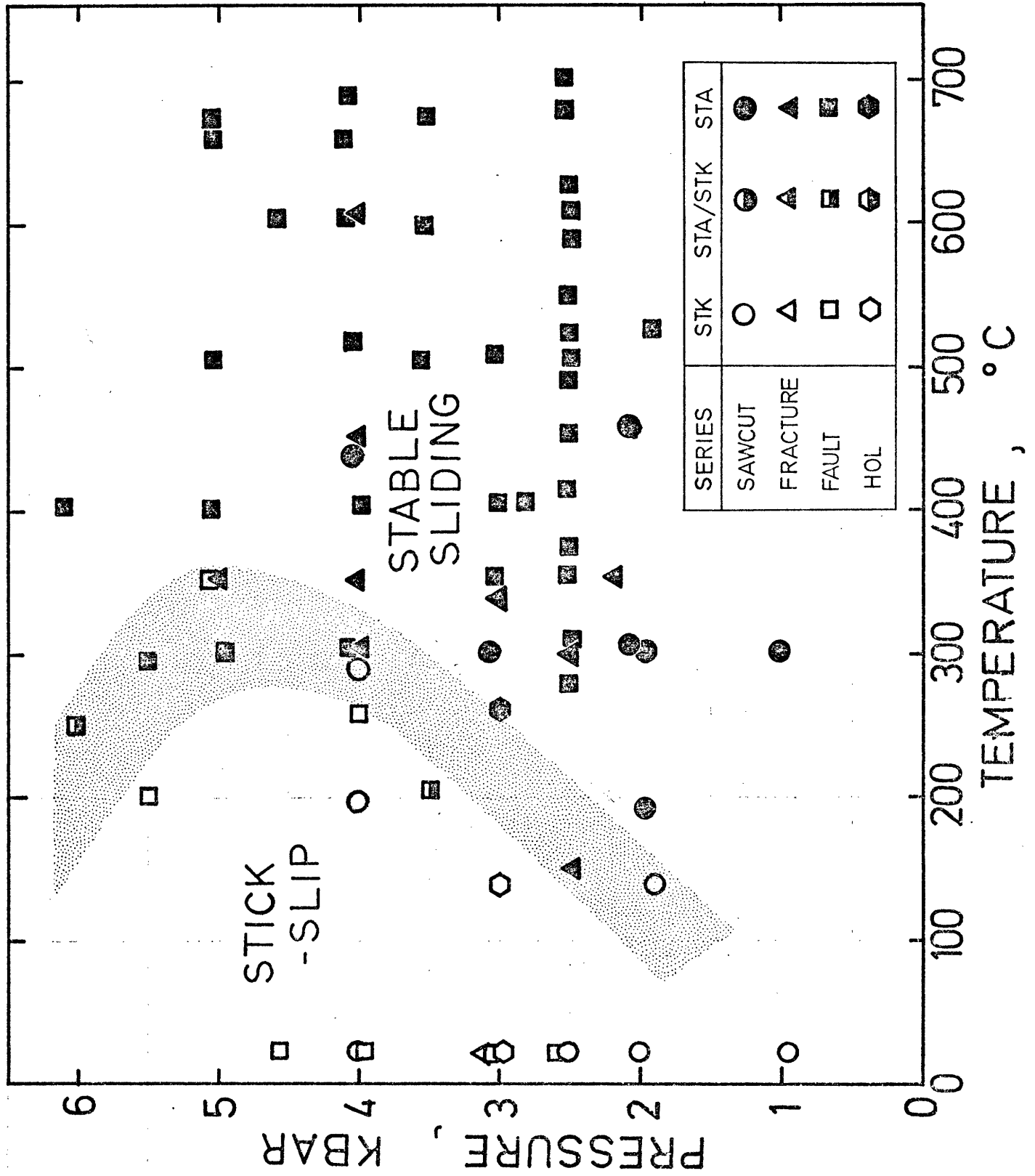


FIG 7

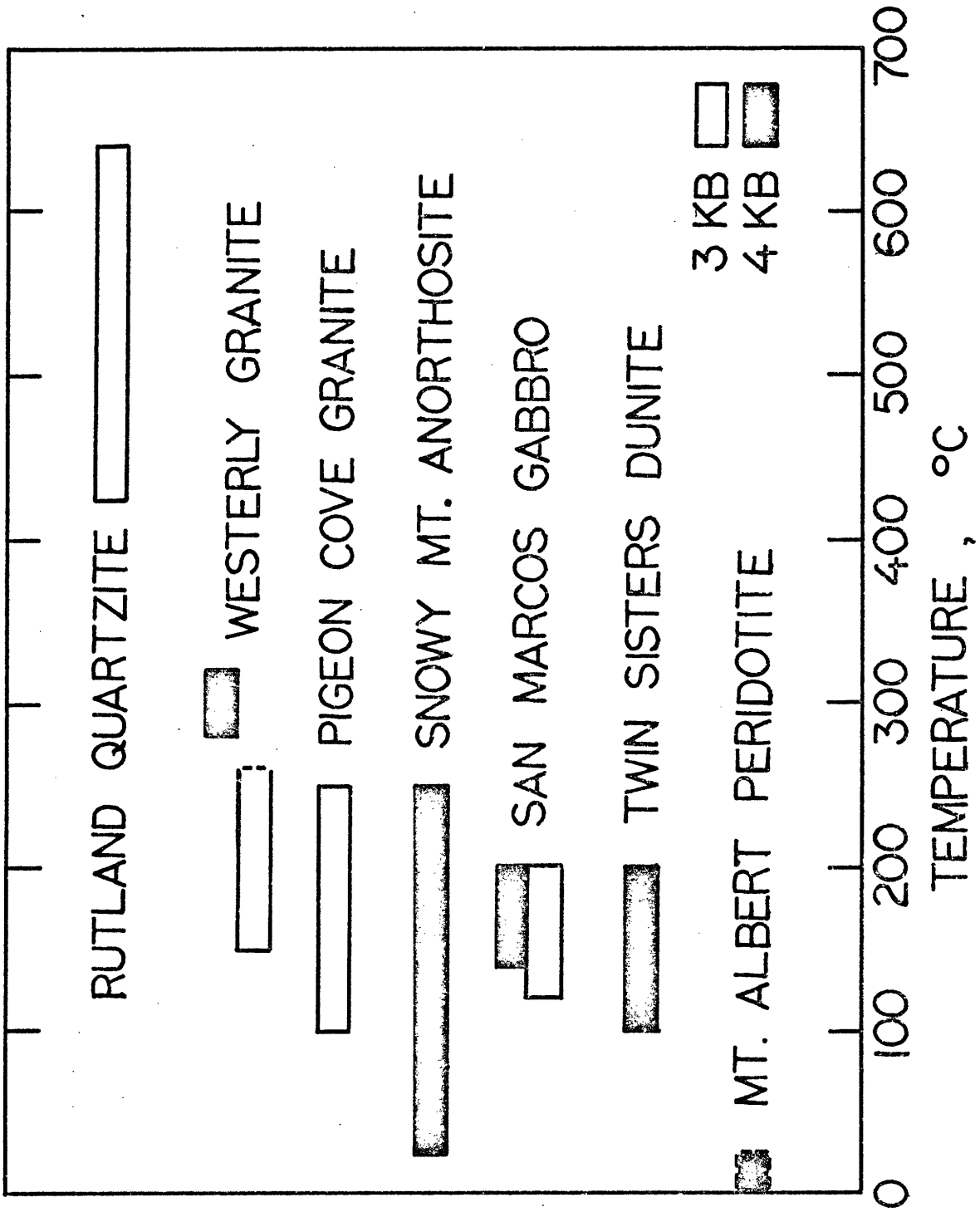


FIG 8

S/S

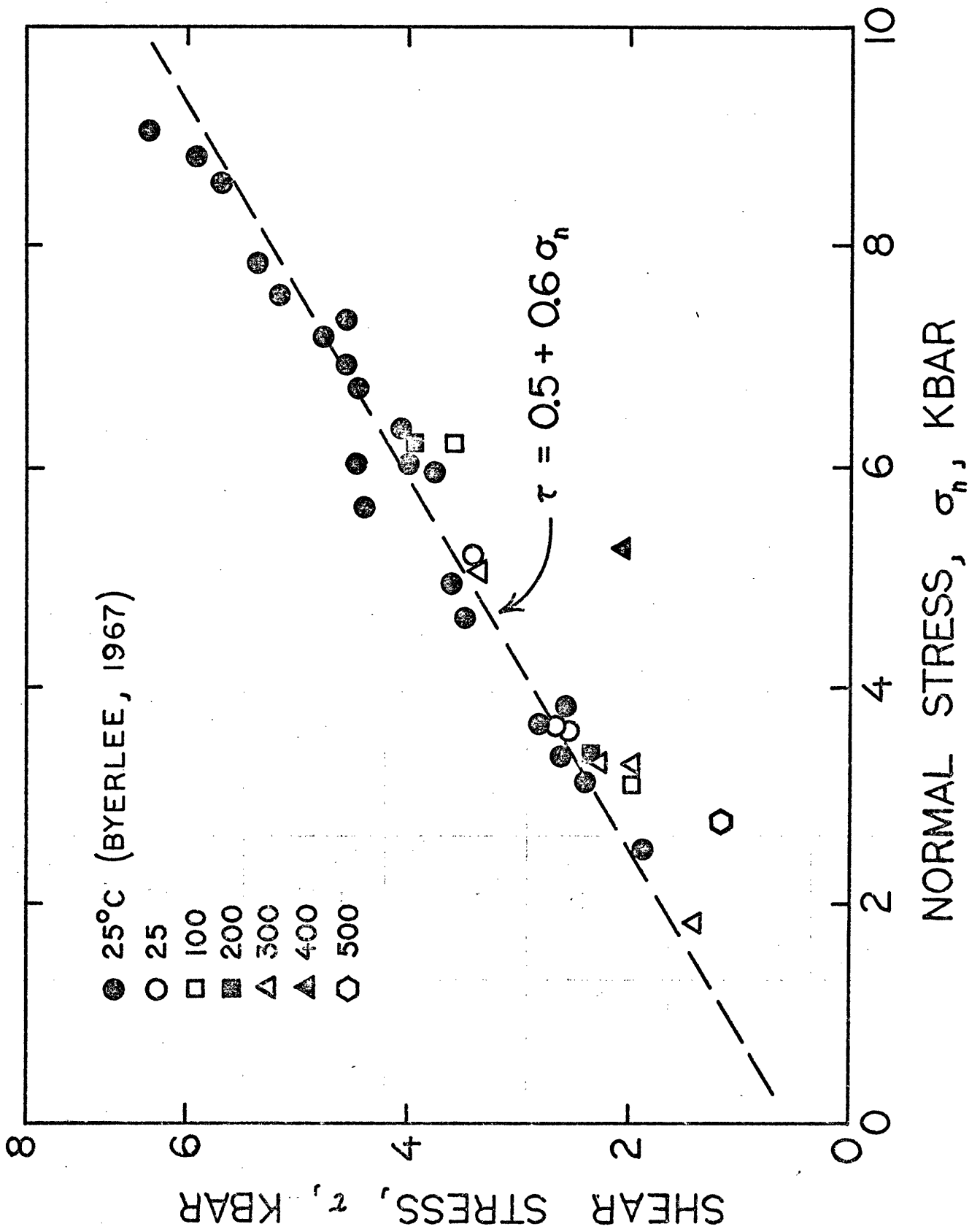


FIG. 9

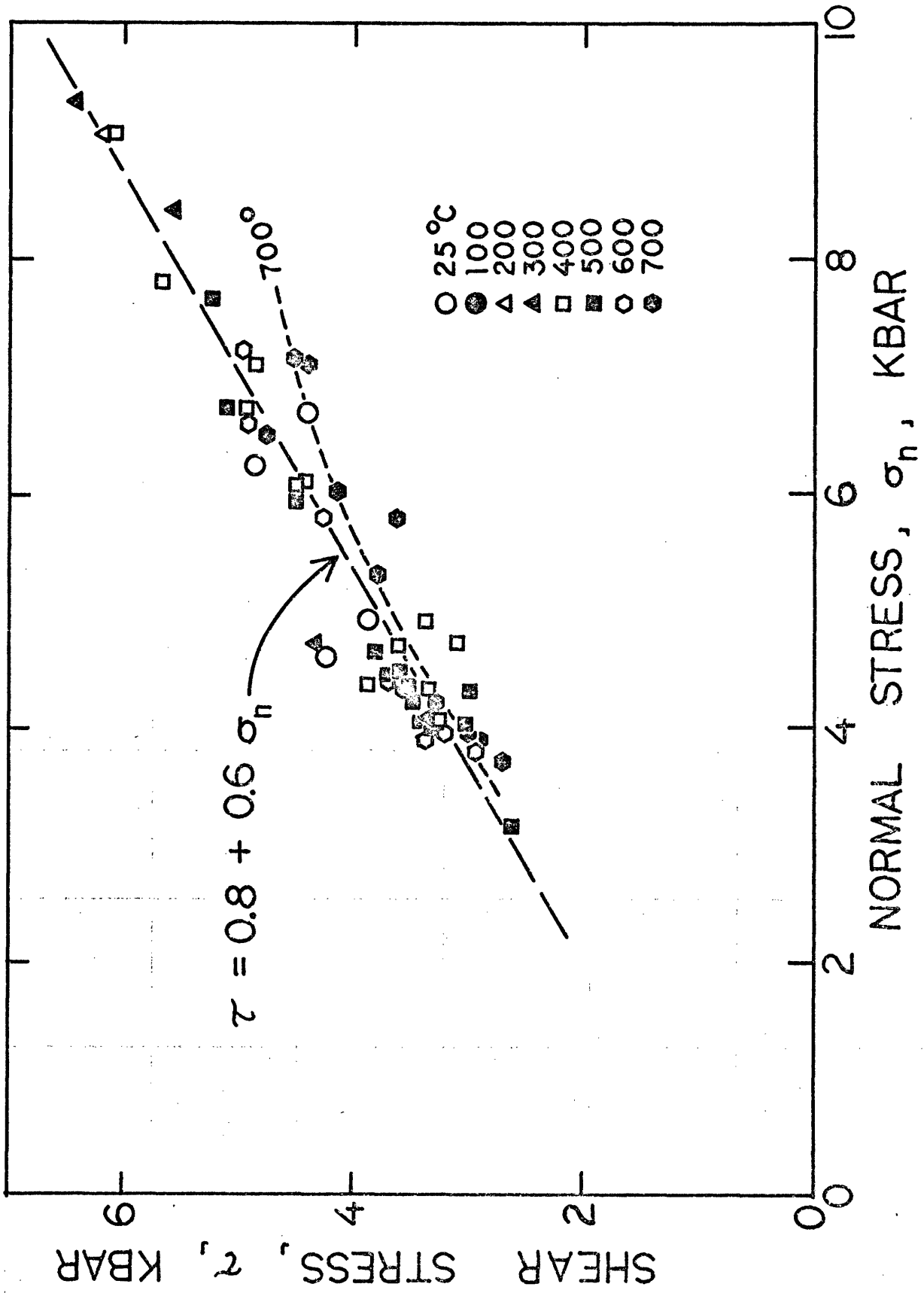


FIG 10

5/5

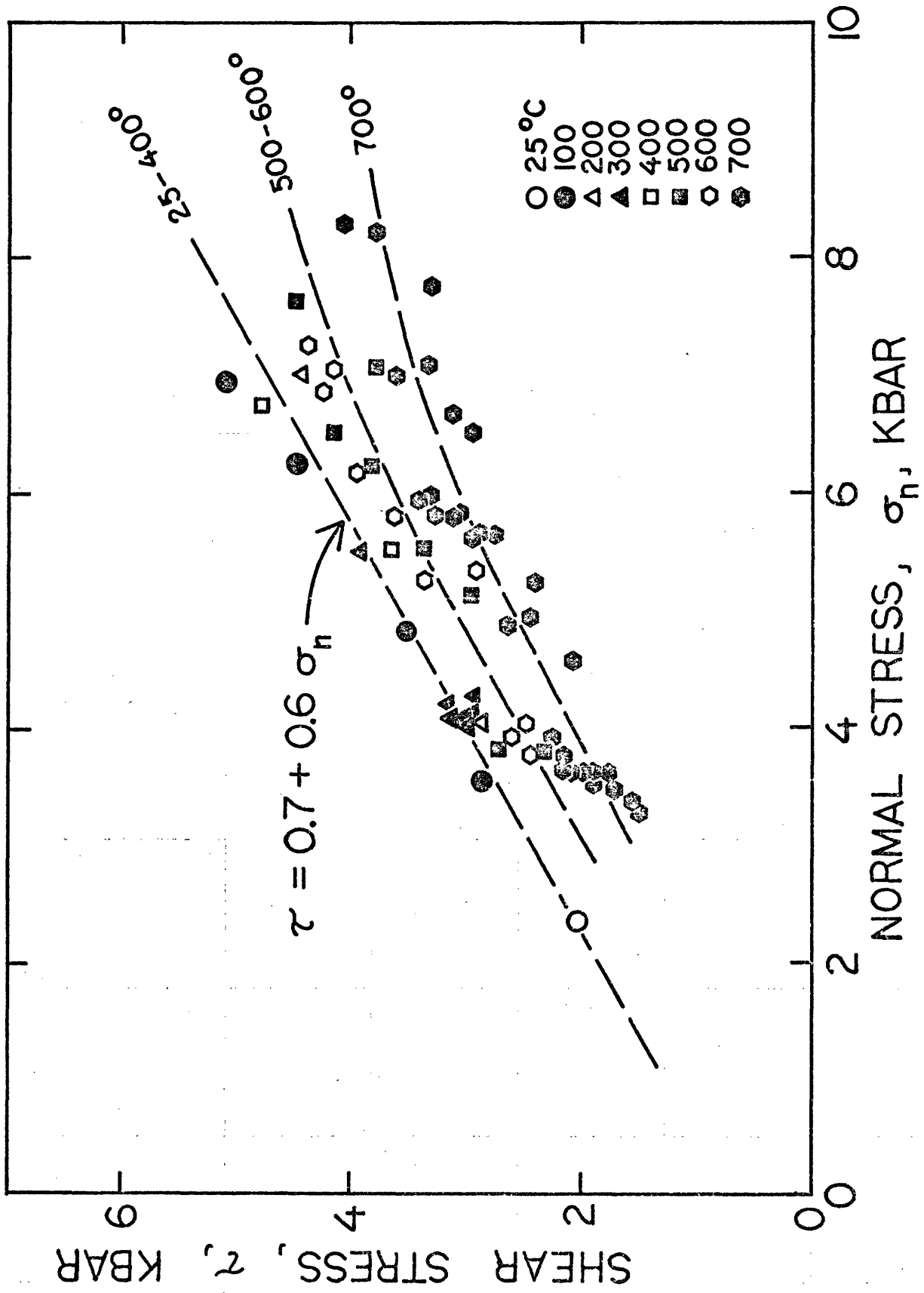


Fig 11

S/S

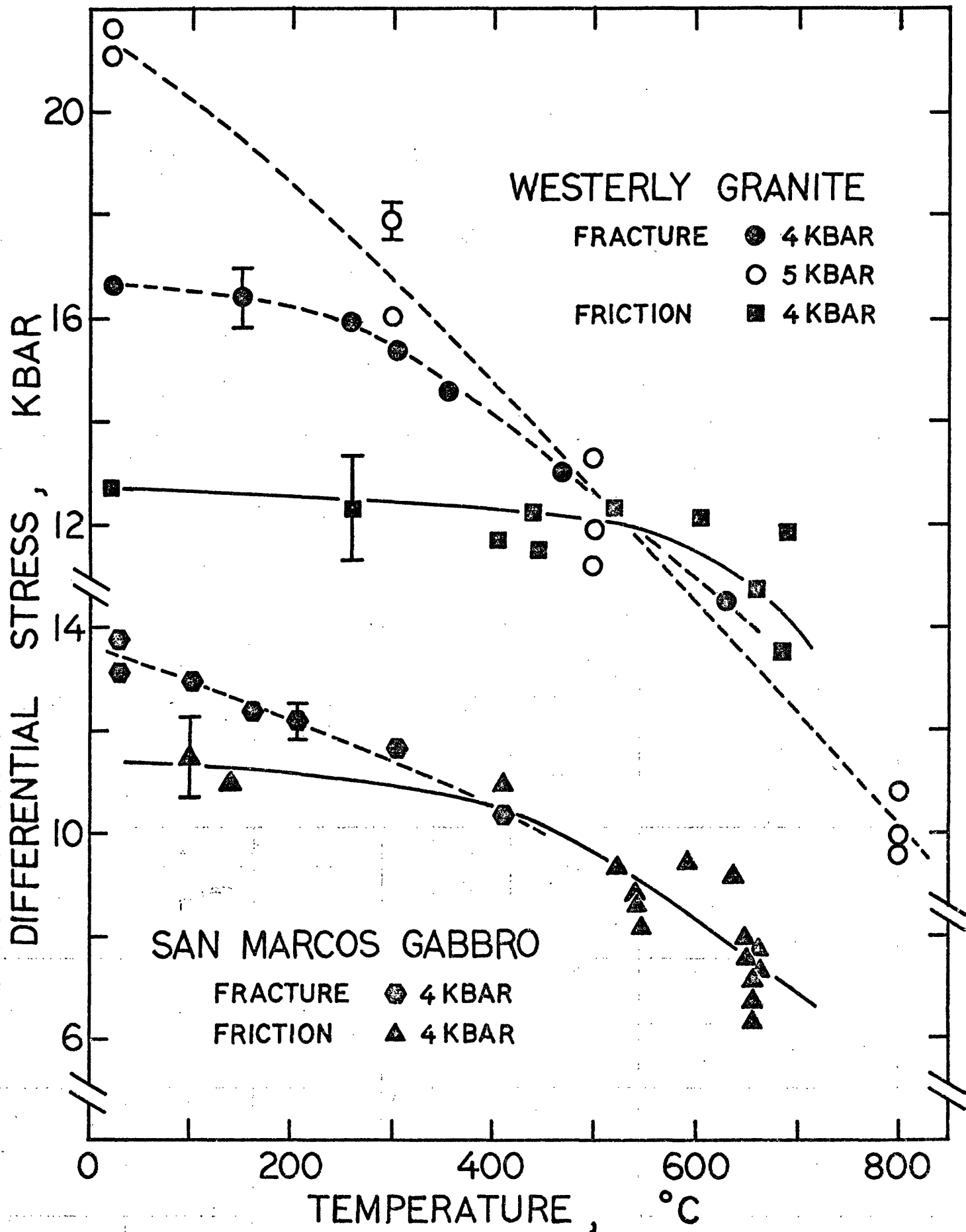
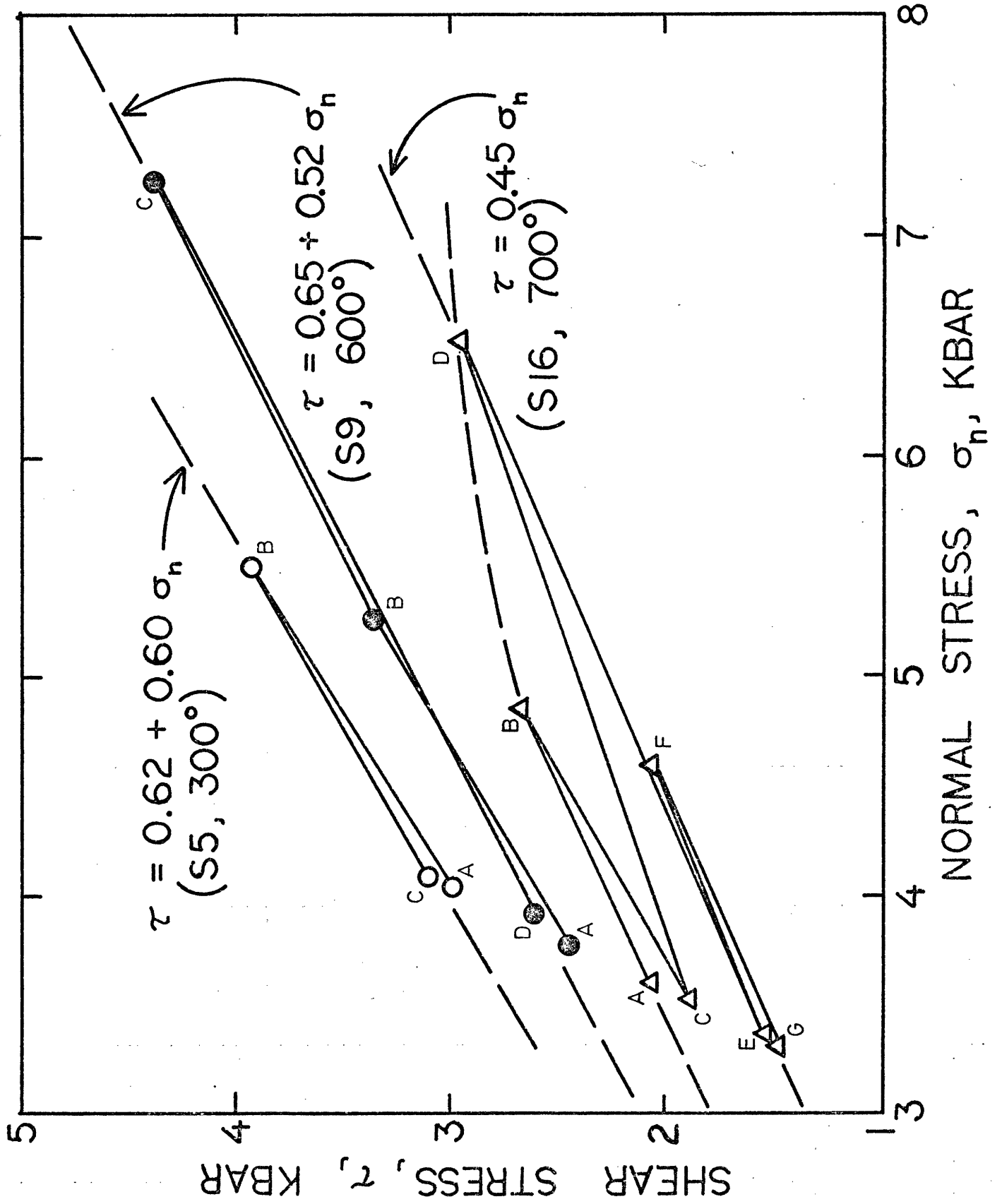


Fig 12

97



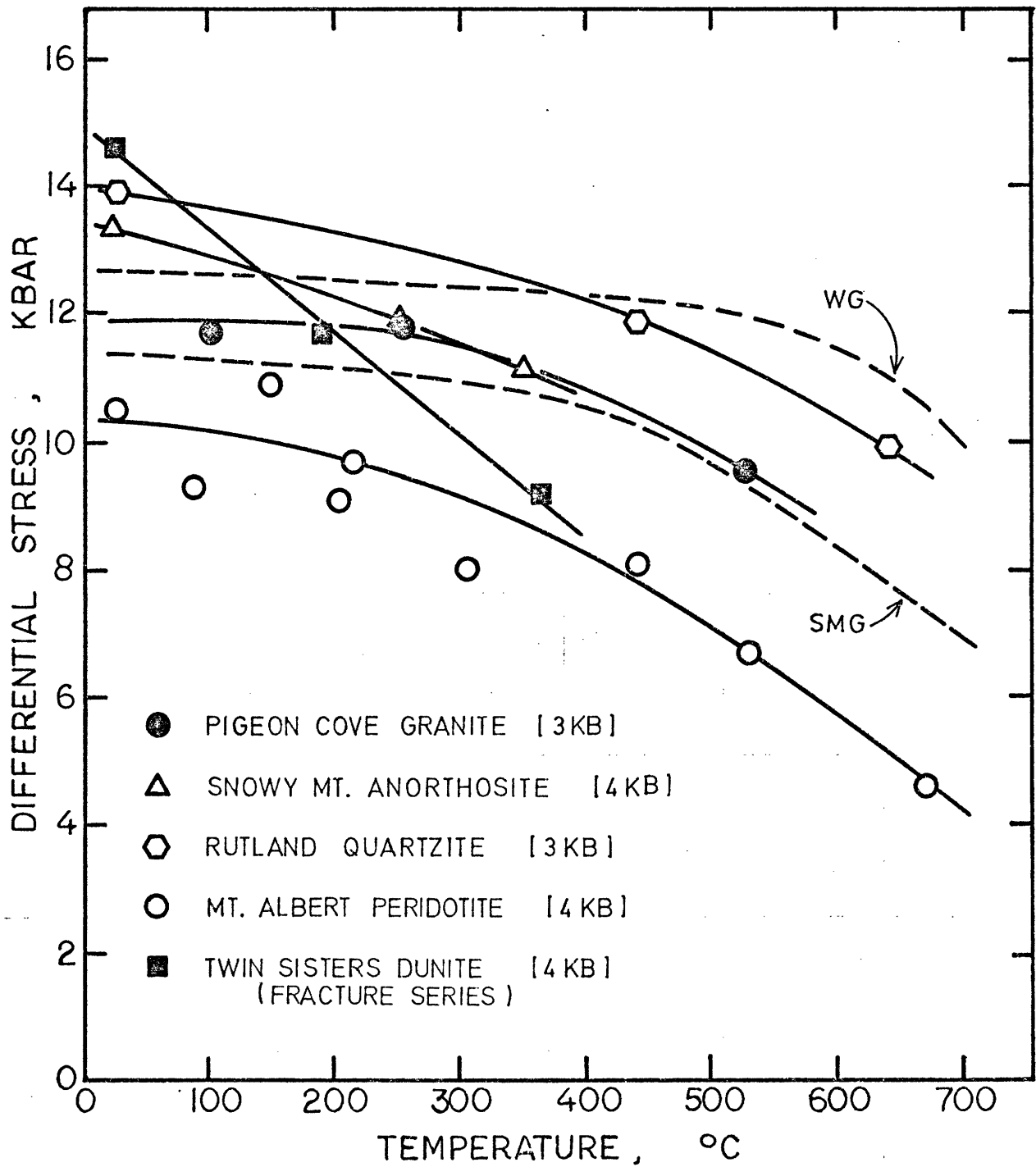


FIG 14

5/5

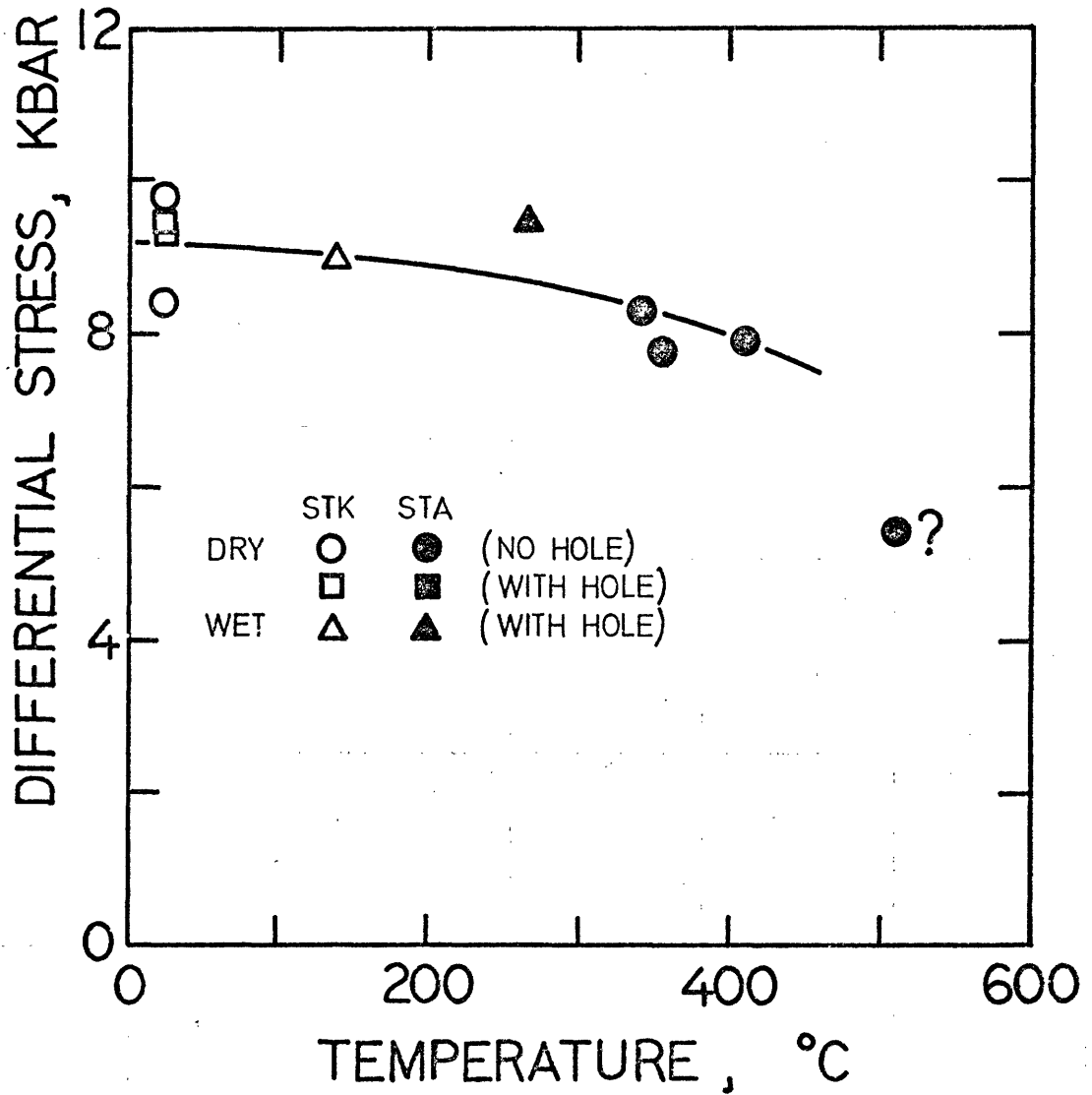


FIG-15

S/S

## CHAPTER II

### TIME-DEPENDENCE OF FRICTION IN FAULTED ROCK AT HIGH TEMPERATURE AND PRESSURE

#### ABSTRACT

The frictional strength of faults during stable sliding was time-dependent. The stress for steady-state sliding increased with increasing sliding rate, the rate sensitivity being greater at higher temperature and higher pressure. Over most of the temperature range the rate sensitivity was very low, lower than that for brittle fracture at room temperature.

Transient phenomena occurred during changes in rate, depending on the boundary conditions. An increase in boundary displacement rate produced a peak in stress before steady-state sliding was reached. The peak height increased with an increase in the change in displacement rate. Holding the boundary displacement constant allowed the fault to continue sliding, but under decreasing stress and sliding rate. However, the stress decreased more rapidly than predicted from the steady-state measurements. If the boundary displacement was held constant for some time and then increased at a constant rate, a stress-peak was produced whose height increased with the time that the boundary displacement was held constant.

A possible explanation for these results may be rate-dependent compaction of the gouge. If the gouge is more compacted at lower rates, then changes in rate will be opposed by changes in compaction to minimize

the variation of stress. Thus a low rate sensitivity is produced. The stress-peak and relaxation phenomena occur during the change in state of compaction.

The time dependence of frictional sliding may explain some observations of stick-slip, episodic fault creep, and displacement changes following many large earthquakes.

#### INTRODUCTION

Abundant evidence shows that the mechanical behavior of natural faults is time dependent. Fault creep often proceeds by alternating periods of rapid and slow displacement (Tocher, 1960; Scholz et al., 1969; Nason, 1971; King et al., 1973; and others). The episodes of rapid creep propagate at rates of up to 10 km/day along the fault trace, with a maximum slip velocity of between  $10^{-5}$  to  $10^{-3}$  cm/sec (King et al., 1973). Following many large earthquakes the sliding rate measured at the fault trace decreased approximately hyperbolically with time, a trend observed also for the frequency of aftershocks (Benioff, 1955; Utsu, 1961; Smith and Wyss, 1968; and Eaton et al., 1970).

Yet the effect of time on friction has been little studied, despite its obvious importance in interpreting field measurements and in understanding the physical processes involved. Most previous measurements were made at low pressures, and all were at room temperature. No measurements were made at the higher temperatures appropriate for the earth's crust, so the data have limited applicability for many geological fault problems.

## PREVIOUS WORK

The effect of time on friction seems to depend upon the type of sliding motion. For stable sliding, the kinetic friction stress was measured at different sliding velocities and, except in a few cases, was unaffected by the sliding rate over several orders of magnitude (Rae et al., 1966; Coulson, 1970; Donath et al., 1972; Christensen et al., 1973 and Olsson, 1974). However, Rae et al. (1966) found that, for limestone, friction decreased with increasing rate up to  $6 \times 10^2$  cm/sec and that, for sandstone, friction decreased only for rates above  $2 \times 10^2$  cm/sec and normal stresses less than 5 bars. Furthermore, Coulson (1970) observed that, for dolomite at normal stresses less than 83 bars, the friction stress increased by 3 to 8% with an increase in sliding rate from  $5.3 \times 10^{-4}$  cm/sec to  $1.2 \times 10^{-2}$  cm/sec.

For stick-slip experiments, rate effects have been observed by varying the loading or piston-advance rate or by varying the amount of time at which the load was held slightly below that required for slip. These two methods are somewhat comparable since both measure the time-dependence of the "static" friction stress, defined as the maximum friction stress prior to sudden slip. In most experiments the stick-slip stress, as well as the stress drop, increased with the logarithm of the time prior to slip (Coulson, 1970; Scholz et al., 1972; Dieterich, 1972; Handin et al., 1972, and Engelder, 1973). For example, Dieterich (1972) observed a 5 to 8% increase in friction stress for a decade increase in time during which the load was held just below the peak stress. He also noted that the time-dependence was more marked for surfaces with gouge than for those without. On the other hand, Byerlee and Brace (1968) and Christensen et al. (1973), using Westerly granite, did not find any change in friction stress with three orders of magnitude change in loading rate. The  $\pm 10\%$  scatter in the

high pressure measurements of Byerlee and Brace could have masked any small rate effects.

#### PRESENT INVESTIGATION

To further understand the time-dependence of frictional sliding we made measurements at high temperature, for several reasons. With higher temperatures we can better simulate the fault conditions at depth in the earth. Also, since many geological rate processes are thermally activated, we might expect the rate effects to be more marked at higher temperatures. The effect of temperature might lead to some insight into the physical processes. However, because of possible jacket constraints in our high-temperature sample configuration (Stesky et al., 1974), friction measurements had to be made at pressures above 2 kbars. As Byerlee and Brace (1968) showed, the variation in peak stress between successive stick-slip events at high pressures is larger than the expected rate effects. Consequently, the experiments were made under conditions where the sliding was stable, that is, above 250°C at 2.5 kbars (Brace and Byerlee, 1970; and Stesky et al., 1974), allowing small stress variations to be measured.

The detailed frictional behaviour seems to depend very much on the applied boundary conditions. For convenience, the piston displacement rate was chosen as the variable boundary condition. The boundary displacement was taken up by sliding on the fault, by elastic shortening of the rock, and, perhaps, by deformation of the rock surrounding the fault. By varying the piston rate, effects were observed which seem to depend on the existence of a transient phenomenon. The characteristics of this transient, as well as of the steady-state behavior, were the subjects of this investigation. Three kinds of rate variations were made: (1) a rate experiment, in which

the piston displacement rate was changed by up to three orders of magnitude during stable sliding; (2) a relaxation experiment, in which the piston was stopped during steady sliding and the stress allowed to relax; and (3) a holding experiment, in which the stress to cause sliding was measured after holding the fault for varying lengths of time under a load below that necessary for slip, or after a relaxation experiment of varying duration. While in hindsight these kinds of variations may not be the best choice for understanding the physical processes, they do exhibit phenomena which may have their counterpart in nature.

## EXPERIMENTAL PROCEDURE

### Apparatus and sample configuration

A detailed discussion of the experimental technique was given by Stesky et al. (1974). The rock sample was precisely ground cylinder, 16 mm in diameter and 35 mm long. It was surrounded by a 1.3 mm thick graphite sleeve and an annealed seamless copper tube, 0.32 mm thick. The triaxial apparatus consisted of an internally heated pressure vessel, the load being applied with a screw-driven piston. The stiffness of the loading system was about  $10^5$  kg/cm. The displacements were measured outside the pressure vessel and are accurate to about 1%. The argon pressure medium was maintained to within 10 bars. The temperature, measured at the base of the sample, was known to within 10 to 15°C, the average variation over the fault surface. The stresses were measured with a conventional strain-gauge load cell and are accurate to within 6 to 8%, although relative values for the same sample were known to within 1 or 2%. Throughout this paper the maximum shear stress on the fault,  $\tau$ , is given, calculated in the usual way from the measured load, the confining pressure, and the fault angle. Corrections were made for the changing fault area during sliding.

In all experiments, the fault was formed by loading the sample at 500 bars pressure and 25°C until failure. The pressure and temperature were then adjusted to the desired conditions. The measurements were made at temperatures up to 700°C and at 2.5 kbars pressure, although a few runs were made at pressures up to 4 kbars. In all cases, the temperatures were sufficient to produce stable sliding (Brace and Byerlee, 1970, and Stesky et al., 1974).

#### Rocks studied

Westerly granite, San Marcos gabbro, and Mount Albert peridotite were selected for study. All are moderately fine-grained, low porosity rocks which have been used in previous studies of friction (Byerlee and Brace, 1968, and Stesky et al., 1974).

#### OBSERVATIONS

##### Rate experiment

The boundary displacement rate,  $\dot{\delta}_a$ , was changed during stable sliding and the change in friction stress,  $\bar{\tau}$ , was measured. A typical stress-displacement curve, uncorrected for area change, is shown in Figure 1. The rising portion of the curve corresponds to elastic shortening of the rock; the horizontal portion to sliding on the fault at a constant rate. The apparent decrease in shear stress with displacement resulted in part from area change, shown by the dotted line, and possibly from changes in fault structure with displacement. Such structural changes were not reproducible from sample to sample for they depended considerably on the initial fault geometry. In the particular example shown, two conjugate faults were formed and required a higher-than-usual stress for sliding. Eventually, one fault became dominant, and the stress decreased.

The steps in the curve correspond to changes in rate. After a rate change and prior to re-establishing steady-state sliding, a brief transition

region occurred. Increasing the rate often produced a slight stress peak (for example, at point A. Fig. 1); decreasing the rate often produced a slight extra weakening (for example, at point B). Typically, steady-state sliding is restored after a displacement of 0.005 to 0.01 cm. These fluctuations in stress and sliding rate do not seem to be attributable to machine effects, so they are a property of the faults.

Two measurements were made for each rate change,  $\Delta\tau_s$  and  $\Delta\tau_p$  (Fig. 1).  $\Delta\tau_p$  was measured for both the stress-peaks and stress-troughs, although for the troughs the stress change was consistently less than for the peaks and often equalled  $\Delta\tau_s$ .

Figs. 2 and 3 show the steady-state sliding measurements,  $\Delta\tau_s$ , for the granite and gabbro with variations in sliding rate,  $\dot{\delta}$ , from  $10^{-5}$  to  $10^{-2}$  cm/sec. at temperatures from  $250^\circ$  to  $700^\circ$ C. The stress changes were calculated relative to  $\dot{\delta}$  at  $10^{-4}$  cm/sec. Two features are observed. (1) The stress change is approximately proportional to  $\log \dot{\delta}$ , although there is a tendency for  $\Delta\tau_s$  to decrease with rate. (2) The slope  $\frac{\Delta\tau_s}{\Delta \ln \dot{\delta}}$ , increased markedly with temperature. This observation is illustrated more clearly in Fig. 4, where the slope, here called the rate sensitivity, is plotted against the reciprocal of the absolute temperature. The stress measurements have been corrected for area change and for a change in normal stress,  $\sigma_n$ . That the normal stress should change with shear stress is inherent in the triaxial method. By making a correction for normal stress change, some of the variability due to fault angle is removed. This correction was made by assuming that the shear and normal stress are linearly related, an approximation that is reasonable for both granite and gabbro at 2.5 kbars (Stesky et al., 1974). Two runs were made at 4 kbars and corrected as above. The bar shown on a few calculated points is the estimated uncertainty. The gabbro results are a

little more scattered, but the stress changes are comparable to that for the granite.

Fig. 5 shows the differential data for the peaks following the rate changes ( $\Delta\tau_p$  of Fig. 1) plotted as in Fig. 4. Again, corrections were made for changes in area and normal stress and the bars denote the measurement uncertainty. Different symbols distinguish peak from trough measurements, and, as suggested earlier, the stress change for a trough is less than that for a peak. No stress peak was observed in the 700<sup>o</sup>, 4 kbar run. The behavior of the granite, observed in two samples, was somewhat unusual at the lowest temperature (305<sup>o</sup>C). The sliding was not entirely steady, but exhibited occasional fluctuations in stress. The temperature for the runs was close to that for which stick-slip motion occurs (Stesky et al., 1974), and the fluctuations may be similar to the episodic sliding events observed by Scholz et al. (1972) in Westerly granite at room temperature and normal stress of 1 kbar.

#### Relaxation experiment

In these runs we stopped the piston once steady-state sliding was attained. A time-dependent decrease in stress was observed and measured with a time-chart recorder. Runs were made with the granite, gabbro, and peridotite at various temperatures and pressures. The results are shown in Fig. 6, where the decrease in shear stress,  $\Delta\tau_R$ , corrected for change in area and normal stress, is plotted against log time.

While there is some scatter in the measurements, several features are evident. Except for the highest temperature runs, the stress decreased approximately linearly with log time after about 50 to 100 seconds. Judging from the granite and peridotite runs, the rate of stress decrease seems to be greater at higher pressure. The effect of temperature on the relaxation

rate is uncertain and unsystematic. For the granite and gabbro, increasing the temperature decreased the rate of stress drop; the opposite was observed for the peridotite. At the highest temperature, a marked change in rate occurred for both the gabbro and peridotite after about 1000 seconds. In the case of the peridotite, this behavior was reproducible with two different samples.

If we assume that all the deformation is occurring by sliding along the fault, we can calculate the change in displacement with time. We have the relation,

$$\Delta\delta = - \frac{\Delta\tau_r}{k \sin \theta \cos^2 \theta} \quad (1)$$

where  $\Delta\delta$  is the change in displacement on the fault surface,  $\Delta\tau_r$  is the change in shear stress on the fault, and  $\theta$  is the angle between the fault plane and the axis of the sample.  $k$  is an elastic constant, defined as,

$$k = \frac{\Delta\sigma_a}{\Delta\delta_a} ,$$

where  $\Delta\sigma_a$  is the change in axial stress and  $\Delta\delta_a$  is the change in axial displacement. These quantities are measured along the rising linear portion of the stress-shortening curve. The angle factors relate the axial loading direction to the sliding direction.

The calculated displacements are shown in Fig. 7. The additional point to note is that the marked change in sliding rate in the highest temperature runs of gabbro and peridotite seems to occur after a displacement of about 0.007 cm. A similar change results in the high pressure, low temperature peridotite run and may have the same cause. The significance of this displacement effect is not certain, since it did not occur in the granite. An observation to be noted, however, is that in the high temperature gabbro runs the steady sliding stress at  $10^{-4}$  cm/sec was

significantly lower (about 11%) after the relaxation measurement than before. This irreversible change in stress cannot be explained by a change in area, but rather suggests some permanent change in the fault surface.

#### Holding experiment

Here the shear stress to cause sliding was observed after holding the fault either for varying lengths of time under a reduced load (the granite runs) or following relaxation experiments of varying duration (the gabbro and two granite runs). This procedure is somewhat analogous to that used by Dieterich (1972) and is a hybrid of the rate and relaxation experiments. In a typical holding experiment (Fig. 8), the faulted rock was loaded at a constant piston rate of  $10^{-4}$  cm/sec until steady state sliding occurred. The machine was then stopped and the stress was lowered manually by about 10 to 15% (as in Fig. 8) or was allowed to relax for some period of time. Upon reloading, a small stress-peak occurred similar to that observed by Jaeger and Cook (1970) and to that found in the rate tests described earlier. The height of the peak was dependent on the holding time.

The measurements for the granite and gabbro are shown in Fig. 9. The shear stress difference,  $\Delta\tau_H$ , is the height of the peak measured relative to the steady sliding stress at a sliding rate of  $10^{-4}$  cm/sec (Fig. 8). Although there is considerable scatter in the results and the accuracy of the measurements is not great, there is a tendency for the peak height to increase with the holding time. The results are little affected by rock type, pressure, and temperature within the range of conditions used and the reproducibility obtained. The more extensive experiments made by Dieterich (1972) for stick-slip sliding at low normal stress and room temperature suggest a semi-logarithmic relationship between stress and time. This

relationship was dependent on the normal stress, the strengthening rate being greater at higher normal stresses.

## DISCUSSION

### Effect of rate on steady-state sliding

The effect of rate on deformation depends very much on the details of the mechanisms involved. It seems a general observation that for processes involving crack growth, the stress for deformation is fairly insensitive to the rate (see, for example, the results of Donath and Fruth, 1971, and the compilations of Brace and Jones, 1971). This feature results in large measure from the high stress sensitivity of crack propagation velocities. For example, Martin (1972) observed that the rate of crack growth in quartz is dependent on the exponential of the stress. For comparison with other deformation processes we can express the stress-rate measurements, over small ranges of stress, in the form  $\dot{\epsilon} = \sigma^n$ , where  $\dot{\epsilon}$  is strain rate and  $\sigma$  is stress. A typical value of  $n$  for crack growth is 19 (calculated from data in Martin's Fig. 4). For room temperature fracturing of brittle rocks,  $n$  is 30 or greater (Brace and Jones, 1971, Fig. 4). High values of  $n$  are typical also for steady-state frictional sliding. Using the measurements of rate sensitivity from Fig. 4 of this paper and of the frictional shear stress at 2.5 kbars confining pressure (normal stress of about 4 kbars for a  $30^\circ$  fault angle from Stesky *et al.*, 1974), we obtain  $n$  values of over 1000 at  $300^\circ\text{C}$  to 30 at  $700^\circ\text{C}$ , similar numbers being obtained for both Westerly granite and San Marcos gabbro. For comparison, plastic deformation of rocks tends to give much lower values of  $n$ , typically below 10 (Kohlstedt and Goetze, 1974, for olivine; Heard and Carter, 1968, for quartz; Heard, 1972, for halite; and Heard and Raleigh, 1972, for marble).

However, a high  $n$  does not necessarily imply a crack-related process;

other mechanisms may have a similarly large stress dependence. For example, dislocation glide velocity is very sensitive to stress. Using the measurements of Johnson and Gilman (1959) in lithium fluoride, we calculate an  $n$  value of 25 at low velocities, decreasing to 2 at high velocities.

A further complication is that competing processes may occur which offset the effect of rate changes and produce high values of  $n$ . One possibility for frictional sliding is a change in gouge compaction with sliding rate. At lower rates, the gouge may be denser. Since an increase in compaction would tend to act on the applied stress in a way opposite to that of a decrease in rate, the resulting change in stress with rate would be less than if the gouge density remained constant. This interpretation is supported by the results at 4 kbars. At 450°C the rate sensitivity at 4 kbars is comparable to that at 2.5 kbars, while at 700°C it is a factor of two higher. Further, the frictional stress at 700°C seems less dependent on pressure at 4 kbars than at 2.5 kbars (Stesky *et al.*, 1974), suggesting that changes in porosity and the porosity itself may be much less at the higher pressure. A decreased influence of compaction would then produce an increased rate sensitivity, as observed. Other possible evidence for the effect of variations in gouge compaction, particularly to explain transitory phenomena, will be discussed later.

The large change in rate sensitivity with temperature also deserves comment. If two competing processes are indeed present--that is, the effect of sliding rate on shear strength on the one hand and the effect of gouge compaction on shear strength on the other--then two possibilities exist to explain the change in rate sensitivity. Either a change in mechanism occurs to alter the relationship between rate and stress, or the gouge may approach zero porosity at high temperatures. The latter possibility seems less likely since at 2.5 kbars the effect of pressure on the shear

stress remains the same over the entire temperature range studied (Stesky et al., 1974). Other evidence to be presented in a later paper also points to a change in deformation mechanism with temperature.

Porosity changes have been observed during the deformation of granular materials. For example, an initially dense sand dilates during shearing and produces a stress-peak very similar to that found in the rate experiments here (Taylor, 1948, p.331). Loose sand, on the other hand, compacts when sheared and no peak is observed. The amount of dilation is dependent on rate. Healy (1963) found that at higher strain rates, dry sand dilates to a greater void ratio or porosity than at lower rates, but that the shear strength is little affected. The origin of the time dependence is not known. He speculated, as we do, that increasing the porosity to lower the shear strength at higher rates is more energetically favorable than increasing the shear strength at constant porosity. However, for other conditions these results may be quite different, depending on the history of the fault gouge and the constraints on sliding. These porosity effects become especially important if water is present in the fault zone. Goodman has shown (Goodman, 1973; Goodman and Ohnishi, 1973) that pore pressure may change during slip on joints and faults. These changes are related to variations in porosity and affect the strength of the fault in accordance with the effective stress principle. Since shallow faults are likely to contain water, the importance of these results to our understanding of fault behavior cannot be understated.

#### Analysis of relaxation measurements

Using adjacent pairs of data points from Figs. 6 and 7, we can calculate the variation of frictional stress and sliding rate during each relaxation run. The results are shown in Fig. 10. Except for the highest temperature

gabbro and peridotite runs, the calculated values scatter about the line,

$$\Delta\tau = s (\ln \dot{\delta}_0 - \ln \dot{\delta}) \quad (2)$$

where  $\Delta\tau = \tau_0 - \tau$  is the change in frictional stress,  $\dot{\delta}$  is the sliding velocity,  $s$  is a constant, and  $\tau_0$  and  $\dot{\delta}_0$  are the initial values. Using equations (1) and (2), we can derive expressions for the variation of stress and displacement with time during a relaxation run, namely,

$$\Delta\tau = -s \ln\left(\frac{t}{p} + 1\right) \quad (3a)$$

and

$$\Delta\delta = \frac{s}{k'} \ln\left(\frac{t}{p} + 1\right) \quad (3b)$$

where  $t$  is time after stopping the piston,  $k' = k \sin \theta \cos^2 \theta$ , and  $p = s/k' \dot{\delta}_0$ . These equations are plotted as solid curves in Figures 6 and 7.

As discussed earlier, the parameter,  $s$ , varies somewhat with temperature and pressure;  $s$  tends to be higher at higher pressures and temperatures, but it does not greatly depend on rock type. When approximately corrected for pressure,  $s$  for Westerly granite is considerably greater than that found for steady-state sliding (Fig. 4) but is about the value for the stress-peak phenomenon (Fig. 5).

The high temperature gabbro and peridotite runs show some unique features in Fig. 10. After a displacement of about 0.007 cm,  $s$  markedly increases in value. The sliding velocity decreases at a lower rate and, for the gabbro, does not appear to decrease at all. The displacement, 0.007 cm, is of the same order as that for the stress-peak phenomenon, a fact that further suggests a relationship between the two kinds of behavior.

#### Transient frictional phenomena

It is quite evident from this study and others that some form of transient

behavior occurs during frictional sliding under changing conditions. The stress peaks following changes in rate (Fig. 1) or in pressure (Handin et al., 1972, p. 125) are two examples. We can gain a qualitative understanding of these transient phenomena by using the concept of an "equilibrium surface structure", a concept similar in principle to that proposed by Jaeger and Cook (1972). The actual surface structure is not known in detail and presumably involves characteristics such as gouge thickness, grain size distribution, porosity, and fault plane curvature. During steady-state sliding, this surface structure does not change with displacement. However, if conditions such as temperature, rate, or pore pressure change, a new equilibrium structure will be established, but only after some finite displacement. The change in equilibrium structure produces transient effects that depend upon what conditions alter and how quickly. Such transient effects tend to be ignored in friction studies; but they may be important in natural faults. Indeed, stick-slip may be such a transient.

The causes of some transients are generally understood. The transients after pressure changes (Handin et al., 1972) may be caused by differences in compaction. The fault gouge during sliding at high pressure is likely to be more compacted than at lower pressure. After decreasing the pressure, a slightly higher stress is necessary to shear through the compacted gouge before steady-state sliding is attained. Dieterich (1972) suggested that time-dependent compaction or some form of junction growth may explain the strengthening observed in his holding tests. These mechanisms, as well as high temperature sintering, may also explain the holding-test results of this study.

But a static compaction or sintering mechanism cannot account for the stress-peaks, since the fault is continually sliding and never stationary.

However, the idea of a rate-dependent gouge porosity, as outlined earlier, is an attractive possibility. How changes in porosity can produce the transient frictional phenomena may be postulated in the following way. Assuming that at higher shearing rates the gouge is less compacted, an increase in sliding rate necessarily involves increasing the porosity of the gouge. Such dilation requires doing work against the normal stress and confining pressure. As a result the initial shearing force to be applied must be greater than that necessary to accommodate the higher shearing rate. Once the gouge dilates, the force to continue shearing decreases because of the less compacted structure. Thus a stress-peak is produced when the sliding rate is increased. In a similar way, a stress-trough forms when the sliding rate is decreased.

The porosity change during shearing can be estimated by assuming as an upper limit that all the stress-peak energy goes into work against the confining pressure. For a peak height of about 20 bars (Fig.9), a displacement of about 0.005 cm, and a fault area of about  $2 \text{ cm}^2$ , the work done is  $10^5$  ergs. Thus, for a confining pressure of 2.5 kbars, the pore volume increase is about  $4 \times 10^{-5} \text{ cm}^3$ . If the dilation is distributed over a fault zone about 0.05 cm thick, then the porosity change is about  $4 \times 10^{-4}$ . This volume change is very small and would require careful experimentation, perhaps with a pore fluid, to detect it.

The relaxation and holding test results, too, are amenable to analysis in this way. In the relaxation experiments, the dependence of shear stress on sliding rate was found to be significantly higher than expected from the steady-state rate tests. As the stress and sliding rate decreases, the fault gouge becomes more compacted, decreasing the rate further. However, because a certain amount of shearing displacement is necessary to alter the porosity, the gouge remains less compacted than that appropriate for the current

sliding rate. Thus during relaxation the stress necessary to shear the gouge at that rate is less than it would be during steady-state sliding at the same rate. The holding tests are a combination of rate and relaxation experiments. While the sample is held at a reduced load or allowed to relax for a time, the sliding rate decreases and the gouge becomes more compacted with time. Upon reloading, the stress necessary to initiate sliding at the higher rate is greater than during steady-state sliding, a phenomenon completely analogous to the stress-peaks of the rate tests.

Support for the hypothesis of the effect of gouge compaction can be found in the measurements at different pressures. At 400°C the height of the stress peak is almost a factor of two greater at 4 kbars than at 2.5 kbars. Such increase could reflect in part the greater amount of work necessary to dilate at the higher pressure. At 700°C, however, no stress peak is produced at 4 kbars, suggesting again that porosity changes are less important at high pressure and temperature.

### Stick-slip

The stress-peaks in the rate and holding tests are a type of instability that could produce stick-slip. An apparatus with a much lower stiffness than that of these experiments might not be able to follow the descending part of the curve, leading to unstable behavior. For example, the maximum negative slope of the stress-peak labelled A in Figure 1 is about  $8 \times 10^4$  kg/cm, comparable to the stiffness of our loading system and of the double shear apparatus of Jaeger and Cook (1972). Such behavior was observed by Jaeger and Cook (1972), who proposed a theory which, in principle, could be extended to include the mechanical properties of the fault itself.

Many stick-slip properties are understandable in terms of the stress-peak phenomenon: the increase of stick-slip stress with decreased loading

rate (Scholz et al., 1972) or with increased holding time (Dieterich, 1972) and the transition from stable sliding to stick-slip with increasing pressure (Byerlee and Brace, 1968; and others) and decreasing rate (Handin et al., 1972). To the extent that the stress drop is related to the height of the stress-peak, one would expect that the stress drops would be larger at lower rates and higher pressure, as observed (Byerlee and Brace, 1968; Scholz et al., 1972; Engelder, 1973). That this stress-peak phenomenon may explain at least some stick-slip observations is suggested by Dieterich's (1972) comment that stick-slip did not seem to occur until at least some amount of time-dependent strengthening took place. If insufficient holding time was allowed, stable sliding resulted; with increased pressure the critical holding time decreased, until stick-slip always occurred. In our holding tests, the slope of the descending part of the stress-peaks increased with the holding time (Figure 8) and presumably could exceed the stiffness of the loading system after some critical holding time was reached.

#### Episodic fault creep

In an attempt to explain the episodic nature of fault creep, Nason and Weertman (1973) suggested that the fault material may exhibit an upper yield point. This phenomenon involves a finite stress to initiate deformation and a smaller stress to continue it. The stress-peak effect observed in the present study shows these characteristics and may be a candidate for explaining episodic creep. In addition, the small stress fluctuations involved in the stress-peaks is in keeping with the low stresses estimated for fault creep events (Nason and Weertman, 1973).

On the other hand, our laboratory study indicates that the sliding velocity during stable sliding increases with increasing stress. One might postulate that the fault creep event is a response to a stress concentration

propagating along the fault, locally increasing the stress and accelerating the sliding. Such events may be initiated by an earthquake, as observed by Burford and others (1973), although the initial slip need not be seismic.

The significant difference between these two possible explanations for episodic creep is the following: for the stress-peak phenomenon, the fault accelerates with decreasing stress, while for the rate effect, the acceleration occurs with increasing stress. In principle, these two possibilities can be tested by making detailed measurements of stress-dependent phenomena associated with creep events, such as seismic velocities (DeFazio et al., 1973), water level changes in wells (Johnson et al., 1973), or piezomagnetism (Breiner and Kovach, 1968; Johnston et al., 1973), or by measuring the stress changes directly by various borehole methods.

#### Relaxation on natural faults

Following many large earthquakes, the tectonic activity has been observed to decrease systematically. The number of aftershocks (Utsu, 1961; Eaton et al., 1970), the accumulated strain recovery (Benioff, 1951; 1955), and the fault displacement (Smith and Wyss, 1968; Scholz et al., 1969) change with the logarithm of the time after the main event. The same time dependence was observed in the relaxation experiments described in this paper. But this relaxation was not the result of creep, in the sense used by Benioff (1951). Rather it was caused by continued sliding at constant boundary displacement and decreasing elastic stress. The time dependence results in large measure from the relationship between the frictional stress and the sliding velocity. This relaxation model may be applicable to the fault creep following an earthquake, but this is less certain in the case of aftershocks. Microfracturing studies, such as that of Scholz (1968), may shed light on this problem. It is interesting to note, however, that Benioff (1951; 1955) found

a marked change in activity following a certain amount of logarithmic relaxation. This change is similar to that observed in the high temperature relaxation runs described here, although in neither case is there any understanding of why the change occurs.

#### CONCLUSIONS

The frictional strength of faults in granite, gabbro, and peridotite during stable sliding is time dependent. The stress for steady-state sliding increases with increasing rate, the rate sensitivity being greater at higher temperature and higher pressure. At temperatures between 200° to 700°C, pressures between 2 and 4 kbars, and sliding rates between  $10^{-5}$  and  $10^{-2}$  cm/sec, the rate sensitivity is low, lower than that for brittle fracture at room temperature. A striking characteristic of stable sliding is that the shear stress can be separated into two parts: a steady-state component dependent only on temperature, pressure and sliding rate, and a component dependent on displacement and history. The latter includes irreversible changes in sliding stress resulting from sliding at different temperatures and pressures, as well as transient changes in frictional strength prior to establishing steady-state. The time dependence of frictional sliding can explain some observations of stick-slip, episodic fault creep, and displacement changes following many large earthquakes.

## REFERENCES

- Benioff, H., 1951. Earthquakes and Rock Creep. I. Creep characteristics of rocks and the origin of aftershocks. *Seismic Soc. Am. Bull.*, 41: 31.
- Benioff, H., 1955. Seismic evidence for crustal structure and tectonic activity. In: Crust of the Earth, Geol. Soc. Am., Spec. Paper, 62: 61-74.
- Brace, W.F. and Byerlee, J.D., 1970. California earthquakes: Why only shallow focus? *Science*, 168: 1573.
- Brace, W.F. and Jones, A.H., 1971. Comparison of uniaxial deformation in shock and static loading of three rocks. *J. Geophys. Res.*, 76: 4913.
- Breiner, S. and Kovach, R.L., 1968. Search for piezomagnetic effects on the San Andreas fault. In: *Proc. Conf. Geologic Problems of San Andreas Fault System*, W.R. Dickinson and A. Grantz (Editors), Stanford Univ. Publ., Vol. II, Stanford, Calif.: 111-116.
- Burford, R.O., Allen, S.S., Lamson, R.J. and Goodreau, D.D., 1973. Accelerated fault creep along the San Andreas fault after moderate earthquakes during 1971-1973. In: *Proc. Conf. on Tectonic Problems of the San Andreas Fault System*, R.L. Kovach and A. Nur (Editors), Stanford Univ. Publ., Vol. XIII, Stanford, Calif.: 268-274.
- Byerlee, J.D. and Brace, W.F., 1968. Stick-slip, stable sliding, and earthquakes--effect of rock type, pressure, strain rate, and stiffness. *J. Geophys. Res.*, 73: 6031.
- Christensen, R.J., Swanson, S.R., and Brown, W.S., 1973. Torsional shear measurements of the frictional properties of Westerly granite. Final Rept., Contract No. DNA001-72-C-0026, Defense Nuclear Agency, Washington, D.C.

- Coulson, J.H., 1970. The effects of surface roughness on the shear strength of joints in rock. Tech. Rept. MRD-2-70, Missouri River Div., Corps of Engineers, Omaha, Neb., 283 pp.
- DeFazio, T.L., Aki, K. and Alba, J., 1973. Solid earth tide and observed change in the in situ seismic velocity. J. Geophys. Res., 78(8): 1319-1322.
- Dieterich, J.H., 1972. Time-dependent friction in rocks. J. Geophys. Res., 77(20): 3690-3697.
- Donath, F.A. and Fruth, L.S., Jr., 1971. Dependence of strain-rate effects on deformation mechanism and rock type. J. Geol., 79: 347-371.
- Donath, F.A., Fruth, L.S., Jr., and Olsson, W.A., 1972. Experimental study of frictional properties of faults. In: New Horizons in Rock Mechanics, 14th Symposium on Rock Mech., University Park, Penn., June 11-14, 1972: 189-222.
- Eaton, J.P., O'Neill, M.E. and Murdock, J.N., 1970. Aftershocks of the 1966 Parkfield-Cholame, California, earthquake: a detailed study. Seism. Soc. Am. Bull., 60: 1151-1197.
- Engelder, J.T., 1973. Quartz fault-gouge: its generation and effect on the frictional properties of sandstone. Ph.D. Dissert., Texas A&M Univ., College Station, Tex., 153 pp.
- Goodman, R.E., 1973. Pore pressure in intact and jointed rocks induced by deformation. Int. Coll. Seism. Effects of Reservoir Impounding, Roy. Soc. Lond., March 1973 (abstract).
- Goodman, R.E. and Ohnishi, Y., 1973. Undrained shear testing of jointed rock. Rock Mech., 5(3): 129-149.

- Handin, J., Friedman, M., Logan, J., Sowers, G.M. and Stearns, D.W., 1972. Mechanical properties of rocks affecting earthquake generation. Ann. Prog. Rept. No. 1, ARPA Contract No. 14-08-0001-12723, Off. Earthquake Res., U.S. Geol. Surv., Menlo Park, Calif., 147 pp.
- Healy, K.A., 1963. The dependence of dilation in sand on rate of shear strain. Sc.D. Thesis, Mass. Inst. of Technol., Civil Eng., Cambridge, Mass.
- Heard, H.C., 1972. Steady-state flow in polycrystalline halite at pressure of 2 kilobars. In: Flow and Fracture of Rocks, Am. Geophys. Union, Monograph 16, Washington, D.C.: 191-210.
- Heard, H.C. and Carter, N.L., 1968. Experimentally induced 'natural' intragranular flow in quartz and quartzite. Am. J. Sci., 266: 1-42.
- Heard, H.C. and Raleigh, C.B., 1972. Steady state flow in marble at 500° to 800°C. Geol. Soc. Am. Bull., 83: 935-956.
- Jaeger, J.C. and Cook, N.G.W., 1970. Friction in granular materials. Proc. Int. Conf. Struct. and Solid Mech. Civ. Eng., Southampton, U.K., Paper 20: 257-266.
- Johnson, A.G., Kovach, R.L., and Nur. A., 1973. Pore pressure changes during creep events on the San Andreas fault. J. Geophys. Res., 78(5): 851-857.
- Johnston, M.J.S., Smith, B.E., Johnston, J.R., and Williams, F.J., 1973. A search for tectonomagnetic effects in California and Western Nevada. In: Proc. Conf. Tectonic Problems of the San Andreas Fault System, R.L. Kovach and A. Nur (Editors), Stanford Univ. Publ., Vol. XIII, Stanford, Calif.: 225-238.
- King, C.Y., Nason, R.D. and Tocher, D., 1973. Kinematics of fault creep. Phil. Trans. Roy. Soc. Lond., A, 274: 355-360.

- Kohlstedt, D.L. and Goetze, C., 1974. Low-stress high-temperature creep in olivine single crystals. *J. Geophys. Res.*, 79(4): 2045-2052.
- Martin, R.J., III, 1972. Time-dependent crack growth in quartz and its application to creep of rocks. *J. Geophys. Res.*, 77(8): 1406-1419.
- Nason, R.D., 1971. Measurement and theory of fault creep slippage in central California. In: Recent Crustal Movements, Roy. Soc. of New Zealand, Bull., 9: 181-187.
- Nason, R. and Weertman, J., 1973. A dislocation theory analysis of fault creep events. *J. Geophys. Res.*, 78: 7745-7751.
- Olsson, W.A., 1974. Effects of temperature, pressure and displacement rate on the frictional characteristics of a limestone. *Int. J. Rock Mech. Min. Sci.*, 11: 267-278.
- Rae, D., Danson, R. and Heathcote, N.L., 1966. The coefficient of friction of some rocks and other high-melting-point materials during continuous rubbing. Safety in Mines Res. Establishment, Res. Rept. No. 237: 17 pp.
- Scholz, C.H., 1968. Microfractures, aftershocks, and seismicity. *Seism. Soc. Am. Bull.*, 58: 1117-1130.
- Scholz, C.H., Molnar, P. and Johnson, T., 1972. Detailed studies of frictional sliding of granite and implications for the earthquake mechanism. *J. Geophys. Res.*, 77(32): 6392-6406.
- Scholz, C.H., Wyss, M. and Smith, S.W., 1969. Seismic and aseismic slip on the San Andreas fault. *J. Geophys. Res.*, 74: 2049-2069.
- Smith, S.W. and Wyss, M., 1968. Displacement on the San Andreas Fault subsequent to the 1966 Parkfield earthquake. *Seism. Soc. Am. Bull.*, 58: 1955-1973.

- Stesky, R.M., Brace, W.F., Riley, D.K. and Robin, P.-Y.F., 1974. Friction in faulted rock at high temperature and pressure. *Tectonophys.*, 23(1/2): 177-203.
- Taylor, D.W., 1948. Fundamentals of Soil Mechanics. J. Wiley & Sons, New York, N.Y., 700 pp.
- Utsu, T., 1961. A statistical study on the occurrence of aftershocks. *Geophys. Mag.*, 30: 521-

## FIGURE CAPTIONS

- Figure 1. Variation of shear stress,  $\tau$ , with boundary displacement,  $\delta_a$ , during a rate experiment. The steps correspond to changes in boundary displacement rate.  $\Delta\tau_s$  is the change in steady-state sliding stress due to a change in sliding rate,  $\dot{\delta}$ .  $\Delta\tau_p$  is the stress change for a stress-peak (A). A comparable stress change is measured for a stress-trough (B).
- Figure 2. Effect of sliding rate,  $\dot{\delta}$ , on the steady-state shear stress,  $\tau_s$ , of granite at different temperatures.  $\Delta\tau_s$  is plotted relative to the value at  $\dot{\delta} = 10^{-4}$  cm/sec. The vertical bar indicates the measurement uncertainty.
- Figure 3. Effect of sliding rate,  $\dot{\delta}$ , on the steady-state shear stress,  $\tau_s$ , of gabbro at different temperatures.  $\Delta\tau_s$  is plotted relative to the value at  $\dot{\delta} = 10^{-4}$  cm/sec. The vertical bar indicates the measurement uncertainty.
- Figure 4. Variation of rate sensitivity of the steady-state sliding stress with temperature. These values are the slopes of the lines of Figures 2 and 3. Estimated error is indicated by the vertical bars, which apply to both rocks.
- Figure 5. Variation of rate sensitivity of the stress-peak and -trough with temperature. The values are calculated in a manner similar to those of Figure 4. Estimated error is indicated by the vertical bars which apply to both rocks.
- Figure 6. The decrease in sliding stress,  $\tau_R$ , with log time,  $t$ , with the boundary displacement held constant (a relaxation experiment). The stresses were measured relative to the initial stress at  $t = 0$ . The solid lines were calculated from Equation (3a).

- Figure 7. The change in fault displacement,  $\delta$ , with log time,  $t$ , calculated from the data of Figure 6 and the measured slope of the elastic portion of the stress-shortening curves. The solid curves were calculated from Equation (3b).
- Figure 8. A typical holding experiment in which the shear stress,  $\tau$ , is held at a reduced level for some time.  $\Delta\tau_H$  is the stress peak produced upon reloading the sample. Note that during holding the fault continued sliding, relaxing the shear stress and producing the short vertical segments of the curves.
- Figure 9. Variation in holding-peak stress,  $\Delta\tau_H$ , with time. Vertical bars denote measurement uncertainty.
- Figure 10. Variation of sliding stress,  $\Delta\tau_R$ , relative to the initial stress, with sliding rate,  $\dot{\delta}$ , during relaxation experiments. These values are calculated from the data of Figures 6 and 7.

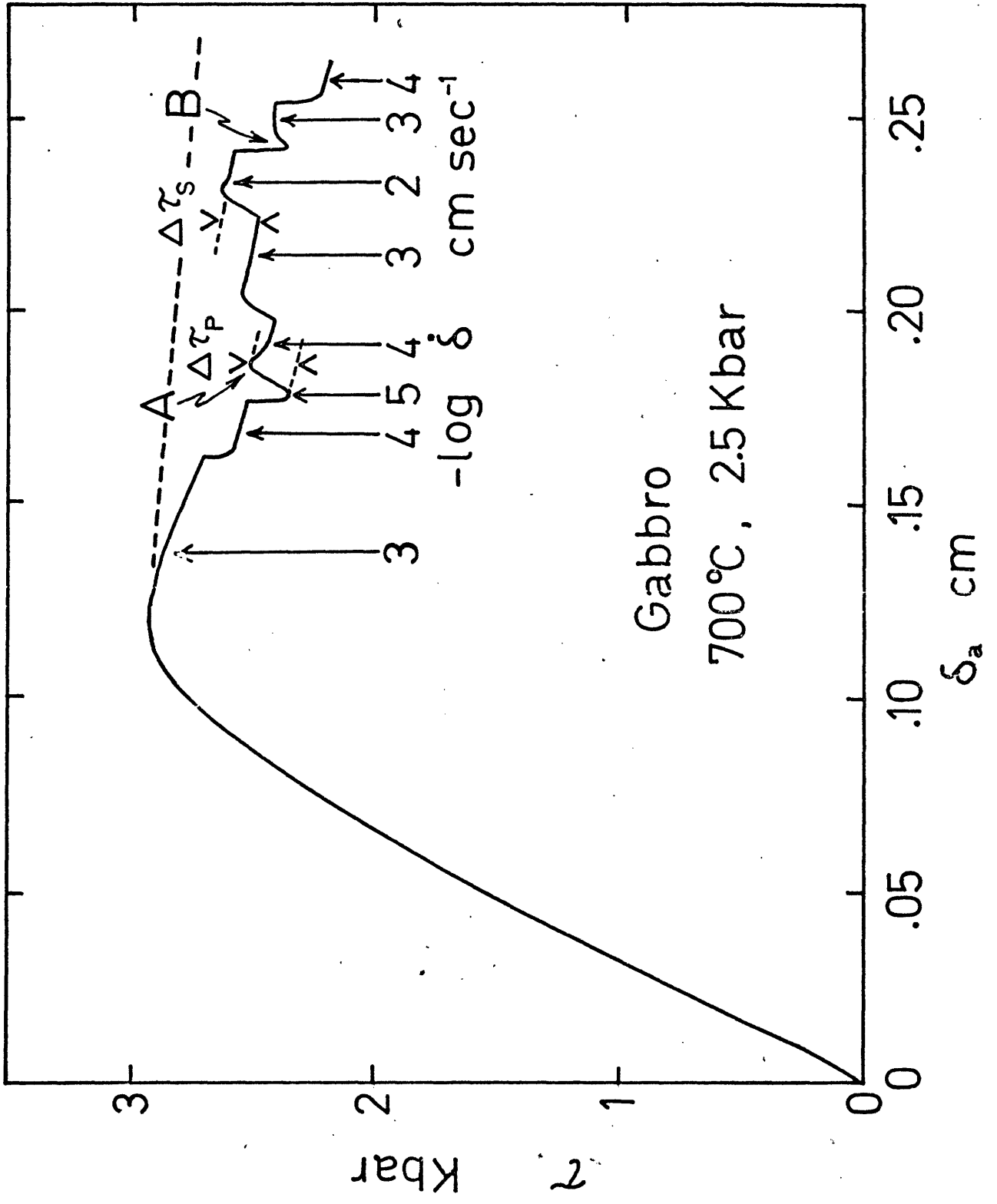


Fig 1

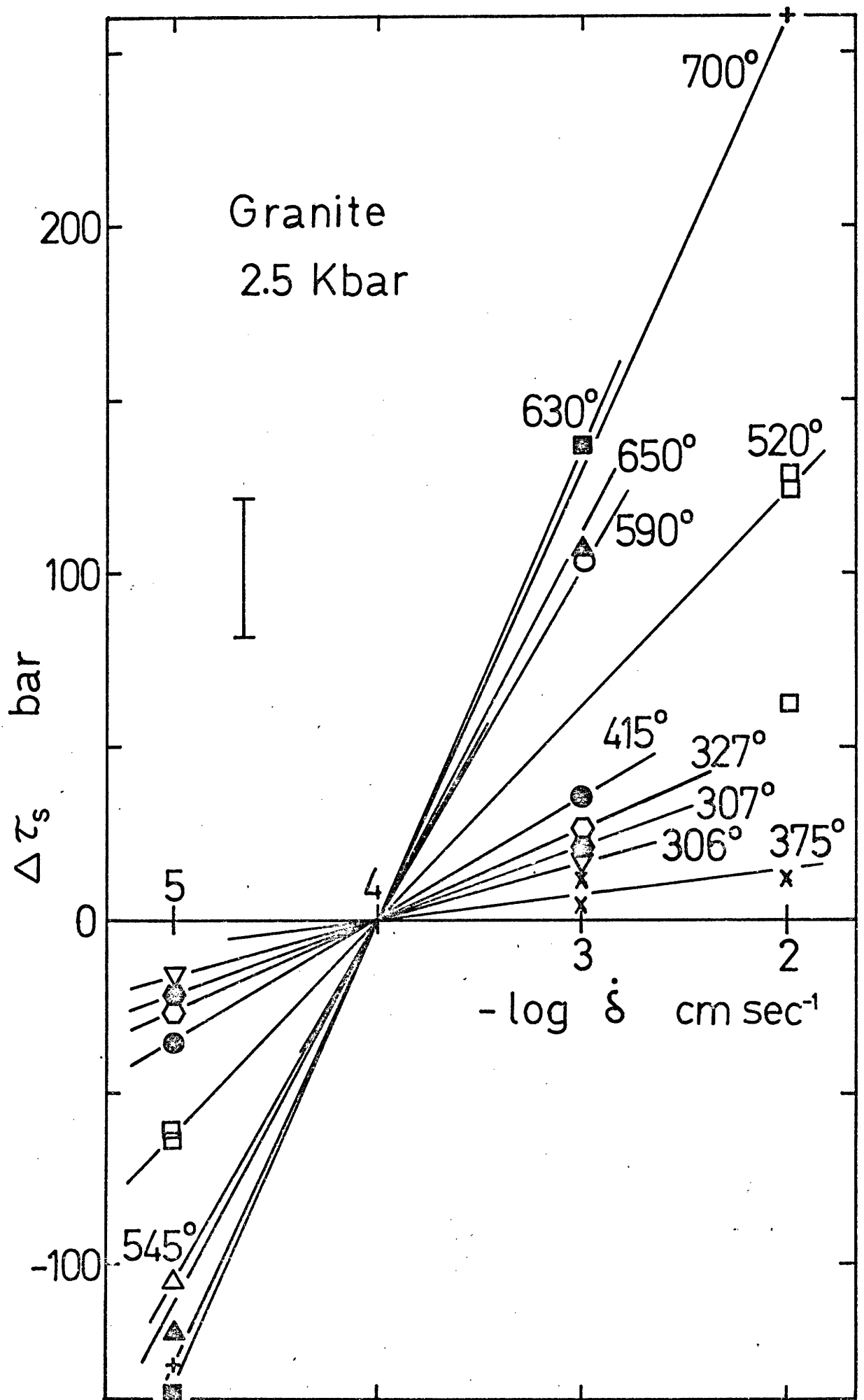


Fig. 2

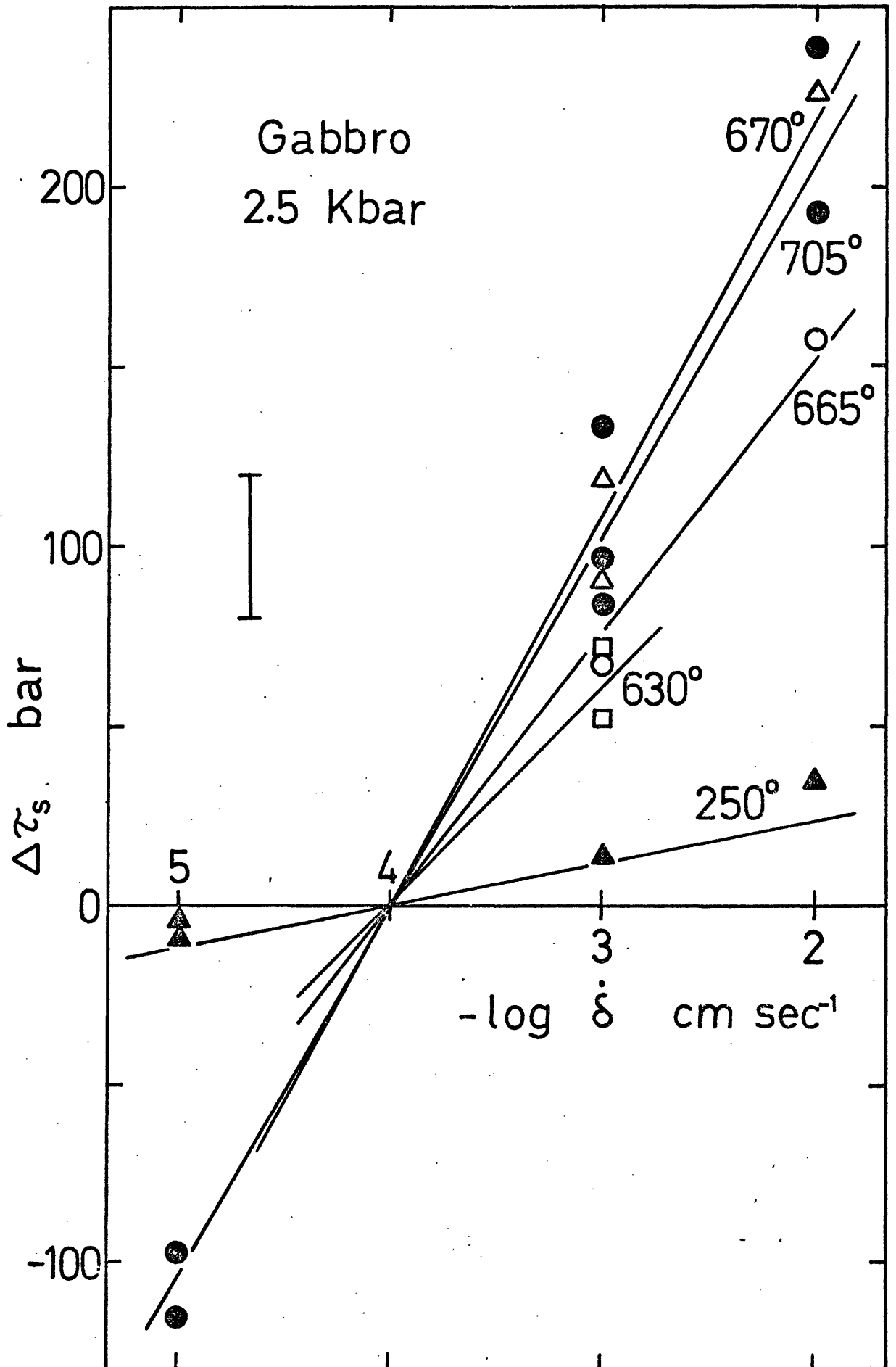


FIG 3

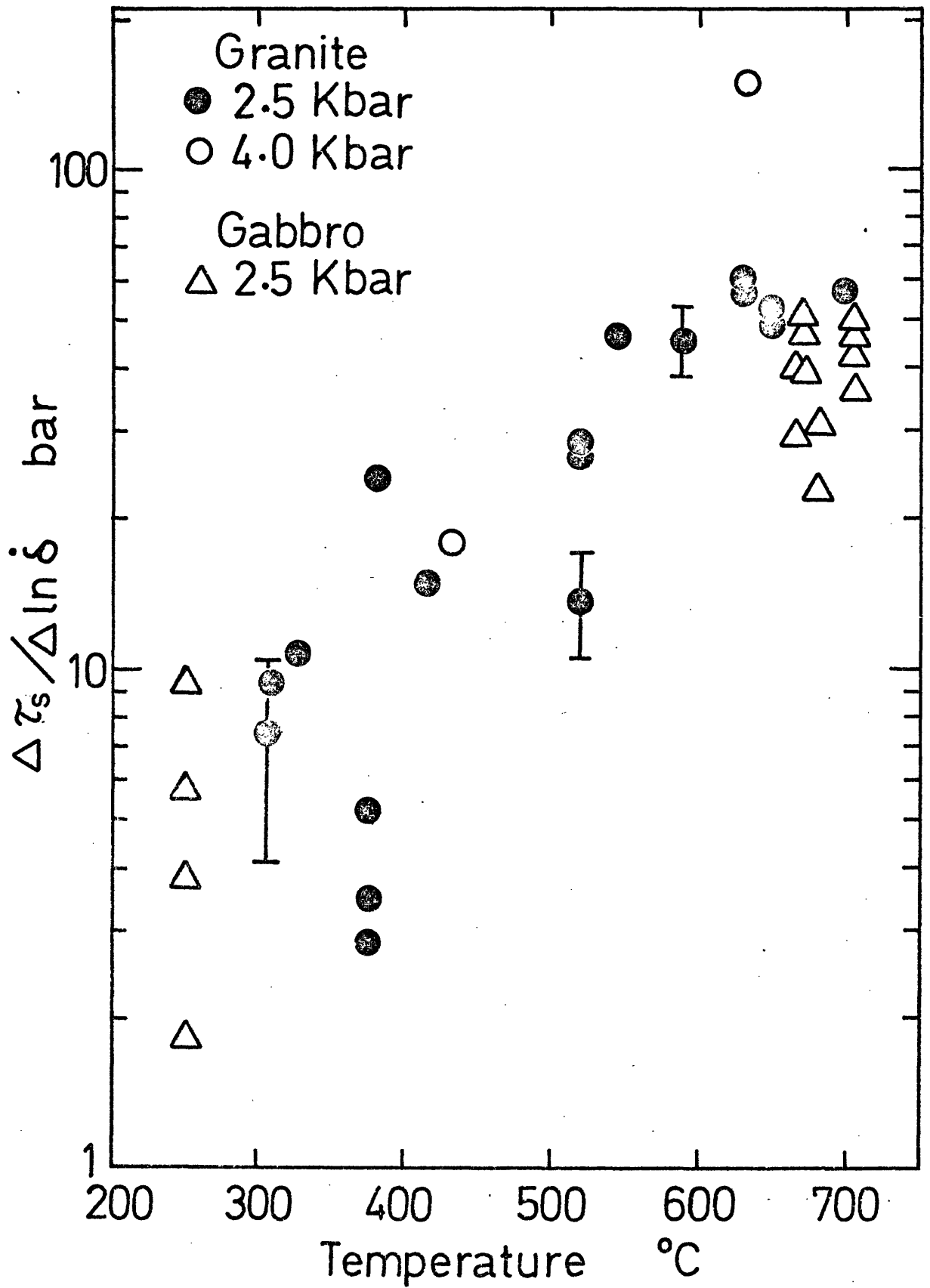


FIG 4

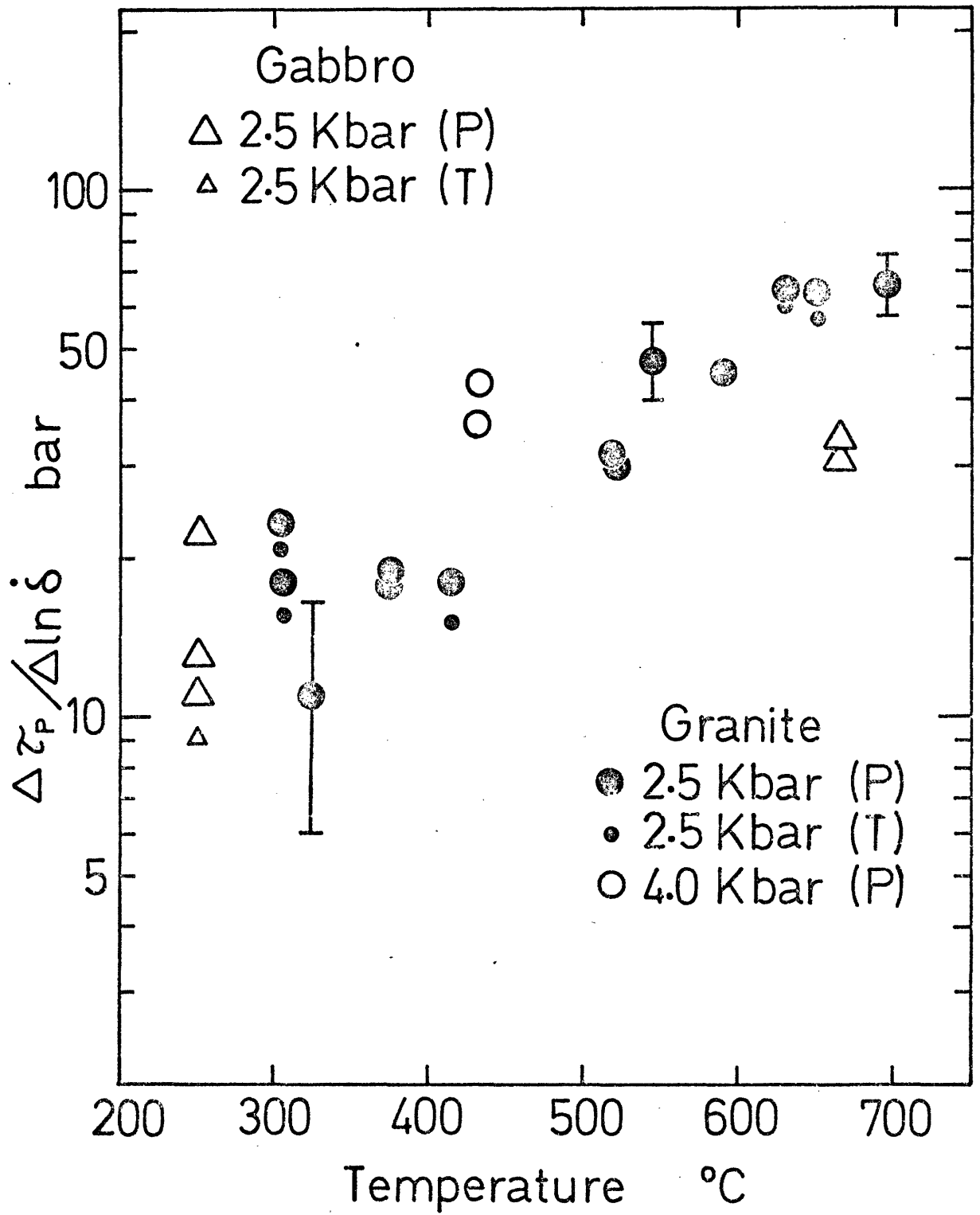


FIG 5

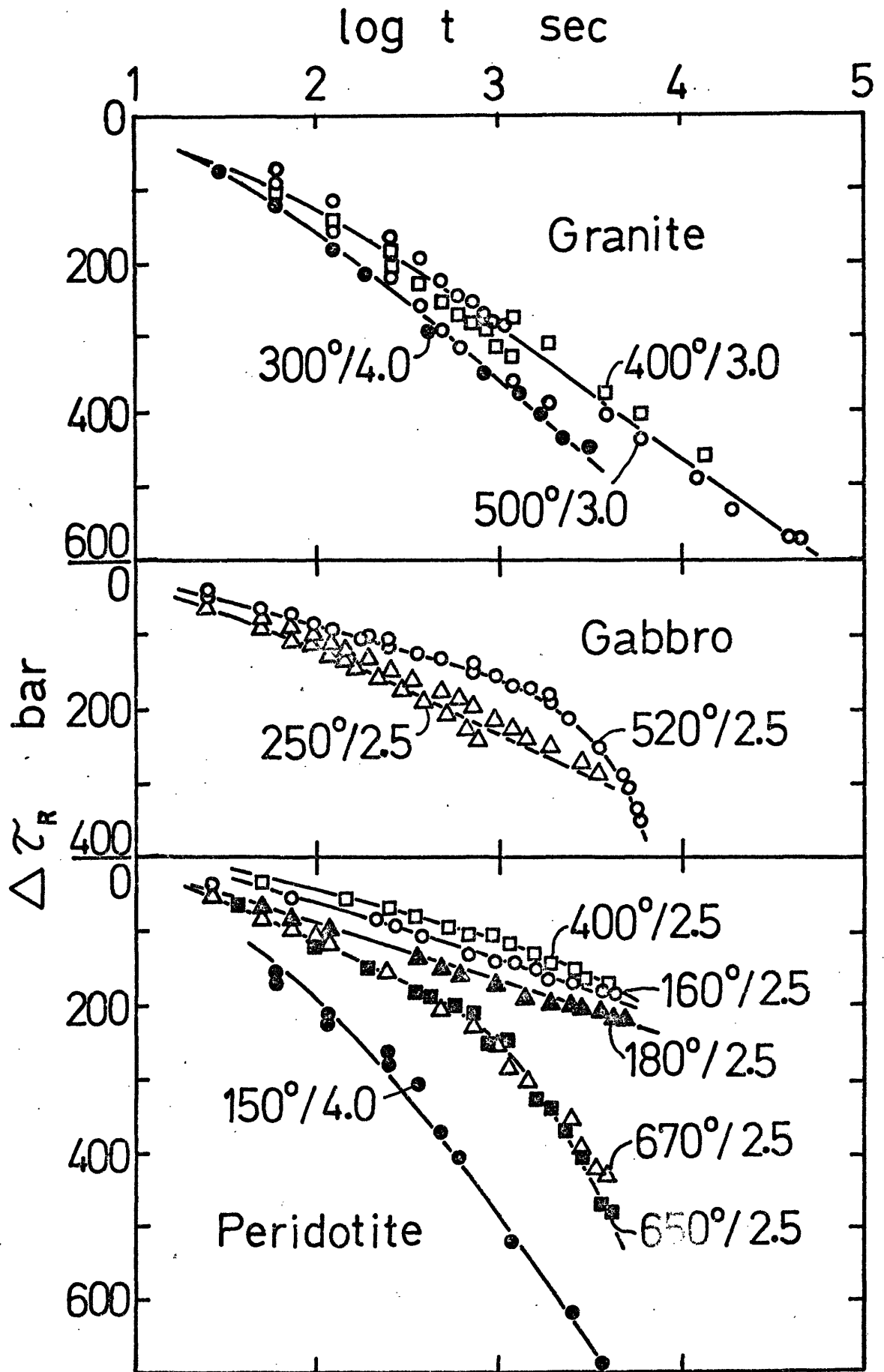


FIG 6

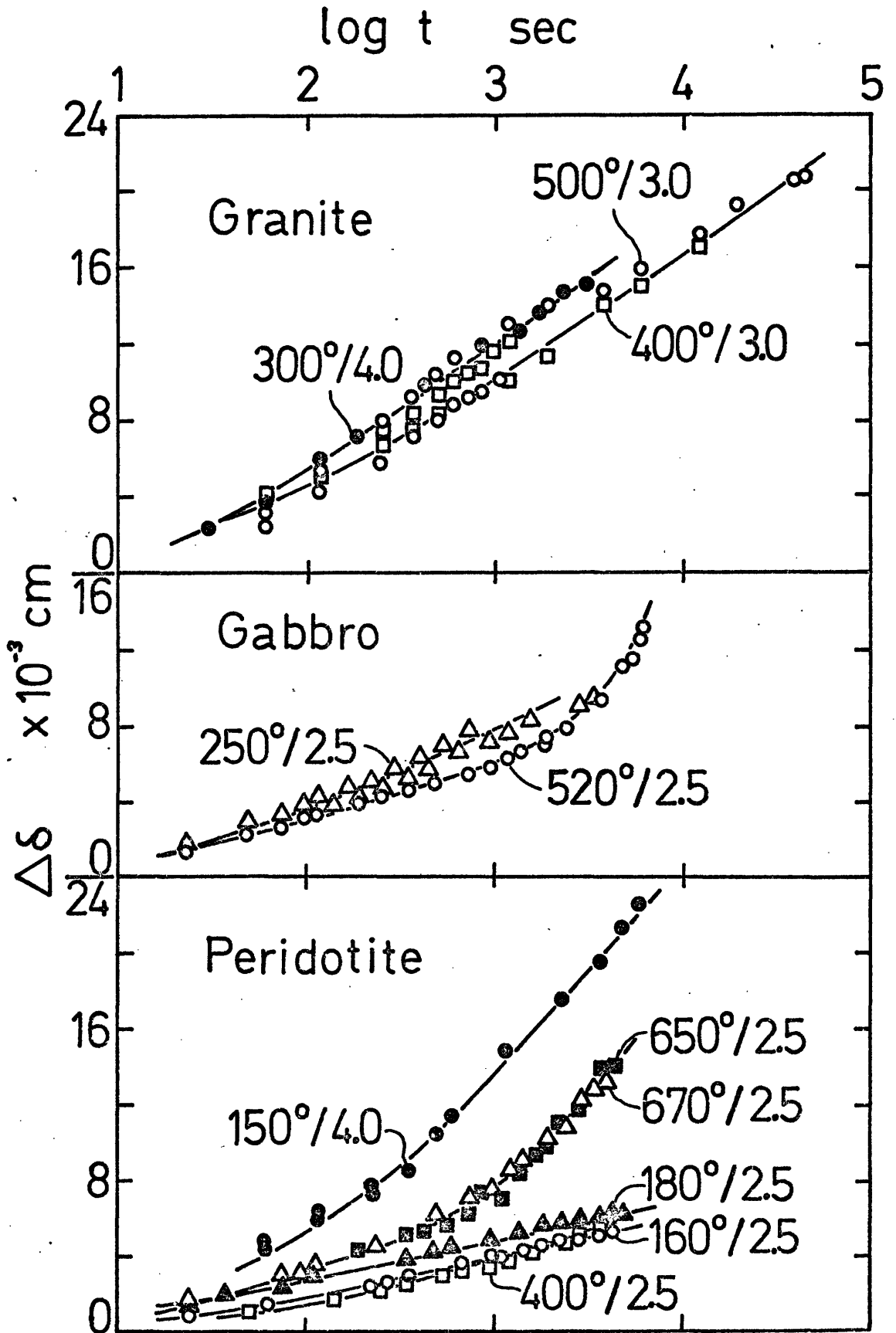


FIG 7

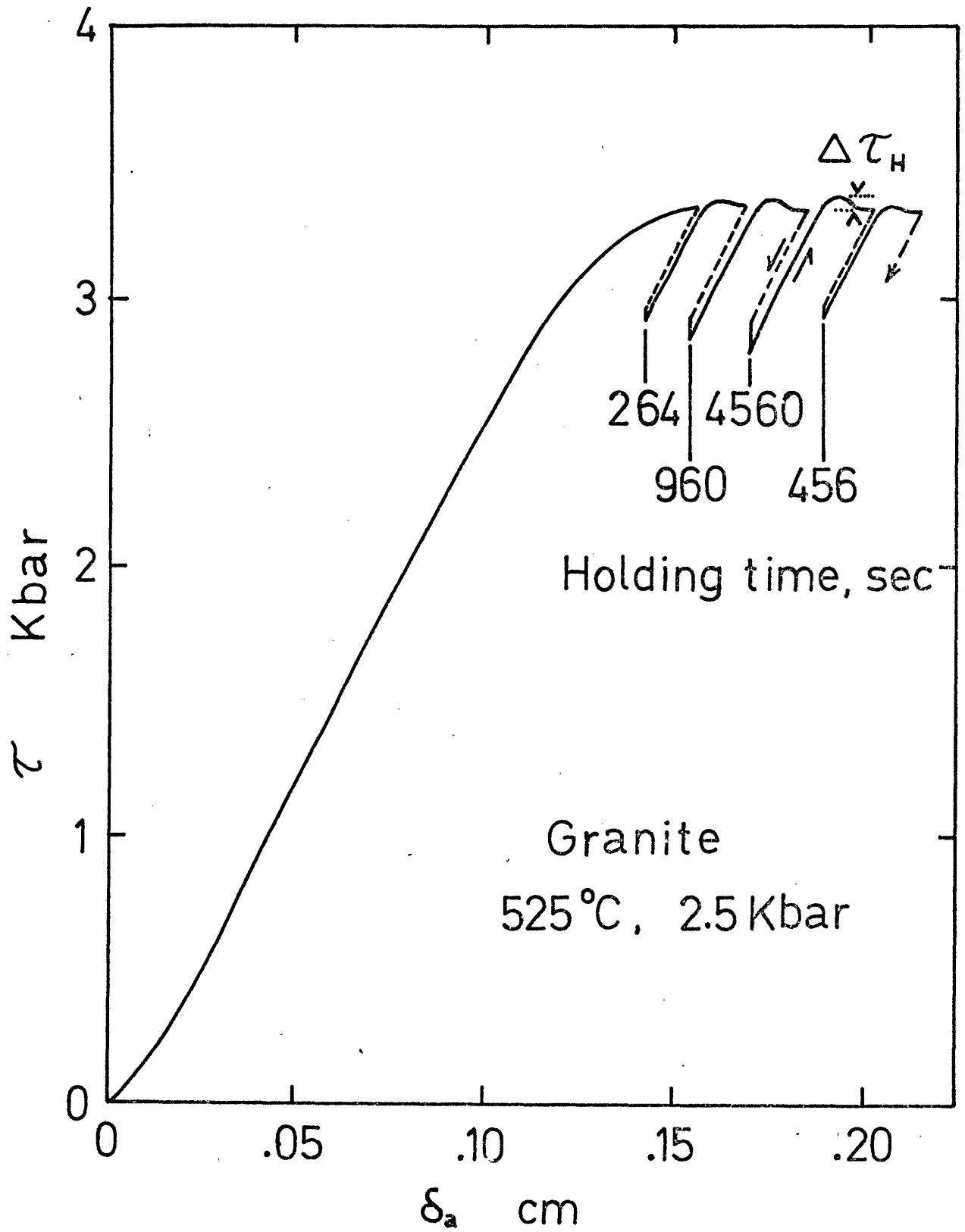


FIG 8

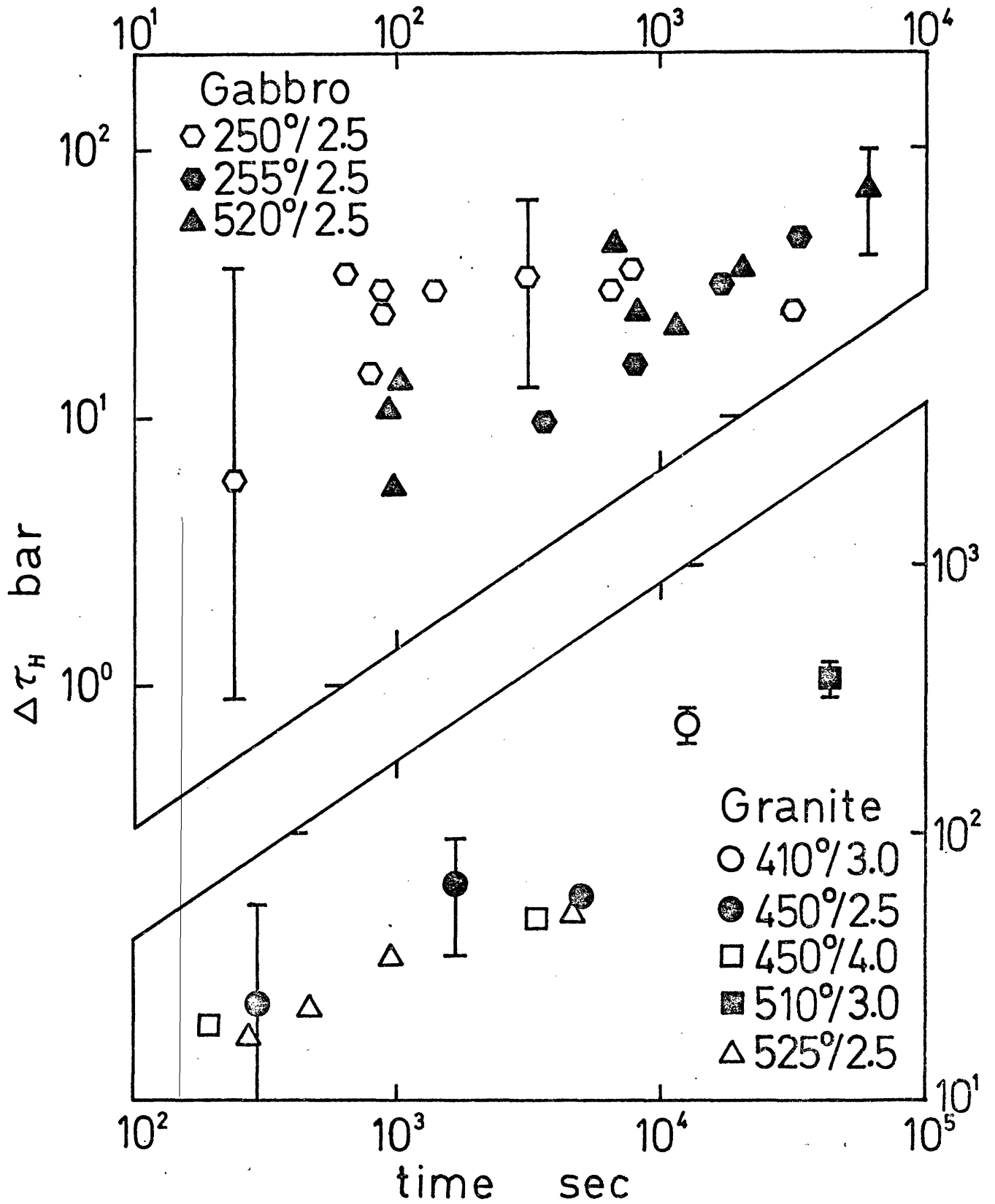
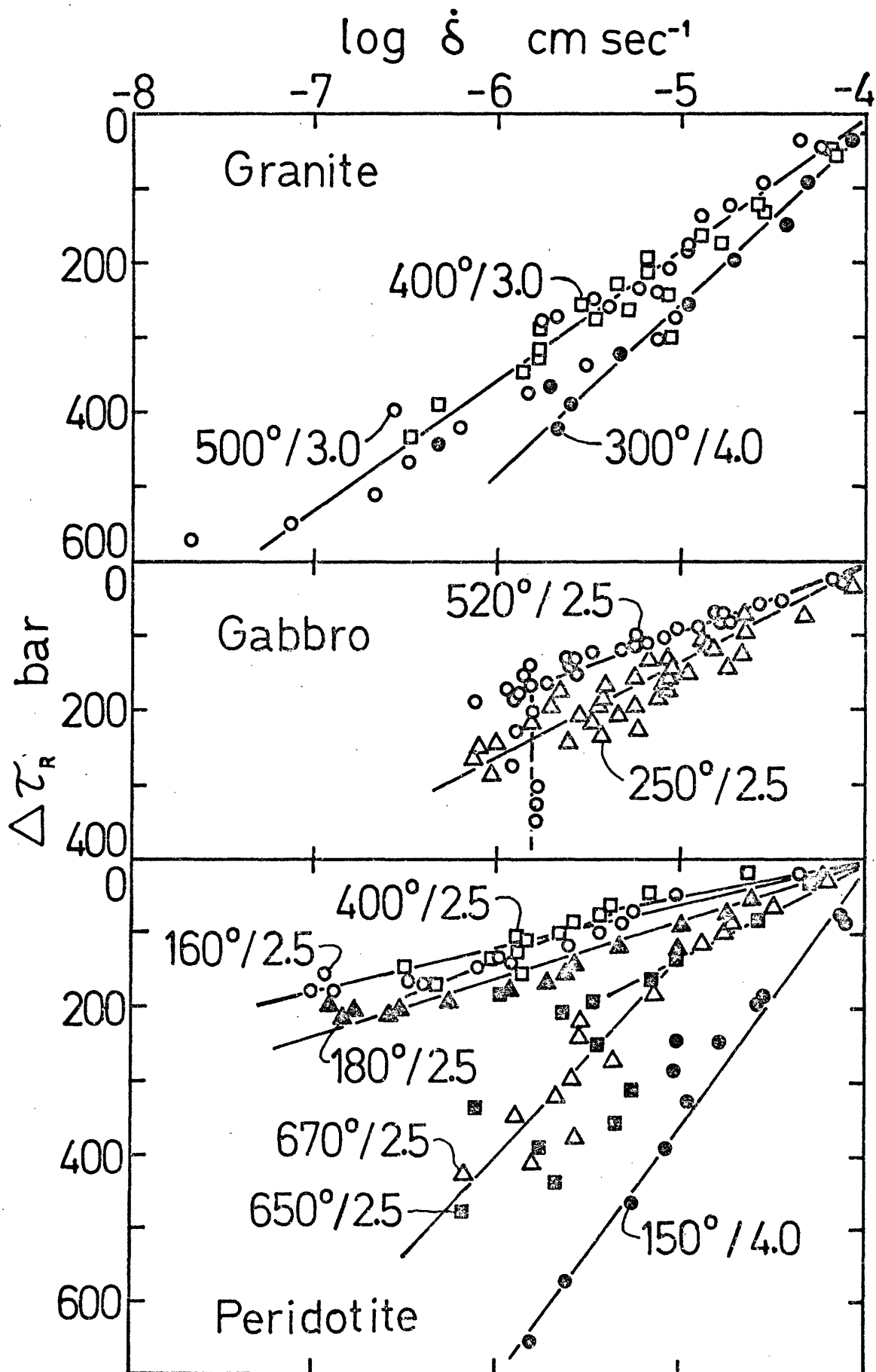


FIG 9



## CHAPTER III

### ACOUSTIC EMISSION DURING HIGH-TEMPERATURE FRICTIONAL SLIDING

#### ABSTRACT

Acoustic emissions during high temperature frictional sliding in faulted granite were detected with a piezoelectric transducer placed outside the furnace and pressure vessel. Suitable choice of materials allowed the transmission of signals sufficiently large for measurement and analysis. Acoustic emissions were also monitored during the fracture runs at room temperature and could be compared with earlier studies. As observed previously, the emission rate increased dramatically prior to failure and the Ishimoto-Iida relationship between emission amplitude,  $A$ , and number of emissions,  $N(A)$ , of amplitude,  $A$ , i.e.,  $\log N(A) = K' - (b+1) \log A$ , was followed. The constant,  $b$ , was typically about 1.4, higher than the value of 1 or less indicated by previous experimental and theoretical studies.

Acoustic emissions were detected during frictional sliding at all temperatures from 25° to 700°C. The activity began at low stresses and accelerated as the stress increased. During sliding the emission rate was nearly constant (with large counts during stick-slip events) at a level which decreased with increasing temperature. This apparent decrease may be explained by a real decrease in the number of emissions or by an increase in attenuation at higher temperatures.

The power-law relationship between amplitude and emission rate seemed to hold for sliding as for fracture. High b-values, between 1.2 and 2.1, are in agreement with earlier studies and are little affected by temperature within the scatter of the measurements. Where the number of emissions allowed its measurement, the b-value of emissions during loading prior to slip was consistently, although only slightly, higher than that during steady sliding.

### 1. Introduction

Acoustic emission during rock deformation has been the subject of much research. It is based on the idea that microfracturing and crack propagation produce elastic wave pulses which are somewhat characteristic of the deformation process. Study of these pulses has led to a further understanding of tensile and shear fracturing, dilatancy, and creep of brittle rocks [1]. However, application of the technique to rock friction is sparse and to friction at high temperature, non-existent.

SCHOLZ [2,3] examined acoustic emissions occurring prior to stick-slip sliding in granite, but limited his study to sawcut samples at room temperature. He found that the level of activity was not reproducible between stick-slip cycles, although it began relatively abruptly during loading and stayed nearly constant as load increased until the sudden stress drop. There was no apparent increase in emission rate prior to sudden slip. The b-values were determined from the relationship of amplitude to emission rate [3],  $N(A) = KA^{-(b+1)}$ , where  $N(A)$  is the number of emissions having peak amplitude  $A$ , and  $K$  and  $b$  are constants.  $b$  is typically greater than 1.0 for frictional sliding, rather than the values of less than 1.0 characteristic of brittle fracture. This result implies that the proportion of small to large events is greater during frictional

sliding than during fracture. BYERLEE and PESELNICK [4] recorded acoustic emissions during sliding of cut glass surfaces at room temperature. They were unable to discern the details of the sliding process, but found that the cumulative results of six cycles of loading and unloading gave a b-value of about 0.9.

These studies represent pioneering work in acoustic emission during frictional sliding, but their results are difficult to apply to natural faults, principally for two reasons. The acoustic emission response from materials is apparently very structure-sensitive [5]; the emissions from clean sawcut surfaces may not have the same characteristics as those from gouge-filled faults, perhaps the more common type in the earth. Secondly, the temperatures at depth on natural faults may be considerably higher than in these room-temperature experiments. Do acoustic emissions occur at high temperature and do their characteristics change? In particular, are there differences in emission activity between low-temperature stick-slip and high-temperature stable sliding? To examine these and other questions I applied SCHOLZ'S techniques to high-temperature friction experiments. Two aspects of the emissions were studied: the emission rate, a measure of the intensity of the processes producing the emissions, and the b-value, that is, the relative proportion of large to small events.

## 2. Experimental Technique

The high-temperature friction apparatus is described elsewhere [6] and illustrated in Figure 1. Briefly, a rock cylinder, 3.5 cm long and 1.6 cm diameter, was placed in a thin graphite sleeve and inserted in an annealed copper foil jacket. Titanium carbide and polycrystalline alumina (Lucalox) were placed above and below the rock in the jacket. A furnace surrounded the jacket and the entire assembly was set inside a gas-medium pressure

vessel. The axial load was applied through a steel piston and measured with a strain-gauge load cell. Because the machine motor produced acoustic noise, the piston was advanced by hand at a nearly constant rate of about  $10^{-4}$  cm/sec, and its displacement was monitored with a time-chart recorder. The temperature was measured with a thermocouple placed at the base of the sample through a 1.6 mm diameter hole in the lower piston and spacers.

For acoustic emission work the problem lay in the location of the detecting transducer. The lack of room, the high temperatures, and the presence of the graphite sleeve prevented bonding the transducer to the side of the sample, as SCHOLZ [2] had done. A simple, yet effective, method of detecting the emissions is shown in Figure 1. A PZT-4 transducer (compressional mode, 1 MHz) was bonded to the steel piston within a cavity in the upper moving platen about 20 cm from the rock sample. Copper foil provided the electrodes, and a piece of thick rubber and a brass backing minimized back reflections. Throughout the experiment the transducer remained unloaded and at room temperature and pressure. The materials between the rock and the transducer were selected to maximize acoustic-impedance matching, with the additional constraints of high strength and suitable thermal properties [6]. Despite the mismatching that remained and despite the separation of rock and transducer, the acoustic emission signals were sufficiently strong for detection and analysis.

The electronics for the signal analysis was similar to that used by SCHOLZ [2]. The emission signal was amplified in three stages using two 40 db amplifiers and the trigger output of the monitoring oscilloscope. Between the first and second stage the signal was filtered to remove the low frequency noise picked up by capacitive coupling with the machine, a

major source of electrical noise. The high frequency noise could not be eliminated and limited the sensitivity of the measurements. The acoustic emission pulses, essentially decaying sinusoids, were rectified and shaped [2] and then fed into a multi-channel analyzer (TMC model 102). The analyzer was used in two ways: to count the number of pulses during successive time periods and to count the pulses having peaks within successive amplitude intervals. The latter method determines the b-values.

Since the transducer remained outside the furnace and pressure vessel, the entire range of pressures and temperatures could be used. This study, however, examined frictional sliding at two pressures, 1 and 2 kbars, and at temperatures from 25°C to 700°C. The procedure used, outlined in detail by SIESKY and others [6], was the following. A fault was first formed by fracturing the rock at 500 bars and 25°C. The pressure and temperature were then raised to the desired conditions and the faulted rock loaded until sliding occurred. Rather than have the sliding continue at constant pressure and temperature to examine the effect of displacement, the temperature of sliding with each sample was varied to observe the effect of temperature on acoustic activity, the object of this study. Thus sliding at each set of conditions was continued only until a reasonable estimate of its emission activity could be made. At this point the load was removed, the temperature changed, and the rock reloaded until sliding again occurred. In this way, several measurements could be made with one sample, thus minimizing the effect of fault variability. For clarity, each measurement will be called here a run and all measurements for one sample, an experiment.

Westerly granite was used in all experiments reported here. Many of the acoustic emission and frictional properties of this rock have been

previously studied [2,3,6,7,9,17] and its physical characteristics are described elsewhere [2,6].

### 3. Observations During Fracture

The acoustic emissions during fracture at 500 bars, 25°C, were monitored as a check on the technique. SCHOLZ [2] observed that during the fracture of brittle rocks at low pressures, two regions of activity occurred: at the low stress region during initial loading where cracks were closed and at stresses greater than half the fracture strength where new cracks were being formed. As the stress approached the fracture strength, the emission rate increased dramatically until fracture. Figure 2 illustrates the emission rates observed during two typical fracture runs in the present study. The pattern of activity is very similar to that found by SCHOLZ. However, the sensitivity of the apparatus for pulse-height analysis was at least an order of magnitude less than in SCHOLZ'S [3] experiments, judging from the b-value plots. The number of events detected was lower than SCHOLZ found and, except at stresses greater than half the fracture strength, was insufficient for adequate b-value calculation. At stresses above half the fracture strength, all the emissions occurring until just prior to fracture were analyzed together, and thus the stress-dependence of the b-value was not determined.

The results of two fracture runs are shown in Figure 3. Here we plot the number of events against the maximum trace amplitude on logarithmic coordinates. The low amplitude range is limited by the ambient noise level. As expected, the measurements follow a power-law relationship and the fall-off in counts at high amplitudes as observed by SCHOLZ [3] is seen here. However, the slope,  $1/m$ , of the lines in Figure 3, or equivalently the b-value, defined as  $b = m - 1$ , is consistently higher than in SCHOLZ'S study.

The b-values of four runs ranged from 1.3 to 1.7. SCHOLZ'S [3] results suggest that for a rock stressed homogeneously (on a macroscopic scale) the b-value should be less than 1.0 and should decrease as the stress level is increased.

The reason for the high b-values in these runs is not known. SCHOLZ [3] suggested that an inhomogeneous stress field could produce b-values greater than 1.0. Some stress inhomogeneity was present in our samples. The hole in the end pieces adjacent to the rock likely induced variations in local stress in the region of the rock near the hole. However, whether this anomalous region, representing less than 25% of the total volume of the rock, was sufficient to affect the b-values is not known.

#### 4. Observations During Frictional Sliding

Acoustic emission measurements were made at two pressures, one experiment at 1 kbar and several at 2 kbar. The low-pressure emission rates are shown in Figure 4, along with the stress-shortening curves. Apparently, the acoustic emission response depends considerably on the details of the process, as well as the temperature of sliding. Initially, at 25°C the emission rate was high, with occasional large counts corresponding to small stick-slips. With displacement, however, the emission rate fell off. At this point the run was stopped and the temperature increased to 225°C. During sliding at this temperature no emissions were detected above the background noise level. The emission rate was slightly higher at 115°C and large counts were detected at two conspicuous small stress-drops. Finally, repeating the room temperature measurement showed that the emission rate was markedly lower than in the first run and that

stick-slip did not occur. The emission rate increased with displacement almost to the level at the end of the first run. Unfortunately the experiment was stopped at that point and we do not know whether the increase in emissions was premonitory to a stick-slip event.

Two points are clear from this experiment. The acoustic emission response during frictional sliding at 1 kbar was complex. In general, however, the emission rate was lower during stable sliding and fell off to negligible values at 200°C. To test whether, indeed, acoustic emissions do not occur during high temperature stable sliding or whether the sensitivity of the detecting system was too low, we ran the sliding experiments at 2 kbars. At the higher pressure the local stresses on the fault would be higher and more energy would be available for the emissions.

Figure 5 shows the results of one experiment at 2 kbars. In each run the emission activity began at fairly low stresses and accelerated as the stress increased. Once steady sliding at constant stress began, the emission rate became nearly constant, a behavior similar to that observed during the cataclastic deformation of marble [2]. Again, as in the 1 kbar experiment, we see a high emission rate at low temperatures (with large counts during stick-slips) and a decrease in activity with successively higher temperatures. In this case, however, the temperatures ranged upwards from 235°C, the lowest temperature used at 2 kbars. Clearly, emissions do occur at high temperature and during stable sliding.

Figure 6 summarizes the results of several experiments. Here the range of emissions rate during steady sliding at different temperatures are plotted, neglecting the high counts measured during stick-slip events. While there may be some influence of fault geometry and of displacement (as in figure 4), the over-all trend is a decrease in emission rate with

increasing temperature. Even at the highest temperature (660°C) emissions were detected above the background noise level.

To test whether the characteristics of the emissions changed with temperature, the relation between amplitude and emission rate during sliding was studied. In many cases, sufficient emissions were produced prior to reaching steady sliding to examine the pre-sliding behavior, although the detailed effect of stress on b-value could not be discerned. Figure 7 shows the measurements for one experiment, plotted as in figure 3. As for fracturing, a power-law relationship between amplitude and count-frequency seems to hold. The b-values, calculated from the slope, seem to be higher than those for fracture.

The results of several experiments are shown in figure 8. Measurements were not made below 300°C because of the unpredictability of the stick-slip events and the influence of machine vibration during the stress drops. For example, note the low b-value obtained in a 370°C run where a large stress drop occurred due to jacket failure. Acoustically, stick-slip consisted of a large-amplitude burst of emissions with a total ring-down time (several milliseconds) larger than the dead-time between counts (40 to 100  $\mu$ seconds). At the highest temperatures, the low emission rate prevented separation of pre-sliding and sliding events and all are counted together. Also included in this plot are measurements made prior to stick-slip on sawcut samples at 2 kbar and 25°C [3].

Several features are evident in figure 8. The b-values are high and in general agreement with SCHOLZ'S measurements. There seems to be no overall change in b-value with temperature within the scatter of the measurements, although there is a weak suggestion, from individual experiments, of an increase in b with temperature. Lastly, the emissions during

initial loading seem to show a small but consistently higher b-value than do those during steady sliding.

### 5. Discussion

Our understanding of the physical mechanisms during high-temperature frictional sliding is meager. BRACE and BYERLEE [7] and, more recently, STESKY and others [6] showed that for all rocks studied the sliding was stable at high temperature. Can the transition from stick-slip to stable sliding at high temperature be attributed to the onset of plastic deformation or, indeed, local melting on the fault surface? At low temperature it is reasonable to assume that most of the emissions in Westerly granite resulted from the brittle cracking of asperities and gouge particles. Such brittle cracking seems to occur even up to 700°C at 2 kbar, as evidenced by the similarity of b-values. That plastic deformation may also have occurred cannot be ruled out. Indeed, BOLAND and HOBBS [8] showed evidence of concurrent fracturing and plastic deformation during high temperature creep of peridotite. Also, acoustic emissions have been observed during the plastic deformation of metals [5]. SCHOLZ [2] similarly observed emissions during the plastic deformation of marble at high confining pressure, although only during yielding and with amplitudes much lower than emissions produced by brittle processes. It seems unlikely that such plastic deformation can account for the emissions found in this study.

The variation of acoustic activity with style of sliding seems to depend on pressure. At 1 kbar stick-slip produced a large number of emissions, while there was almost no activity during stable sliding. That this difference cannot be entirely due to temperature can be seen by comparing the two 25°C runs (Figure 4). In contrast, at 2 kbar there was little difference in activity (neglecting the high counts during stress drops) between stick-slip and stable sliding other than that due to differences in temperatures as in Figure 6.

This pressure dependence is puzzling and may be indicative of the mechanisms of gouge deformation. For example, grain crushing may be more significant at higher pressure, producing high emission rates even during stable sliding. At lower pressure, stable sliding may result more from grain rolling or sliding, mechanisms perhaps less conducive to acoustic activity.

The cause of the decrease in emission rate with temperature is not known. During loading of a faulted sample, the emission rate depended on the stress level. But for stable sliding the change in stress with temperature was fairly small (less than 10% between 250° and 650°C) and cannot explain the order of magnitude change in emission rate. Two possible explanations seem most likely: either the decrease in number of emissions is real or the attenuation of the stress waves increases with temperature. If the emissions reflect the occurrence of brittle cracking, then a decrease in the proportion of brittle to plastic deformation will produce a simultaneous decrease in acoustic emission rate. On the other hand, an increase in attenuation with temperature would cause the amplitude of the large number of small events to fall below the noise level so that these events would not be counted. Since all emissions would be attenuated by the same proportion, the b-value would not change with a change in attenuation. At present we cannot distinguish between these possibilities since we have little knowledge of the characteristics of brittle deformation nor of stress-wave attenuation in faulted rock at high temperature.

The pre-sliding behavior is also significant. As shown in figure 5, the emissions began early in the loading history and the emission rate increased continually with stress until steady sliding occurred. This behavior differs from that of initial fracturing and of sliding on sawcut samples [2]. In intact rocks the emission rate began to increase at about

half the ultimate strength, a higher relative stress level than in faulted rocks (figure 2). On the other hand, in sawcut samples the emission rate increased abruptly at a high stress level, above half the ultimate strength, and remained nearly constant until sudden stick-slip 2. These results indicate fundamental differences between the mechanical behavior of faulted rock and that of intact or sawcut rock.

From an analysis of the time-dependence of high temperature friction in faulted rocks [9], I observed that transient frictional phenomena occurred when the deformation conditions changed. In that study, changes in the applied boundary displacement rate produced time- and displacement-dependent changes in shear strength and sliding rate. Similarly, HANDIN and others [10] observed transient changes in shear strength following pressure changes. I suggested that during steady-state sliding an equilibrium fault structure is developed that depends on temperature, pressure, sliding rate, and possibly other variables. If conditions change, a new equilibrium structure will be established, but only after some finite displacement. The change in structure may produce transient mechanical behavior. By understanding the fault structure and the factors that affect it, we may be in a better position to explain transient frictional phenomena in the laboratory and in the field. Indeed, stick-slip and perhaps earthquakes may be such transients.

The acoustic emission results give us some insight into the mechanisms of deformation prior to reaching steady-state sliding. In this case, the altered conditions were mainly pressure and temperature. The deformation seems to begin at very low stresses, considerably lower than can be detected by measuring the fault displacement. The intensity of the deformation, as indicated by the emission rate, increased until steady sliding

was reached. One would expect then, according to this hypothesis, that if the faulted sample was unloaded after sliding and then reloaded without changing pressure and temperature, little or no emissions would occur prior to reaching steady sliding. Preliminary work by the author indicated that this supposition seems to be correct at room temperature, but this aspect was not examined in the present study. Often a slight peak in shear strength occurred prior to steady sliding, similar to the stress-peaks observed following changes in boundary displacement rate [9] and pressure [10]. However, no significant increase in emission rate corresponding to the stress drop was observed (Figure 5). The b-value analysis indicates that b may be slightly greater for the emissions produced during loading than during steady-state sliding. Thus the pre-slip deformation consists of a larger number of small emissions, perhaps related to the readjustments of the fault to a new equilibrium structure.

## 6. Conclusions

Brittle cracking occurred during stable frictional sliding in dry Westerly granite at 2 kbar confining pressure,  $10^{-4}$  cm/sec sliding rate, and temperatures up to  $660^{\circ}\text{C}$ . This conclusion is based on the observation of acoustic emissions whose distribution of amplitudes remained the same at all temperatures. Cracking during sliding consisted of a much higher proportion of small events than during fault formation, as indicated by the high b-values, ranging from 1.2 to 2.1.

### 7. Acknowledgements

This work was carried out under U. S. Geological Survey contracts 14-08-0001-13229 and 14-08-0001-14551. I thank W. F. Brace for his encouragement and supervision and for making his laboratory available to me. Discussions with C. Goetze, K. Hadley, and D. Fitterman were helpful. I also thank P.-Y. F. Robin for reviewing the manuscript.

### REFERENCES

- 1 H. R. HARDY, Application of acoustic emission techniques to rock mechanics research, Am. Soc. Test. Mat., Spec. Tech. Publ. 505 (1972), 41.
- 2 C. H. SCHOLZ, Microfracturing and the inelastic deformation of rock in compression, J. Geophys. Res. 73 (1968), 1417.
- 3 C. H. SCHOLZ, The frequency-magnitude relation of microfracturing in rock and its relation to earthquakes, Bull. Seismol. Soc. Am. 58 (1968), 399.
- 4 J. D. BYERLEE and L. PESELNICK, Elastic shocks and earthquakes, Naturwissenschaften 2 (1970), 82.
- 5 H. L. DUNEGAN and A. T. GREEN, Factors affecting acoustic emission response from materials, Am. Soc. Test. Mat., Spec. Tech. Publ. 505 (1972), 100.
- 6 R. M. STESKY, W. F. BRACE, D. K. RILEY, and P.-Y. F. ROBIN, Friction in faulted rock at high temperature and pressure, Tectonophysics 23 (1974), 177.
- 7 W. F. BRACE and J. D. BYERLEE, California earthquakes: why only shallow focus?, Science 168 (1970), 1573.
- 8 J. N. BOLAND and B. E. HOBBS, Microfracturing processes in experimentally deformed peridotites, Int. J. Rock Mech. Min. Sci. 10 (1973), 623.

- 9 R. M. STESKY, Time-dependence of friction in faulted rock at high temperature and pressure, in preparation (1975).
- 10 J. HANDIN, M. FRIEDMAN, J. LOGAN, G. M. SOWERS, and D. W. STEARNS, Mechanical properties of rocks affecting earthquake generation, Ann. Prog. Rept. No. 1, ARPA Contract No. 14-08-001-12723, Office of Earthquake Res., U.S. Geol. Survey, Menlo Park, Calif. (1972) 147 pp.

## FIGURE CAPTIONS

- Figure 1 Experimental configuration.
- Figure 2 Two fracture experiments in Westerly granite at 500 bars confining pressure and 25°C. Stress and microfracturing rate are plotted against axial strain.
- Figure 3 Number of microfracturing events of a given maximum signal amplitude versus amplitude for two fracture experiments in Westerly granite at 500 bars pressure and 25°C. The emissions were accumulated during loading from about half the fracture strength until just prior to failure. The slope of the fitted lines,  $1/m$ , is calculated from  $m = \Delta \log (\text{number of events}) / \Delta \log (\text{amplitude})$ . The b-value is then  $b = m - 1$ .
- Figure 4 Emission rate and shear stress during frictional sliding in a single faulted sample of Westerly granite at 1 kbar pressure and different temperatures. Note the change in scale of the emission rate between the upper and lower figures. Roman numerals denote the order of the runs. The vertical arrows indicate stick-slips.
- Figure 5 Emission rate and shear stress during frictional sliding in a faulted sample of Westerly granite at 2 kbar pressure. Roman numerals denote the order of the runs. The vertical arrows indicate stick-slips.
- Figure 6 Variation of acoustic emission rate with temperature during stable sliding in Westerly granite at 2 kbar pressure. The vertical bars indicate the range of rates observed and the horizontal bars denote the variation of temperature over the fault surface. Several measurements were made with each sample, the samples being distinguished by different symbols.

- Figure 7 Microfracturing frequency versus maximum signal amplitude for two frictional sliding runs in Westerly granite at 2 kbar pressure. The open symbols indicate the emissions during loading up to stable sliding, while the closed symbols refer to emissions occurring during stable sliding.  $b$  is calculated as in figure 3.
- Figure 8 Variation of  $b$ -value, calculated from the slope of the frequency-amplitude curve, with temperature during frictional sliding of Westerly granite at 2 kbar pressure. Except for the two at room temperature, like symbols indicate measurements made with the same sample. The open symbol denotes  $b$  for pre-sliding emissions and the closed symbol denotes  $b$  for stable sliding emissions. The two measurements at 25°C are from SCHOLZ [3]. The vertical error bar has been visually estimated from plots such as in figure 7 and may be larger for the pre-sliding emissions. The horizontal bar indicates the range of temperature over the fault surface.

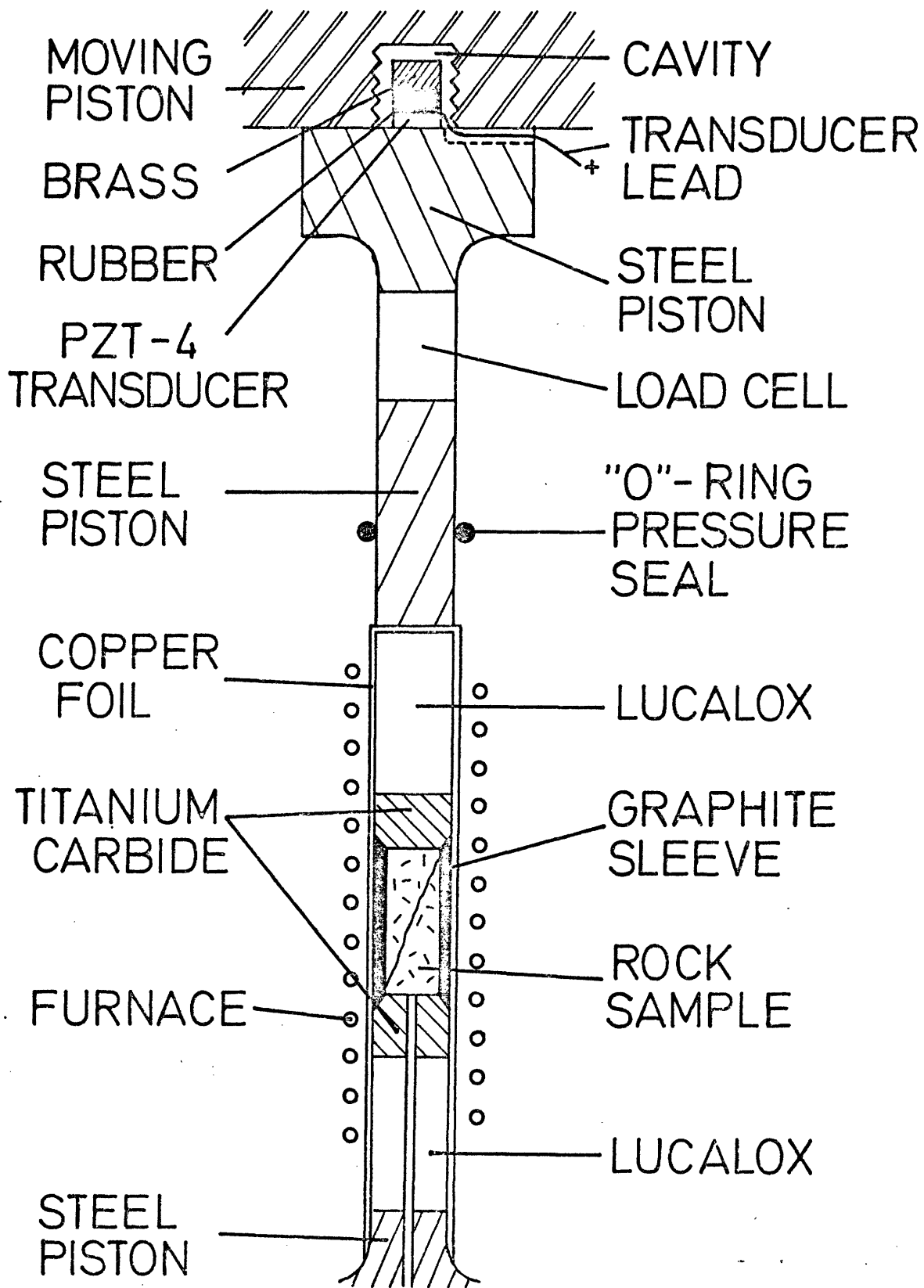
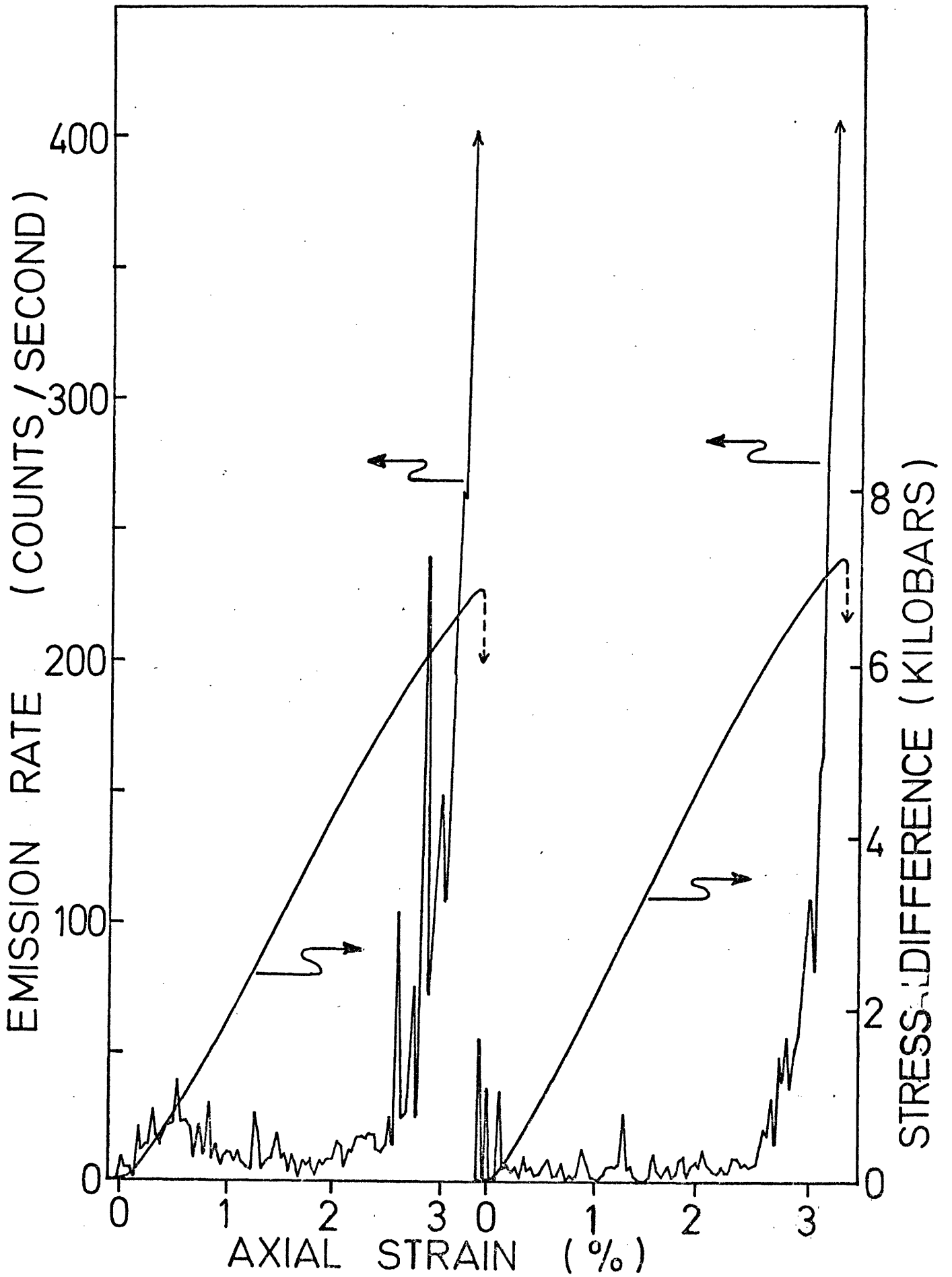


Fig 1



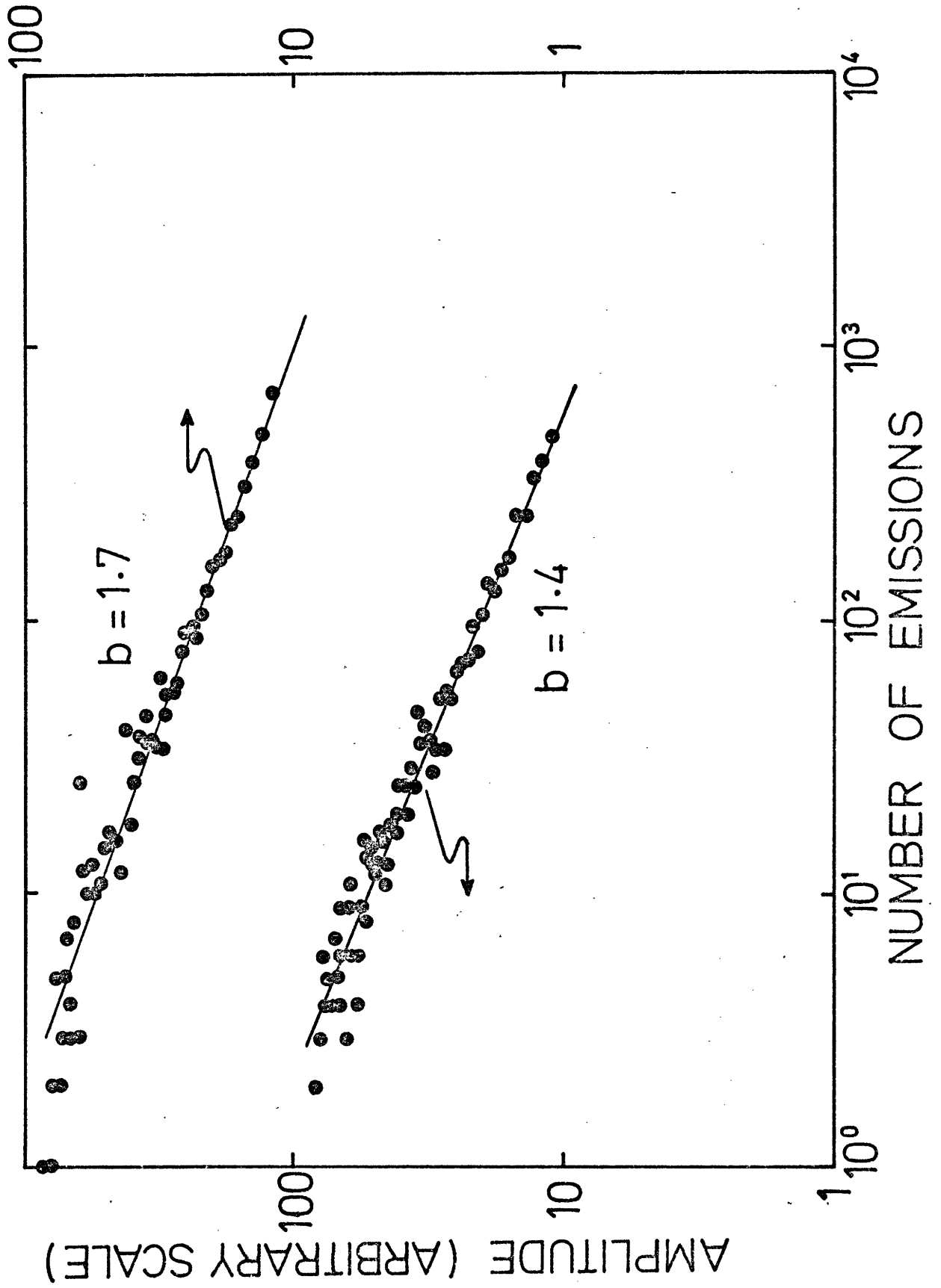


FIG 3

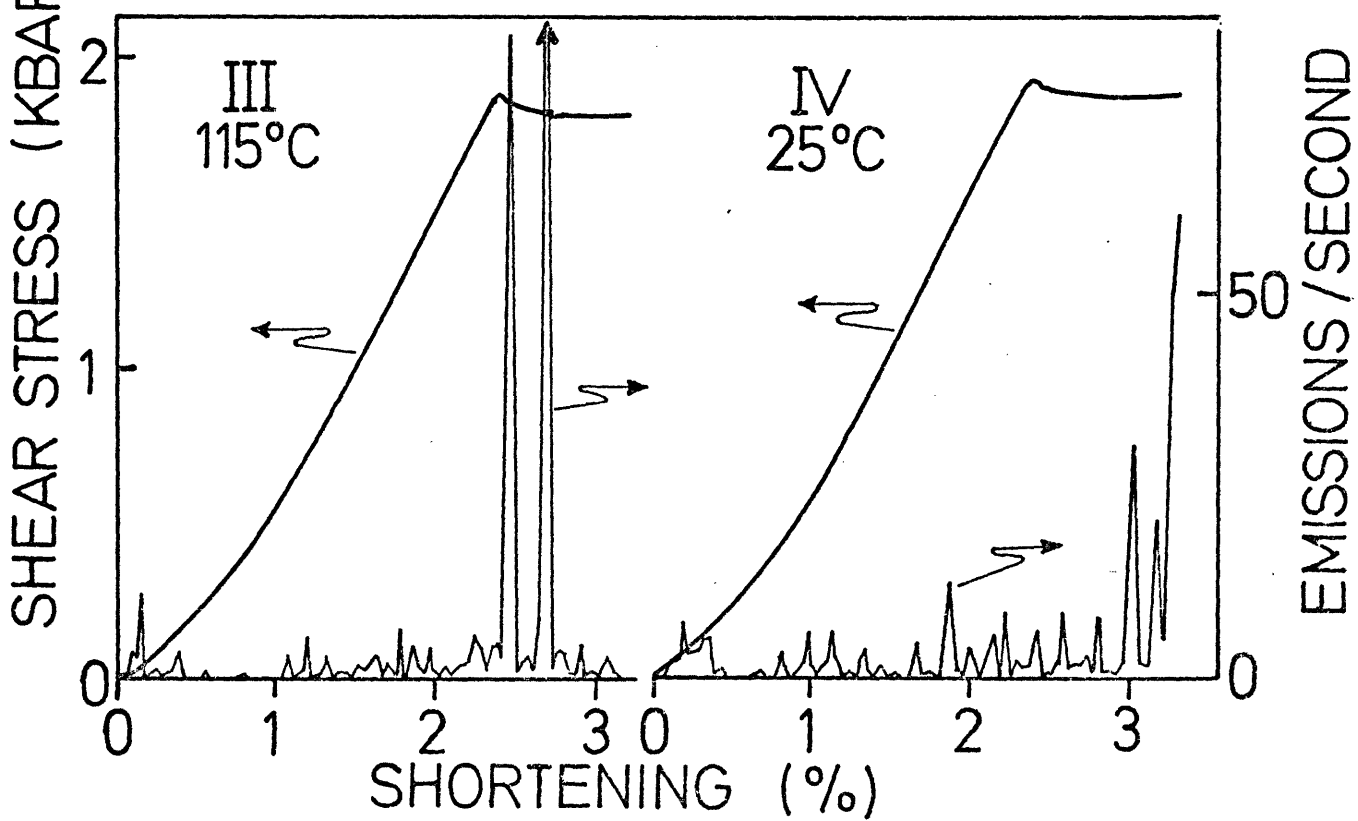
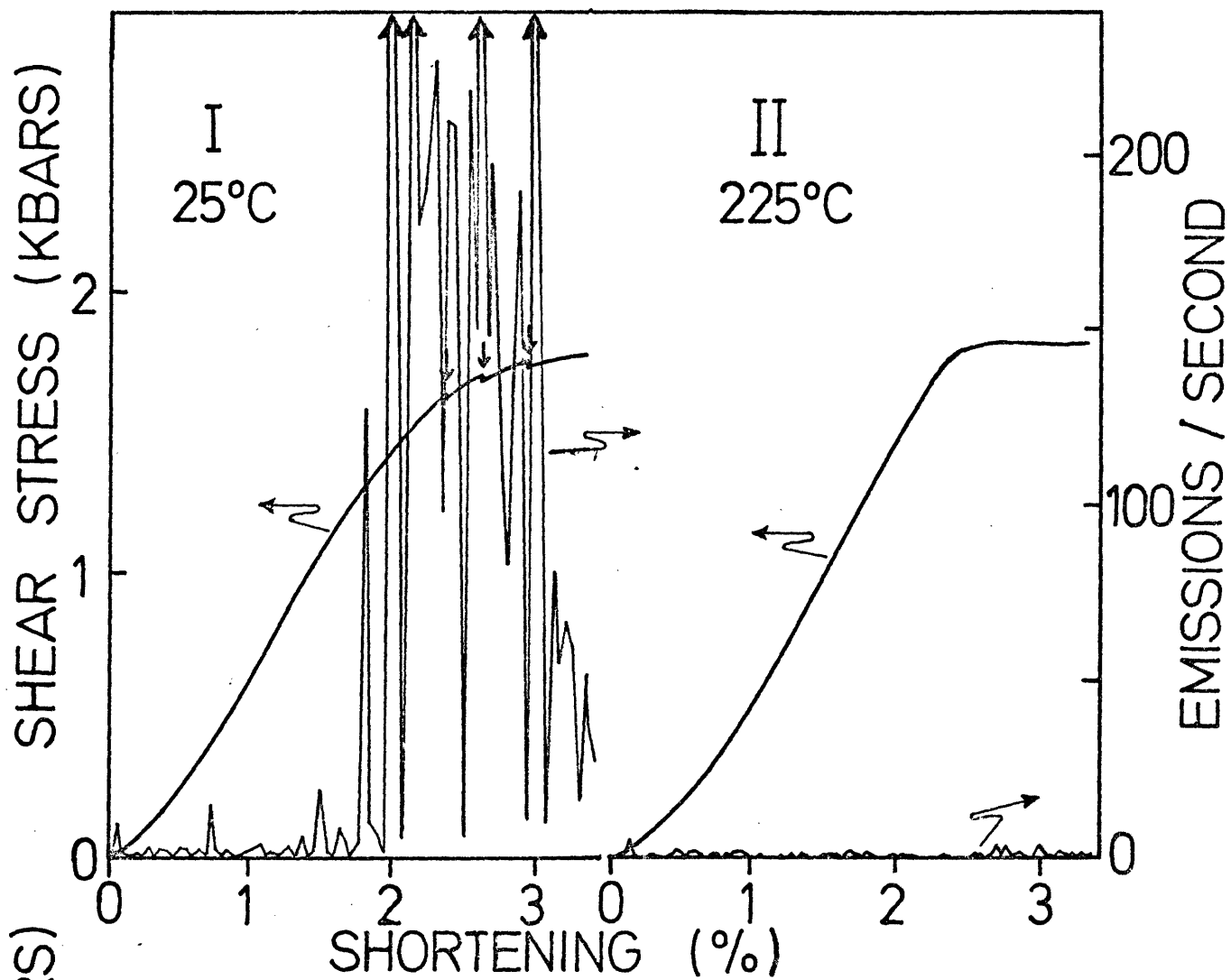
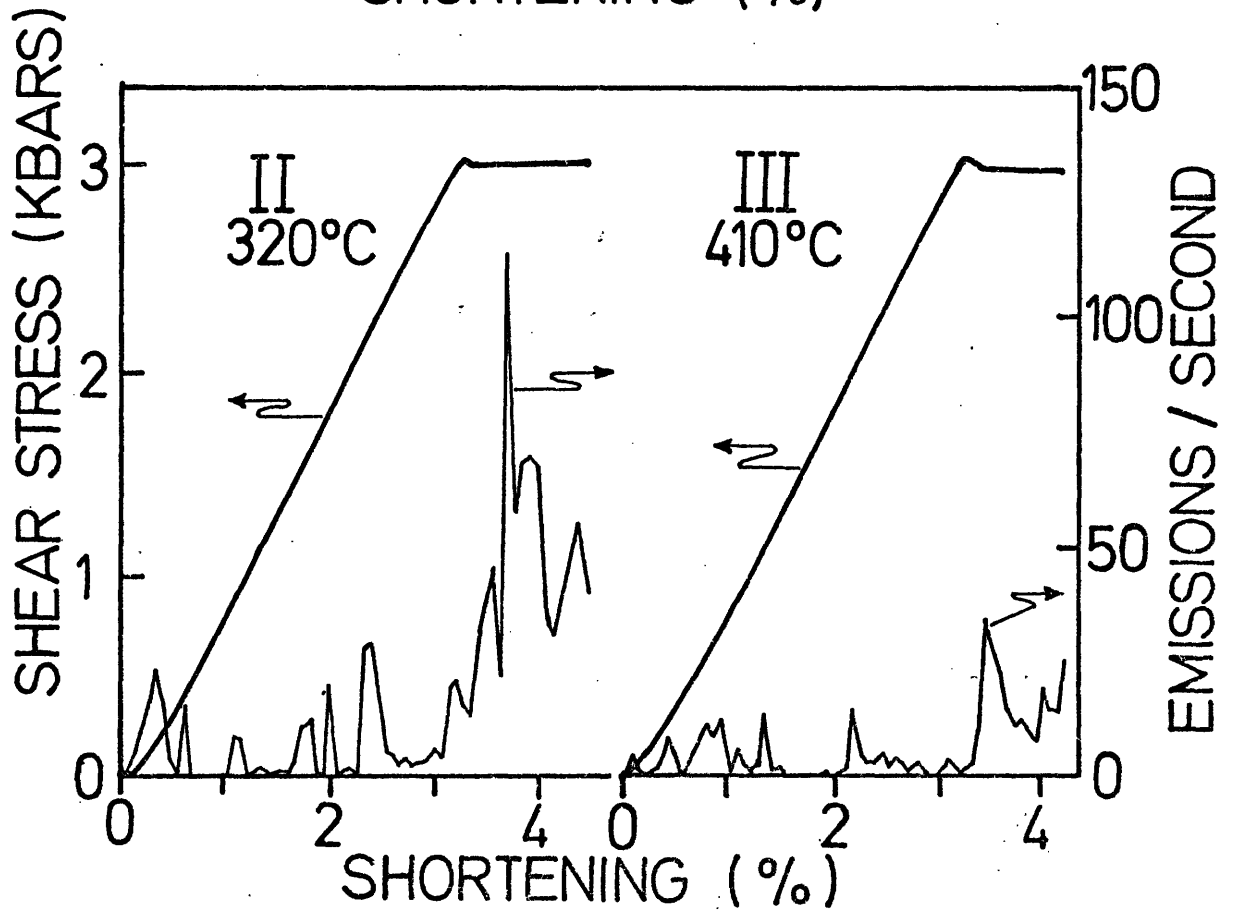
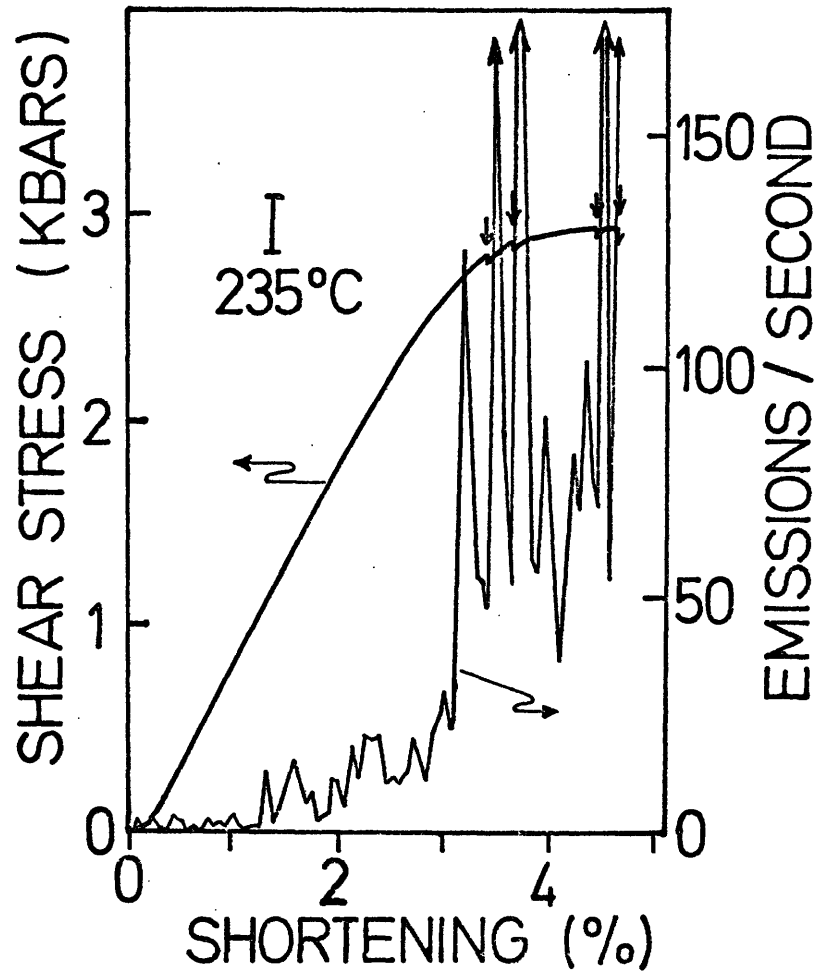


FIG 4



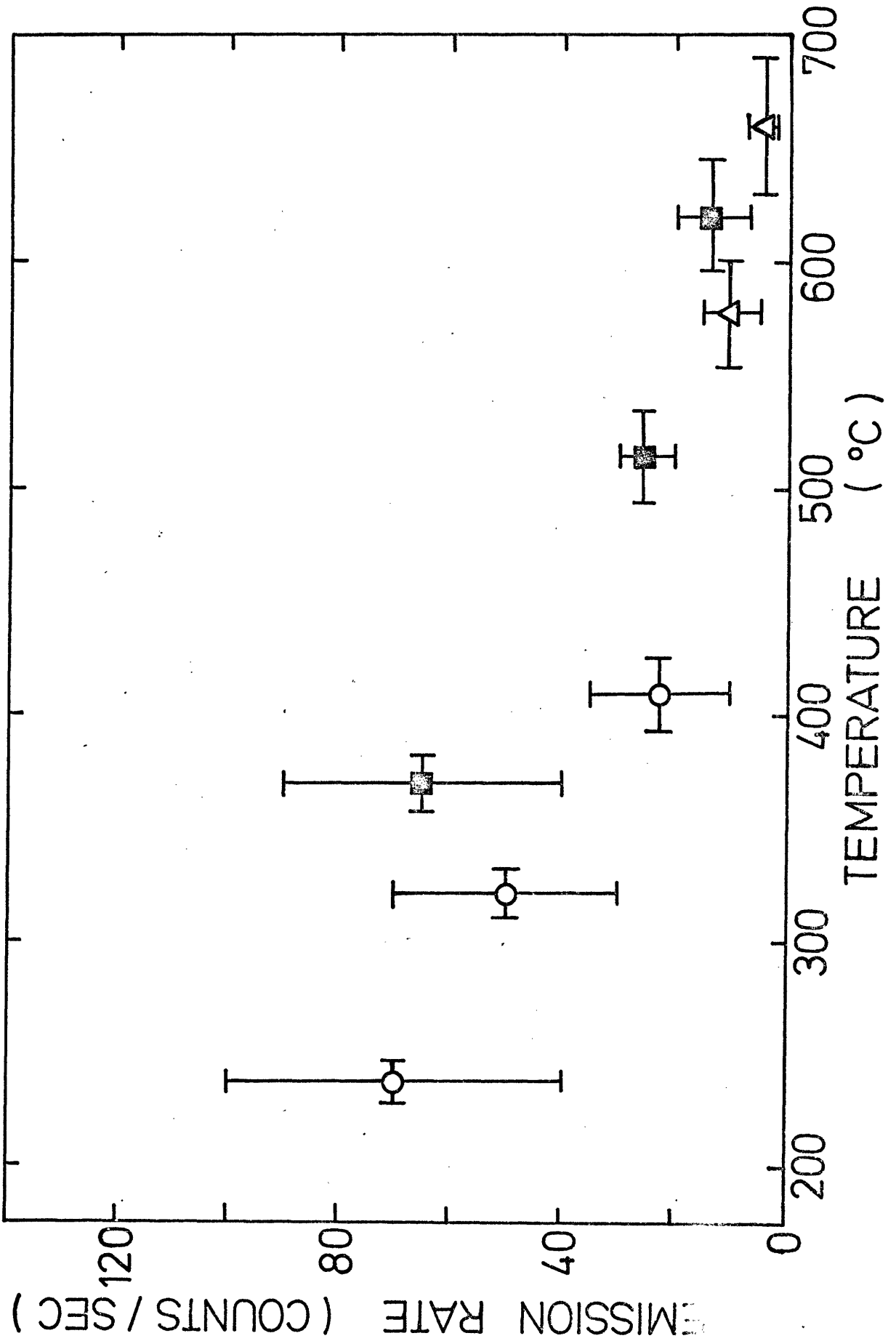


FIG. 6

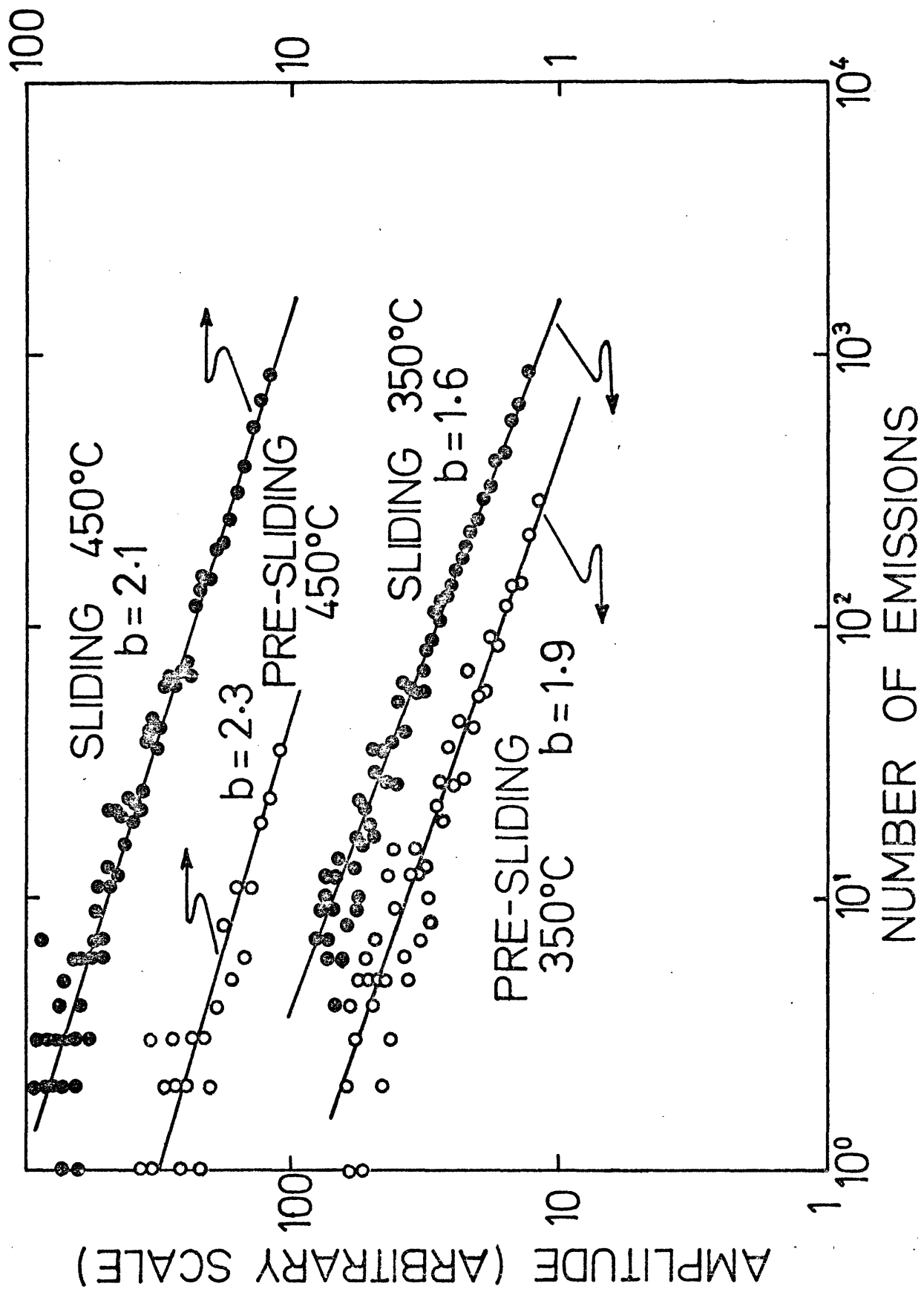


FIG 7

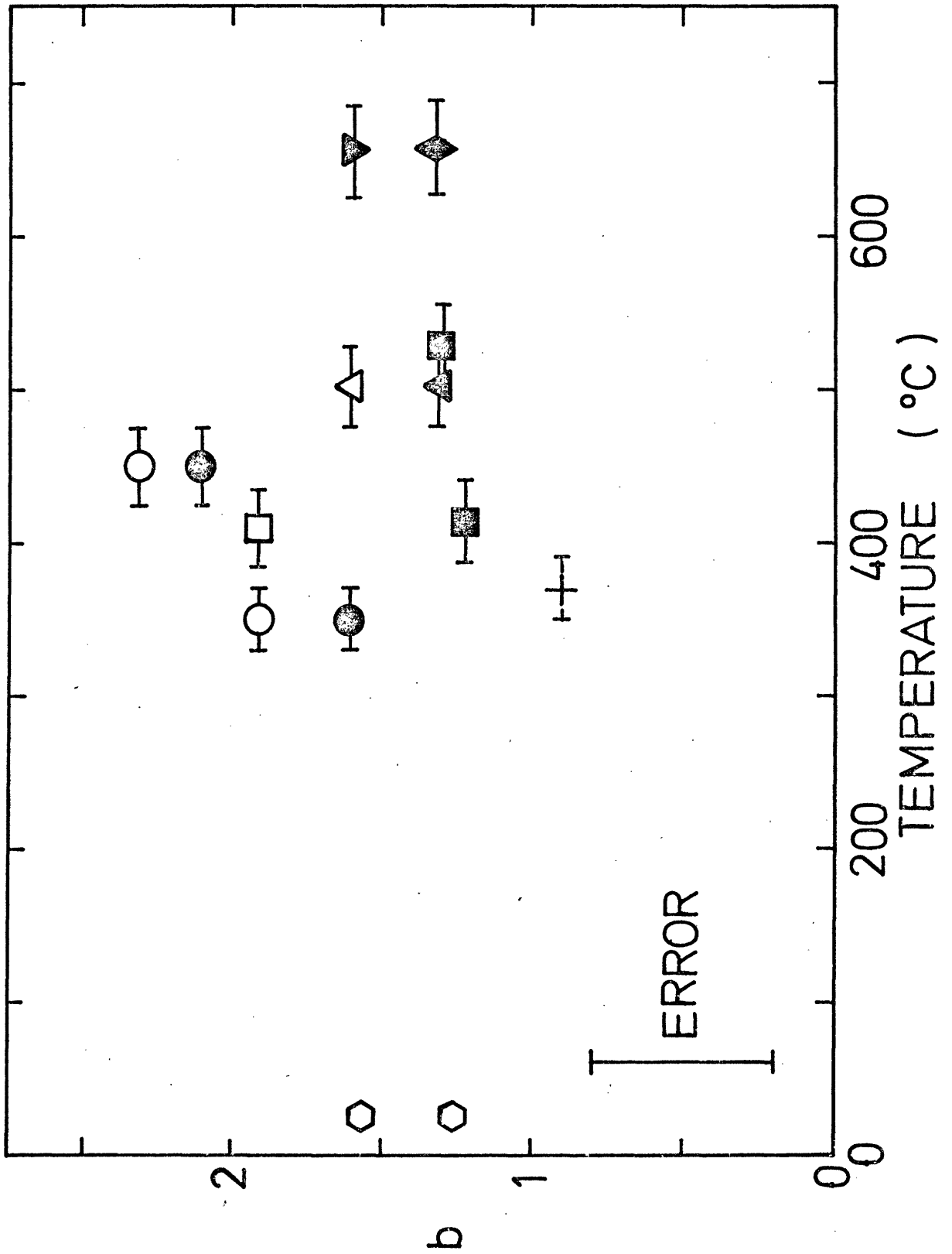


FIG 8

## CHAPTER IV

### MECHANISMS OF HIGH TEMPERATURE FRICTIONAL SLIDING IN WESTERLY GRANITE

#### ABSTRACT

The mechanisms of frictional sliding in faulted Westerly granite were studied in two ways. Firstly, the experimental activation energy was measured from 300° to 700°C at 2.5 kbar pressure and sliding rates from  $10^{-6}$  to  $10^{-3}$  cm/sec. Secondly, fault samples were examined with an optical and a transmission electron microscope. Below 500°C the activation energy was about 30 kcal/mole. The fault gouge was porous and consisted of angular, randomly oriented grains. The quartz and the feldspars were unstrained, similar to the grains in a room-temperature fault. Above 500°C the activation energy increased to about 85 kcal/mole. Plasticity in quartz above 500°C was observed optically by the presence of highly strained gouge grains and with the transmission electron microscope by a marked increase in dislocation density from  $3 \times 10^8$  cm<sup>-2</sup> initially to greater than  $10^{11}$  cm<sup>-2</sup> at 700°C. The quartz grains away from the fault were strain-hardened with inhomogeneously distributed, dense tangles of dislocations. In contrast, the small grains (< 10<sub>μ</sub>m) in the gouge contained a low density of dislocations. The feldspars showed no sign of plasticity up to 700°C. Biotite and muscovite were plastic at all temperatures, forming thin ribbons along slip surfaces in the fault zone.

## INTRODUCTION

We now have many observations of the mechanical behavior of faulted rock over a wide range of pressures and temperatures. These observations include some details of the effects of rock type, temperature, pressure, and time on the shear strength and sliding behavior of faults. However, the deformation mechanisms remain largely unknown. Yet without detailed knowledge of the mechanisms, application of the results to natural faults remains empirical and consequently speculative.

Some progress has been made in deducing the mechanisms. Engelder (1973) has shown that the shearing of fault gouge in quartzose sandstone at 500 bars and 25°C consisted in part of grain crushing and rolling. He inferred, from the angularity of the gouge particles and the presence of conchoidal fractures, that brittle fracture was the primary deformation mechanism. Byerlee (1967) reached a similar conclusion from optical observations of granite gouge at 25°C and pressures to 4 kbar. On the other hand, Friedman and others (1974) suggested that shear-induced melting may occur during steady sliding on faults, even at room temperature. Using optical and scanning electron microscopy, they found evidence of glass on sawcut surfaces, presumably related to shearing at local high-stress points. At higher ambient temperatures, the amount of glass produced during sliding appeared to be greater. This increase in glass production was coincident with an increase in the shear strength of the sawcut, an effect that Friedman and his coworkers attributed to an increase in total contact area. Jackson and Dunn (1974) similarly observed "glass-like welded gouge" after sliding in sawcut samples of gneiss and mylonite initially containing a 1 mm layer of 120-250  $\mu\text{m}$  granulated sample material; they likened this glass to pseudotachylite (Higgins, 1971), found in many natural faults.

Clearly a problem exists. Cataclasis and melting are quite different mechanisms and extrapolation of the laboratory measurements to the conditions in the earth would yield a different understanding of natural faults depending on the assumption of deformation mechanisms. Furthermore, at high temperatures new deformation mechanisms may play an important role. For example, deformation by dislocation glide has been observed in natural quartz experimentally strained at 400°C (Tullis et al., 1973). Also, recrystallization and phase changes are other possibilities. Under what conditions and to what extent these and other mechanisms are important during frictional sliding is not known. Nor do we know what effect they have on sliding behavior.

#### PRESENT STUDY

The object of the present study was to gain some understanding of what deformation mechanisms operate during sliding at temperatures up to 700°C. Two approaches were used. Firstly, the experimental activation energy for sliding was measured at different temperatures. The procedure used followed that of many other high temperature studies (for example, Kohlstedt and Goetze, 1974), with some modifications. Since the measurements were made at constant stress, the technique was limited to stable sliding. While experimental activation energies are not meaningful in themselves unless the deformation mechanisms are known, they do provide additional constraints on possible physical processes when considered with other information. In particular, changes in apparent activation energy may signal changes in the deformation process.

The second approach was observational and involved several techniques. The exposed sliding surface and fault gouge from samples deformed at different temperatures were examined with an optical microscope. Other

samples were impregnated with epoxy, sectioned, and studied by optical and transmission electron microscopy. The aim was to identify the characteristics of the faults and to observe changes in these characteristics with temperature. In an earlier study (Stesky *et al.*, 1974), we attempted to observe differences in fault characteristics related to the stick-slip to stable-sliding transition. In the present work the observations were extended to higher temperatures and used the greater resolution of detail available with the transmission electron microscope.

#### EXPERIMENTAL PROCEDURE

##### Activation energy measurement

Rock cylinders (35 mm long and 16 mm in diameter) were fractured at 500 bars and 25°C to produce the experimental faults used for the friction study. The faulted rock, jacketed with a graphite sleeve in seamless copper tubing, was heated and compressed to the temperature and pressure of interest and axially loaded until sliding occurred. The details of this procedure and of the apparatus and measurement techniques were described by Stesky and others (1974).

The determination of experimental activation energies entailed measuring the sliding rate at different temperatures while holding the shear stress constant. The activation energy was then calculated from the relation:

$$-\frac{E}{R} = \frac{\ln \dot{\delta}_1 - \ln \dot{\delta}_2}{\frac{1}{T_1} - \frac{1}{T_2}}$$

where E is the experimental activation energy, in cal/mole,  $\dot{\delta}_1$  and  $\dot{\delta}_2$  are the sliding velocities in cm/sec at absolute temperatures  $T_1$  and  $T_2$ , respectively, and R is the gas constant. The constraint of a constant shear stress posed an extra problem. During sliding the total fault area

in contact decreased by as much as 10%. Thus the applied load needed to be lowered accordingly to maintain constant applied shear stress. Other work on the time dependence of friction showed that the shear strength was relatively insensitive to the sliding rate, or conversely that the sliding rate was very sensitive to variations in shear stress (Brace and Stesky, 1973; Chapter II). For example, a 10% change in shear stress would produce a rate change of two orders of magnitude at 700°C and more than ten orders of magnitude at 300°C (Chapter II). Consequently the area correction was very significant. This correction was calculated using the fault angle, measured after initial faulting, the sample dimensions and the scale factors of the instrumentation. Once the desired sliding stress was reached, a predetermined load line was drawn on the X-Y plotter. At each temperature the machine piston was advanced by hand keeping the load at the specified value; piston advance, and hence the sliding displacement, was plotted on a time chart recorder, from which plot the sliding rate was calculated. By cycling the temperature, allowing sufficient time at each temperature for steady-state sliding to be reached, several measurements could be made with one sample. The uncertainty in the individual activation energy values was large (typically  $\pm 35\%$ ) and comparable to the scatter of repeated measurements.

### Microscopy

The faulted rock samples were examined in several ways. The copper and graphite jackets were carefully removed from a suite of samples representing a range of deformation temperature and the fault surfaces and gouge were studied optically. A similar suite of samples was impregnated with epoxy (ERL 2795 Bakelite Epoxide, Union Carbide Corp.) under vacuum prior to jacket removal. The rocks were then cut along the plane containing

the cylinder axis and the direction of fault slip, and thin sections were prepared for optical study. Selected areas of the sections were further thinned by ion bombardment. Remarkably, the epoxied gouge remained intact during this process so that adequate thinned areas were produced. These sections were studied in a Philips EM300 transmission electron microscope (TEM) operating at 100 kV.

## OBSERVATIONS

### Experimental activation energy

An example of a sequence of sliding rate measurements is shown in Figure 1. Here the sample was deformed at a number of different temperatures between  $416^{\circ}$  and  $538^{\circ}\text{C}$ , where the temperature is the average over the fault. The sliding rate measured represents an average over the displacement. Evidently, there is a systematic change in sliding rate, as shown by measurements repeated at the same temperature ( $460^{\circ}$  and  $538^{\circ}\text{C}$ ). This change may be due to error in maintaining a constant shear stress or to some unknown displacement effect. By comparing, for each sample, the measurements at the same temperature and assuming the same drift at other temperatures, we can roughly correct for the drift. Except where small temperature changes were made, this correction probably is reasonable since differences between adjacent measurements only are used in the calculations.

The calculated activation energies for the temperature range  $325^{\circ}$  to  $650^{\circ}\text{C}$  are shown in Figure 2. The most striking result is the marked temperature dependence of the experimental activation energy. The scatter in the values is relatively large and comparable to the error of each measurement. However, there is a significant difference between the values at  $350^{\circ}$  (averaging 25 to 30 kcal/mole) and at  $625^{\circ}\text{C}$  (averaging 80 to 90 kcal/

mole). The nature of the transition between these two extreme values is uncertain, although there appears to be an increase from the low activation energy to the high near 500°C. The transition does not seem to be related to a change in shear or normal stress with temperature. The shear stress was 3.52 to 3.85 kbar at 400°, 3.85 kbar at 500°, and 2.98 to 3.37 kbar at 600°. The corresponding normal stresses were 4.53 to 4.84 kbar, 4.75 kbar, and 3.90 to 4.30 kbar, respectively.

#### Optical microscopy

A striking feature of the faults deformed at high temperature was observed when a series of samples were unjacketed (Figure 3). The 300° and 375° samples separated into two halves as does a room-temperature sample. The 450° sample, however, required force to be applied by hand to separate the halves, and even then the separation was not complete. The 500° and 700° samples could not be separated by hand at all, although the 500° sample broke along an extension fracture surface approximately normal to the maximum compressive stress. This "welding" of the fault was confirmed by testing a few other samples. The transition from unwelded to welded appears to be at about 500°C at 2.5 kbars.

The fault surfaces were examined under reflected light with a low power binocular microscope. A 700° surface was exposed by carefully wedging apart the fault. All fault surfaces were nearly planar with a maximum relief of surface irregularities of about 1 mm. In part, this relief is related to the distribution of gouge between the two exposed halves of the samples. Except for a sample which was faulted only, all surfaces were very similar. In each case, the gouge was very fine-grained (<100 μm) and tended to clump into flat platelets which could easily be disaggregated with a pointed tool. Such clumping did not occur in the

room temperature fault sample and seems to be related to large amounts of sliding rather than to the temperature of deformation. In all cases the biotite was smeared and slickensided along the fault surfaces, although to a lesser extent in the fault sample. In general, there were no observable differences in appearance of the sliding surfaces which could be related to the temperature of sliding. Even in the 700° sample there was no discoloration which might be indicative of dehydration of the biotite.

In a further search for differences between high and low temperature faults, gouge fragments were observed under oil immersion and in thin sections. Again no obvious differences were found. A particular study was made for the possibility of glass being present, especially in clumped gouge, as observed by Friedman and others (1974) and Jackson and Dunn (1974). None was found. In each case of clumped gouge, careful observation showed that the clump was composed of fine grained crystals with no optically isotropic "glass" being present, at least down to a resolution of 10  $\mu\text{m}$  (Fig. 4).

Thin sections of impregnated samples, however, revealed some differences in fault character that could be related to the temperature of deformation. In the room-temperature fault, the gouge was angular and randomly oriented (Figure 5). All minerals were brittle, except for biotite and muscovite. These were kinked near the fault zone and were somewhat smeared along the fault (Figure 6a). The quartz showed relict strain and sub-boundary formation, observed in undeformed samples of Westerly granite.

At higher temperature and pressure, the fault material changed somewhat. In part, the gouge was still angular, poorly sorted, and randomly oriented. In such areas the gouge often showed distinct slip surfaces,

subparallel to the fault trace and occasionally marked by stringers of deformed biotite and muscovite (Figure 7). These slip surfaces were less prominent where the fault was bifurcated with less sliding on each branch. Often, however, the gouge fragments appeared highly strained, particularly where quartz is predominant and at the highest sliding temperatures. The quartz grains became elongated parallel to the fault surface and showed extreme undulatory extinction (Figure 8). The micas were highly kinked near the fault, while within the fault zone they were smeared out into thin ribbons parallel to the shear zone (Figure 6b, 6c, 6d). This smearing, observed earlier by Borg and Handin (1966), seems to result from a breakdown of the crystal structure. The boundary between kinked and smeared mica is fairly sharp and often related to kink bands (Figure 6a, 6b). However, cases can be found where the boundary is at a high angle to the kink bands (Figure 6c, 6d), so that no one mechanism, such as shear along kink-band boundaries, can account for this sharp change in deformation behavior in the mica. Similar intense shearing was observed in amphibole at high temperature (Stesky *et al.*, 1974), although there appeared to be no associated kinking. The only mineral which showed relatively little change in behavior was feldspar. It appeared to remain brittle over the entire range of temperatures and pressures, with no tendency to develop undulatory extinction. Occasionally, large fractured grains were found surrounded by fine grained gouge (Figure 9), resembling an incipient mylonitic texture.

#### Transmission electron microscopy

Room-temperature fault. Away from the fault zone, the rock was little strained, so the starting material could be examined. The most conspicuous mineral was quartz; it could be identified by the radiation damage produced

by the high intensity electron beam (McLaren and Phakey, 1968). Quartz was the only phase in which dislocations were observed. They occurred as loops, low-angle tilt boundaries, and free dislocations (Figure 10a, 10b). The density,  $\rho$ , of free dislocations was high, averaging about  $3 \times 10^8 \text{ cm}^{-2}$ , suggesting that the maximum differential stress was about 1 kbar at the time the dislocations were frozen in (Goetze, personal communication, 1975). The presence of dislocation loops and tilt boundaries indicates that climb was important at the conditions of tectonic deformation.

Little can be said about the micas. They did not seem to thin very well, although we did not make a specific effort to obtain good sections for TEM study. Only in one section of a high temperature fault did we get sufficiently thinned muscovite (Figure 16); the observations will be noted later. In any case, optical study indicated that the micas were plastic over the entire range of temperature.

The feldspars were more of a problem. Two feldspars were present in the granite: microcline and partially altered oligoclase ( $\text{An}_{17}$ ). Under the TEM they had two forms. In one the crystal consisted of two orthogonal sets of fine, lenticular lamellae having an average width of about 100 to 200  $\text{\AA}$  (Figure 11). The diffraction pattern for this crystal showed streaking of the spots in two orthogonal directions. Although this type of fine, cross-hatched structure has been observed in both microcline and oligoclase ( $\text{An}_{23}$ ) (McLaren, 1972), optical examination indicated that in most cases here the mineral was microcline. The oligoclase was less distinctive. It resembled quartz but lacked the dislocations and was not as easily damaged by the electron beam. Occasionally inclusions were observed in this feldspar which are presumably related to alteration (Figure 15).

The room-temperature gouge fragments were angular and incohesive and had a very wide range of grain sizes from greater than 200  $\mu\text{m}$  (Figure 5) to less than 50  $\mu\text{m}$ , the smallest observed (Figure 12a, 12b, 12c). Dislocations were observed in quartz grains down to about 0.5  $\mu\text{m}$  in diameter (Figure 12d). The corresponding dislocation densities were comparable to that of the original large grains.

High-temperature friction samples. The most dramatic change to occur after sliding at high temperature was in the dislocation substructure of the quartz, observed in grains away from the fault zone. The density of free dislocations increased, particularly at the highest temperature (700°C) (Figure 13a, 13b). Here, dense tangles of dislocations ( $\rho > 10^{11} \text{ cm}^{-2}$ ) formed, typical of cold-working. The distribution was quite inhomogeneous, however, so that regions of low dislocation density remained. These areas resemble the low-temperature substructure, with loops and tilt boundaries evident (Figure 13b). Ardell and others (1974) observed similar structure in a quartzite experimentally deformed at 600°C and a strain rate of  $10^{-5} \text{ sec}^{-1}$ . To quantify this variation of density with sliding temperature, the dislocations were counted in a series of micrographs of samples deformed at different temperatures. The calculated density for each micrograph is plotted in Figure 14, along with the average density at each temperature. For the 700°C sample the measurements were made only where individual dislocations could be distinguished in the micrographs; the maximum density is much higher, as is the average. The densities at the highest temperature are comparable to those observed by Ardell and others (1974) at 600°C. Below about 500°C, however, the dislocation density is similar to that at 25°C indicating that at 500°C quartz begins to deform plastically at a strain-rate of  $10^{-5} \text{ sec}^{-1}$ . That the transition is not

more definitive may result, in part, from the small amounts of strain undergone by the crystals far from the fault zone, evidenced by negligible thickening of the rock cylinder during deformation. The other mineral constituents showed little change with the deformation temperature. No dislocations were observed to develop in the two feldspars nor was there any apparent difference in the diffraction spots, as might be expected if the grains are strained. Figure 15 shows what is inferred to be oligoclase with large featureless areas and structures that resemble healed cracks or inclusions.

We obtained thinned area in only one kinked grain of muscovite adjacent to the fault in the 700°C sample. Scanning the area revealed little substructure, although on closer examination the crystal appeared finely mottled and had thin, diffuse, parallel bands (Figure 16). This texture is similar to that in muscovite found in slate (Phakey *et al.*, 1972). No transmission electron microscopy study seems to have been done on deformed micas, however.

Observation of the high temperature fault gouge was both aided and hampered by the impregnated epoxy. It was resistant enough to ion erosion to hold the small grains in place, but it often eroded unevenly, producing an apparent grain structure due to differential electron absorption (Figures 17a, 17b). However, for grains larger than about 0.1  $\mu\text{m}$ , the crystallinity of the minerals, and even some fine structure, could be seen. The belief that the amorphous material was epoxy, and not fault-generated glass, is based on three observations: the material was found along grain boundaries away from the fault zone; its speckled texture (Figure 17a) was similar to that of epoxy in the 25°C fault (Figure 12c); and its diffraction pattern showed a broad ring similar to that of the epoxy. This latter

observation is not conclusive since we did not know what the pattern for glass would look like.

The presence of epoxy establishes one conclusion: the high-temperature fault gouge was quite porous (on the order of ten percent, judging from the micrographs) (Figure 17). The gouge was much more compacted than that in the 25°C fault (compare with Figure 12), but in the high-temperature faults the degree of compaction seemed not to depend on temperature, at least at 2.5 kbars confining pressure. At 4 kbars the same may not be true (Figure 18). The 450°C fault zone had an apparent porosity comparable to that at lower pressure. On the other hand, the 630°C fault appeared much more compacted, although the difference may be one of grain size and sorting, rather than porosity. In addition, this method of estimating porosity may not be reliable because of possible changes during foil preparation.

In general, the gouge fragments were angular and poorly sorted. As with the 25°C fault, the grain size varied from hundreds of microns (Figure 8) down to at least 0.1  $\mu\text{m}$  (Figure 17). The submicron-sized grains formed a small component of the volume of gouge, except in the 4 kbar, 630°C fault. Here the volume fraction was significantly larger, apparently at the expense of micron-sized grains. This separation of grain sizes occasionally resulted in a mylonitic texture with large fragments surrounded by a matrix of very fine grains (Figure 18c).

The detailed microstructure of the gouge grains was difficult to observe because of thickness variations, except for grains larger than about  $\frac{1}{2}$   $\mu\text{m}$ . The dislocation density in quartz in the 700°C fault zone was comparable to that in the 25°C fault, as observed in a few micron-sized grains. This lack of high strain was confirmed by a study of the diffraction patterns. Single spots, or clusters of two or three, were observed,

but with no streaking, as might be expected (Figure 19). The splitting of spots probably resulted from fracture and a slight rotation of the parts of the grain. The feldspar similarly showed no sign of plastic deformation (Figure 17c). The diffraction spots showed some streaking, probably related to the fine lamellae.

## DISCUSSION

### Deformation mechanisms during sliding

Several lines of evidence point to a change in physical processes during sliding in Westerly granite near  $500^{\circ}\text{C}$  at 2.5 kbar pressure. There was a marked increase in rate sensitivity of the shear stress (Chapter II, Figure 4), in experimental activation energy, and in dislocation density of quartz above  $500^{\circ}\text{C}$ . Also, above this temperature the faults were cohesive after sliding. It is useful then to discuss separately the results below and above  $500^{\circ}\text{C}$ , since different mechanisms seem to be operating and different macroscopic behaviors occurred. The transition temperature,  $500^{\circ}\text{C}$ , is not very well defined and is chosen merely for convenience of discussion. Also, the value applies only at 2.5 kbars pressure; the data are scant for other pressures, although we have some information at 4 kbars.

For sliding at temperatures below  $500^{\circ}\text{C}$ , the evidence strongly indicates that deformation was brittle. At 2.5 kbars the sliding stress was very dependent on the pressure, to the same degree as at room temperature (Chapter I, Figure 10). Acoustic emissions (presumably from brittle cracking) were detected during sliding over the entire temperature range, although the emission rate decreased with increasing temperature (Chapter III, Figure 6). The gouge fragments were angular, randomly oriented and incohesive, with appreciable pore space later filled by epoxy during

microscope sample preparation. TEM examination revealed no change in microstructure of the three dominant minerals--microcline, oligoclase, and quartz--that might be indicative of plastic strain. In contrast, however, the micas--biotite and muscovite--constituting 5% of the volume of the granite, appeared to be plastic at all temperatures, at least in the high strain regions near the fault zone.

The final piece of evidence, the experimental activation energy measurements, deserves special attention. The relationship between rate and temperature was studied under conditions of constant applied stress. Below 500°C the activation energy had an average value of 25 to 30 kcal/mole, comparable to the values obtained for stress-corrosion cracking in quartz (Scholz and Martin, 1971). But the determination of activation energy requires keeping all factors, except temperature and rate, constant, in particular, the local stress. This requirement was closely approached in the crack studies, but probably not in the case of frictional sliding. For a granular material, the local stress is a function not only of the applied stress, but also of the porosity, grain size and angularity, degree of interlocking, and so on. Grain size and angularity would be slowly varying parameters, but porosity and degree of interlocking will depend on temperature, shearing rate, and stress and so will vary as any of these quantities are changed. Thus the structure of the fault zone may not remain constant during an activation energy experiment, resulting in an apparent energy value that may reflect many effects.

How variations in porosity could affect the observed activation energy can be seen very simply. Experiments have shown that at constant temperature and applied stress, the creep rate of a porous solid increases with porosity (Coble and Kingery, 1956; Spriggs and Vasilos, 1964). Thus as the temperature was altered in a constant stress experiment, a coincident change

in porosity would either increase or decrease the rate change produced by temperature alone. Porosity could change for two reasons: the gouge would compact more under pressure at the higher temperature, but the increase in shearing rate would tend to dilate the fault zone. We cannot decide a priori the net porosity change since it depends on the relative magnitude of the two effects. Thus no conclusions can be drawn from the activation energy experiment other than that the results do not conflict with the idea that the deformation is predominantly brittle.

Above 500°C the situation is more complicated. The dominant process still seems to be brittle cracking, for several reasons: the pressure dependence of the shear stress remained high, acoustic emissions occurred up to 700°C, the gouge grains were angular and supported observable porosity, and no plastic deformation was detected in the feldspars, the dominant minerals. Yet there was a marked difference in frictional behavior. The rate sensitivity of the friction stress was almost an order of magnitude greater than at low temperature. The experimental activation energy increased by a factor of three, to about 90 kcal/mole. Also, the fault zones became welded together during sliding. The coincident increase in dislocation density in quartz suggests that the onset of plasticity of quartz may account for the change in behavior. This suggestion is supported by the observation of welding. Hardman and Lilley (1973) found that compacted halite powders had a much higher tensile strength than powdered sucrose and coal, compacted under the same pressure. The plastically deforming halite powders compacted to a much lower porosity than did the brittle sucrose and coal, presumably attaining a greater contact area between surfaces and a greater degree of interlocking.

The lack of observed plastic deformation of the quartz gouge poses a problem, however. Marked asterism of the diffraction spots should have been observed if the fragments contained dislocations with a density of  $10^{11} \text{ cm}^{-2}$  (Ardell et al., 1974). It is possible that, in the areas studied, quartz formed a minor component of the gouge. But quartz constituted almost a third of the granite by volume and so it should form a comparable fraction of the gouge. In some cases even, as for the area of Figure 19, the fault was bounded on both sides by large quartz grains, suggesting that here a much larger fraction of the gouge was quartz. If, as seems most likely, the quartz gouge does not contain the high density of dislocations apparent in the quartz of the wallrock, then this difference in behavior needs to be explained.

Several explanations are possible. The crystals may have been annealed during the brief minute or two after the load was removed but before the temperature dropped appreciably. However, there seems to be no evidence in the larger crystals that recovery was significant. On the other hand, the dislocations may have been removed by glide due to the proximity of free surfaces. If we assume, as a minimum, that the glide of one dislocation in quartz requires a shear stress of 350 bars, estimated from the onset of yielding in synthetic single-crystal quartz (Hobbs et al., 1972), we can calculate the maximum distance a dislocation could lie away from a free surface and not be removed by the image force. For reasonable values of Burgers vector and shear modulus, this distance is about  $0.03 \mu\text{m}$ , corresponding to a grain size of about  $0.06 \mu\text{m}$  (Friedel, 1964, p. 44). For grains smaller than this size, all dislocations would be removed by the image force. If the glide stress is greater than that assumed, then the critical grain size is even smaller. But the majority of the grains were

much larger than this maximum and would retain their dislocations. The third, and more likely, possibility is that dislocations were able to glide out of the crystal during shearing. This would be possible if the grain size was comparable to the mean dislocation spacing, so that tangles would not form. For a density of  $10^8 \text{ cm}^{-2}$ , the mean spacing is about  $1 \mu\text{m}$ ; thus a  $1\text{-}\mu\text{m}$  grain would contain one dislocation, as in Figure 12d. Grains much larger than this size were observed optically to be highly strained in the fault zone (Figure 8). Since at these temperatures there was only one slip system active (Heard and Carter, 1968), general strain of each grain was not possible. Rather, only those grains suitably oriented would deform plastically, although the process would be assisted by the presence of free pore space by removing some of the restrictions on the strain. However, brittle fracture and grain rotation would likely accompany plastic-deformation, so that evidence of extensive strain, such as ribbon-shaped grains, may not be preserved.

The high apparent activation energy for friction above  $500^\circ\text{C}$  is difficult to explain. The available data indicate that the activation energy for creep of quartz is between 20 and 40 kcal/mole (data summarized by Balderman, 1974), comparable to that for static fatigue cracking. Thus the activation energy should remain nearly constant with temperature. As at lower temperatures, the effect of porosity cannot be decided. The gouge is likely to be somewhat more compacted at the higher temperature because of plasticity of the quartz, although no evidence for such increased compaction could be found in the optical and TEM micrographs. It seems unlikely that the relative magnitude of compaction and shearing dilatancy would change markedly with temperature or with a change in deformation mechanism since the same mechanism probably controls both.

Thus porosity effects may not be able to explain the increase in apparent activation energy near 500°C. The other possibility is that the high apparent activation energy may be real and appropriate for the rate controlling process. Goetze (1971) found that for low-stress transient creep of Westerly granite at 600° to 700°C the activation energy was about 80 kcal/mole, similar to that for friction at the same temperature. It is noteworthy that he found measurable creep strain only above 500°C, presumably related to plasticity of quartz. However, the rate controlling process remains unknown.

#### Processes of frictional sliding in granite

The question then arises: how do these deformation mechanisms act to produce the observed sliding behavior? It seems clear that the process is complex, but despite the complexities, a few statements can be made. The dominant process at 2.5 kbars pressure,  $10^{-4}$  cm/sec sliding rate, and temperature to 700°C is brittle shear of the gouge. This is clear from the fact that over the entire temperature range the pressure dependence was high and constant. In contrast, above 40 kbar at 700°C the pressure dependence appeared to decrease. Under these conditions the friction and fracture stresses were equal. The processes during this frictional sliding are not likely to be the same as at lower pressure, accounting in some way for the lower pressure dependence and significantly higher rate sensitivity. TEM observation also showed the gouge to be markedly different: finer grained, on average, and apparently more compacted. The decrease in pressure dependence with temperature was more marked with the San Marcos gabbro (Stesky et al., 1974), but in neither case is it clear why.

At low temperatures, below 500°C, the rate sensitivity of the sliding stress was low, even for a brittle process, as discussed in Chapter II. In

addition, unusual time-dependent yielding, relaxation, and strengthening phenomena occurred that have their counterpart in few other deformation processes. A simple way to account for these results is in terms of two competing processes: compaction and shear of the gouge. Both are time-dependent processes, but of opposite sense; that is, an increase in shear rate requires an increase in stress, but also produces a decrease in compaction and hence a decrease in stress. The overall effect is a low rate-dependence for steady-state sliding. The yielding, relaxation, and strengthening phenomena occur during the transition from one state of compaction to another, requiring a finite amount of shearing to complete the change. These processes have been documented for sand at low pressure (Healy, 1963), but, except for some static compaction studies (for example, Maxwell, 1960), little work has been done at high pressures and temperatures. Even studies of the porosity dependence of shear rate, such as that of Coble and Kingery (1956), offer little help. In their study the shear rate resulted from an imposed porosity; in the fault gouge the reverse was true. The two processes are not simply related, so their conclusions cannot be directly applied to the friction problem.

The onset of plasticity in quartz above 500°C at 2.5 kbars altered only some of the friction properties. The shear stress and its variation with pressure changed very little. Again, these properties were controlled mainly by brittle shear of the gouge. On the other hand, the marked increase in rate sensitivity for steady-state sliding seems to be correlated with the plastic flow of quartz. The rate-dependence, though, was not as high as for the deformation of quartz-rich rocks (Heard and Carter, 1968; Hobbs et al., 1972). Presumably the effect of the quartz was much reduced because of its relatively low concentration. This conclusion is

supported by our earlier observation that the friction strength of faulted Rutland quartzite decreased more rapidly with temperature than did that of Westerly granite (Stesky et al., 1974). The effect of the micas, preferentially distributed along slip surfaces in the gouge, is uncertain. Jackson and Dunn (1974) found a small variation in friction stress with mica abundance, a variation that depended somewhat on the orientation of the fault relative to the foliation. At temperatures above the 25°C used in their experiments the effect may be more pronounced because of increasing ductility of the mica.

Flow law for stable sliding in granite at high temperature.

Knowledge of the apparent activation energy and rate sensitivity of the shear stress allows us to derive an approximate flow law for sliding. Because of the change in behavior around 500°C, two laws are required, representing the low and high temperature processes. For steady-state sliding, assuming no history dependence, we can write:

$$d \ln \dot{\gamma} = \left. \frac{\partial \ln \dot{\gamma}}{\partial \tau_a} \right|_T d\tau_a + \left. \frac{\partial \ln \dot{\gamma}}{\partial (\frac{1}{T})} \right|_{\tau_a} d\left(\frac{1}{T}\right) \quad (7)$$

neglecting higher order terms. The porosity variations have been included as part of the variation of the applied shear stress,  $\tau_a$ , and activation energy, E, since they are uncontrollable. The first derivative can be approximated by the reciprocal of the rate sensitivity, while the second is the experimental activation energy. The simplest fit to the data (Figure 4 of Chapter II and Figure 2 of this chapter) is a constant value for activation energy and rate sensitivity, independent of temperature, except for a change at 500°C. Using these approximate values and integrating equation (7), we get:

$$\dot{\delta} = \dot{\delta}_0 e^{0.1 \tau_a} e^{-\frac{30,000}{RT}} \quad (8a)$$

$$\dot{\delta} = \dot{\delta}'_0 e^{0.02 \tau_a} e^{-\frac{85,000}{RT}} \quad (8b)$$

where  $\tau_a$  is in bars and T is  $^{\circ}\text{K}$ . As a test of these equations we can calculate the variation with temperature of shear stress at constant rate fitted at  $500^{\circ}\text{C}$  and compare it with the measured values from Chapter I. Figure 20 shows the results. Measurements made on the same sample at different temperatures are shown by joined dots. The measured variations agree reasonably well with those predicted by equations (8a) and (8b), except in the region around  $500^{\circ}\text{C}$ . Also the fit to the absolute stress level is poor above  $500^{\circ}\text{C}$ . A much better fit is obtained if the transition temperature is raised to  $550^{\circ}\text{C}$ . The curve cannot be extrapolated reliably to temperatures below  $300^{\circ}\text{C}$  since the granite undergoes a transition to stick-slip sliding, where we have little idea of its mechanical properties.

The final figure shows the "sliding law" with the new transition temperature of  $550^{\circ}\text{C}$ , plotted for a range of temperatures and sliding rates (Figure 21), preferentially selecting that equation, (8a) or (8b), which gave the lowest stress at any given temperature and rate. This choice produces a decrease in transition temperature as the rate is lowered. There was some suggestion during the rate tests of Chapter II that the rate sensitivity was slightly higher at low rates near the transition. However, the range of rates used was too narrow for any definitive conclusion. In any case, if we assume that the "sliding law" is reasonable and that we can extrapolate to lower or higher rates, at least a few orders of magnitude, then the results predict that granite

fault gouge remains brittle up to about 450°C at a geological sliding rate of 1 cm/yr. This temperature corresponds to a depth of about 14 km for the Basin-and-Range geotherm (Roy et al., 1968). The coincidence of this depth with the lower limit for earthquakes on the San Andreas fault (Eaton et al., 1970) is fortuitous, however, since the effect of pressure has not been considered. These curves are for sliding at 2.5 kbars. Increasing the pressure would shift the curves to higher stresses. Brittle fracturing would tend to be inhibited and hence restricted to lower temperatures. However, our data for other pressures are sparse and not sufficient to predict the pressure effect in any more detail. In any case, our results do suggest that some rocks may behave brittly even to moderately high temperatures under geological conditions.

#### CONCLUSIONS

Stable sliding in Westerly granite at 2.5 kbars confining pressure occurs dominantly by brittle shear of the fault gouge at all temperatures up to 700°C and at sliding rates between  $10^{-5}$  and  $10^{-2}$  cm/sec. Feldspar, forming 65% of the rock, remains brittle over the entire temperature range. Quartz becomes plastic at temperatures above about 500°C. Mica, on the other hand, deforms plastically at all temperatures.

## REFERENCES

- Ardell, A.J., Christie, J.M., and Tullis, J.A., 1973. Dislocation substructures in deformed quartz rocks. *Cryst. Lattice Defects*, 4: 275-285.
- Balderman, M.A., 1974. The effect of strain rate and temperature on the yield point of hydrolytically weakened synthetic quartz. *J. Geophys. Res.*, 79(11): 1647-1652.
- Borg, I. and Handin, J., 1966. Experimental deformation of crystalline rocks. *Tectonophys.*, 3(4): 251-367.
- Brace, W.F. and Stesky, R.M., 1973. Time-dependence of frictional sliding in gabbro at high temperature and pressure. *Trans. Am. Geophys. Union*, 54(4): 466 (abstract).
- Byerlee, J.D., 1967. Frictional characteristics of granite under high confining pressure. *J. Geophys. Res.*, 72(14): 3639-3648.
- Coble, R.L. and Kingery, W.D., 1956. Effect of porosity on physical properties of sintered alumina. *J. Am. Ceram. Soc.*, 39(11): 377-385.
- Eaton, J.P., Lee, W.H.K. and Pakiser, L.C., 1970. Use of micro-earthquakes in the study of the mechanics of earthquake generation along the San Andreas fault in central California. *Tectonophys.*, 9: 259-282.
- Engelder, J.T., 1974. Cataclasis and the generation of fault gouge. *Bull. Geol. Soc. Am.*, 85: 1515-1522.
- Friedel, J., 1964. Dislocations. Pergamon Press, London: 491 pp.
- Friedman, M., Logan, J.M. and Rigert, S.A., 1974. Glass-indurated quartz gouge in sliding-friction experiments on sandstone. *Bull. Geol. Soc. Am.*, 85(6): 937-942.

- Goetze, C., 1971. High temperature rheology of Westerly granite. *J. Geophys. Res.*, 76(5): 1223-1230.
- Hardman, J.S. and Lilley, B.A., 1973. Mechanisms of compaction of powdered materials. *Proc. Roy. Soc. Lond.*, 1, 333: 183-199.
- Healy, K.A., 1963. The dependence of dilation in sand on rate of shear strain. Sc.D. Thesis, Dept. of Civ. Eng., Mass. Inst. of Technol., Cambridge, Mass.: 45 pp.
- Heard, H.C. and Carter, N.L., 1968. Experimentally induced "natural" intragranular flow in quartz and quartzite. *Am. J. Sci.*, 266: 1-42.
- Higgins, M.W., 1971. Cataclastic Rocks. U.S. Geol. Surv. Prof. Paper 687: 97 pp.
- Hobbs, B.E., McLaren, A.C. and Paterson, M.S., 1972. Plasticity of single crystals of synthetic quartz. In: Flow and Fracture of Rocks, H.C. Heard, I.Y. Borg, N.L. Carter, and C.B. Raleigh (Editors), Am. Geophys. Union, Geophys. Monograph 16: 29-54.
- Jackson, R.E. and Dunn, D.E., 1974. Experimental sliding friction and cataclasis of foliated rocks. *Int. J. Rock Mech. Min. Sci.*, 11(6): 235-250.
- Kohlstedt, D.L. and Goetze, C., 1974. Low-stress high-temperature creep in olivine single crystals. *J. Geophys. Res.*, 79(14): 2045-2051.
- Maxwell, J.C., 1960. Experiments on compaction and cementation of sand. In: Rock Deformation (A Symposium), D.T. Griggs and J. Handin (Editors), Geol. Soc. Am., Mem., 79: 105-132.
- McLaren, A.C., 1972. Transmission electron microscopy of the feldspars. In: The Feldspars, W.S. McKenzie and J. Zussman (Editors), Manchester Univ. Press, Manchester, U.K.:

- McLaren, A.C. and Phakey, P.P., 1965. A transmission electron microscope study of amethyst and citrine. *Austral. J. Phys.*, 18: 135-141.
- Phakey, P.P., Curtis, C.D. and Oertel, G., 1972. Transmission electron microscopy of fine-grained phyllosilicates in ultra-thin rock sections. *Clays Clay Mins.*, 20: 193-197.
- Roy, R.F., Blackwell, D.D., and Birch, F., 1968. Heat generation of plutonic rocks and continental heat flow provinces. *Earth Plan. Sci. Lett.*, 5: 1-12.
- Scholz, C.H. and Martin, R.J., 1971. Crack growth and static fatigue in quartz. *J. Am. Ceram. Soc.*, 54(9): 474.
- Spriggs, R.M. and Vasilos, T., 1964. Functional relation between creep rate and porosity for polycrystalline ceramics. *J. Am. Ceram. Soc.*, 47: 47-48.
- Stesky, R.M., Brace, W.F., Riley, D.K. and Robin, P.-Y.F., 1974. Friction in faulted rock at high temperature and pressure. *Tectonophys.*, 23: 177-203.
- Tullis, J., Christie, J.M. and Griggs, D.T., 1973. Microstructures and preferred orientations of experimentally deformed quartzites. *Bull. Geol. Soc. Am.*, 84(1): 297-314.

## FIGURE CAPTIONS

- Figure 1. Variation of sliding rate,  $\dot{\delta}$ , with displacement,  $\delta$ , at nominally constant stress and cycled between different temperatures (numbered in  $^{\circ}\text{C}$  at each point). The horizontal bars indicate the amount of displacement occurring at each temperature interval. The sliding rate is calculated as the average over the displacement interval, except for an initial transient. The lines join pairs of points at the same temperature or are parallel to the pair lines. The change in sliding rate was calculated from the offset of these lines.
- Figure 2. Calculated activation energy at different temperatures for sliding at 2.5 kbar pressure. The horizontal bars denote the change in temperature used for the measurement and the vertical bar, the estimated uncertainty.
- Figure 3. A series of deformed fault samples with their jacket removed. The temperature and pressure of sliding are indicated with each sample. WG-S-18 and WG-S-1 were forceably pulled apart, while WG-S-6 could not be separated.
- Figure 4. Thin section of a platelet of clumped gouge from a fault deformed at  $650^{\circ}\text{C}$  and 2.5 kbar. Crossed nicols.
- Figure 5. Fault gouge from sample fractured at  $25^{\circ}\text{C}$  and 500 bars. Crossed nicols.
- Figure 6A. Kinked and highly sheared biotite at the boundary of the fault in a sample fractured at  $25^{\circ}\text{C}$  and 500 bars. Crossed nicols.
- Figure 6B. Highly sheared biotite in the fault zone of a sample deformed at  $700^{\circ}\text{C}$  and 2.5 kbar. Plane light.

- Figure 6C. Same area as Figure 6B. Crossed nicols.
- Figure 6D. Sheared biotite in fault zone of sample deformed at 450°C and 4 kbar. Note the stringers of biotite in the fault gouge. Plane light.
- Figure 7. Slip surfaces in fault gouge deformed at 530°C and 2.5 kbar. Crossed nicols.
- Figure 8. Plastically strained quartz grain in a fault deformed at 700°C and 2.5 kbar. Crossed nicols.
- Figure 9. Fractured feldspar grain in fault gouge deformed at 700°C and 2.5 kbar. Crossed nicols.
- Figure 10A. Dislocation substructure of quartz from the wall rock of sample fractured at 25°C and 500 bars. Note the abundant loops, low-angle boundaries, and free dislocations. The fine speckling is radiation damage produced by the electron beam.
- Figure 10B. Well-formed low-angle boundary in quartz from the wall rock of sample fractured at 25°C and 500 bars.
- Figure 11. Electron micrograph of microcline showing orthogonal sets of fine lamellae.
- Figure 12A. Low-power overview of gouge fragments from sample fractured at 25°C and 500 bars.
- Figure 12B. Closer view of gouge in area of Figure 12A.
- Figure 12C. High magnification view of small grains in area of Figure 12A.
- Figure 12D. Fragments of quartz gouge with dislocation, from sample faulted at 25°C and 500 bars.
- Figure 13A. High dislocation density ( $\sim 2 \times 10^9 \text{ cm}^{-2}$ ) in quartz deformed at 530°C and 2.5 kbar.

Figure 13B. Dense tangles of dislocations ( $\rho \sim 10^{11} \text{ cm}^{-2}$ ) in quartz deformed at  $700^{\circ}\text{C}$  and 2.5 kbar. Note the undeformed areas having dislocation substructure similar to that of quartz in  $25^{\circ}\text{C}$  sample.

Figure 14. Density of free dislocations in quartz deformed at various temperatures in faulted granite. Each open circle represents the count from one micrograph irrespective of the area of the micrograph; the black square is the average dislocation density, averaged over the area. The arrowed circles represent the maximum density measurable in areas of dense tangles; the true maximum was much higher. All samples shown were deformed at 2.5 kbar, except that at  $630^{\circ}\text{C}$ , deformed at 4 kbar.

Figure 15. Oligoclase feldspar at the edge of a fault deformed at  $700^{\circ}\text{C}$  and 2.5 kbar.

Figure 16. Muscovite at the edge of a fault deformed at  $700^{\circ}\text{C}$  and 2.5 kbar.

Figure 17A. Fault gouge deformed at  $700^{\circ}\text{C}$  and 2.5 kbar. The light speckled region is inferred to be epoxy.

Figure 17B. Fault gouge deformed at  $700^{\circ}\text{C}$  and 2.5 kbar.

Figure 17C. Fault gouge deformed at  $700^{\circ}\text{C}$  and 2.5 kbar. The gouge in this region is composed mainly of microcline.

Figure 17D. Fault gouge deformed at  $450^{\circ}\text{C}$  and 2.5 kbar.

Figure 18A. Fault gouge deformed at  $450^{\circ}\text{C}$  and 4 kbar.

Figure 18B. Fault gouge deformed at  $630^{\circ}\text{C}$  and 4 kbar.

Figure 18C. Fault gouge deformed at  $630^{\circ}\text{C}$  and 4 kbar. Note the large grain of microcline containing fine cross lamellae.

Figure 19. Electron diffraction pattern of fault gouge, containing predominantly quartz, deformed at 700°C and 2.5 kbar.

Figure 20. Shear stress for sliding in granite at different temperatures at 2.5 kbar pressure and a sliding rate of  $10^{-4}$  cm/sec. The joined points are measurements made on the same sample. The heavy line is the empirical flow law derived from rate and activation energy measurements and fitted at an assumed transition temperature of 500°C. The dotted curve is the same equation assuming a transition at 550°C. The dashed portion of the curve is the extrapolation below the stick slip--stable sliding boundary (shown at about 250°C).

Figure 21. Relation between sliding rate and shear stress at different temperatures calculated from the empirical sliding law. The vertical bar shows the range of experimental sliding rates used in this study.

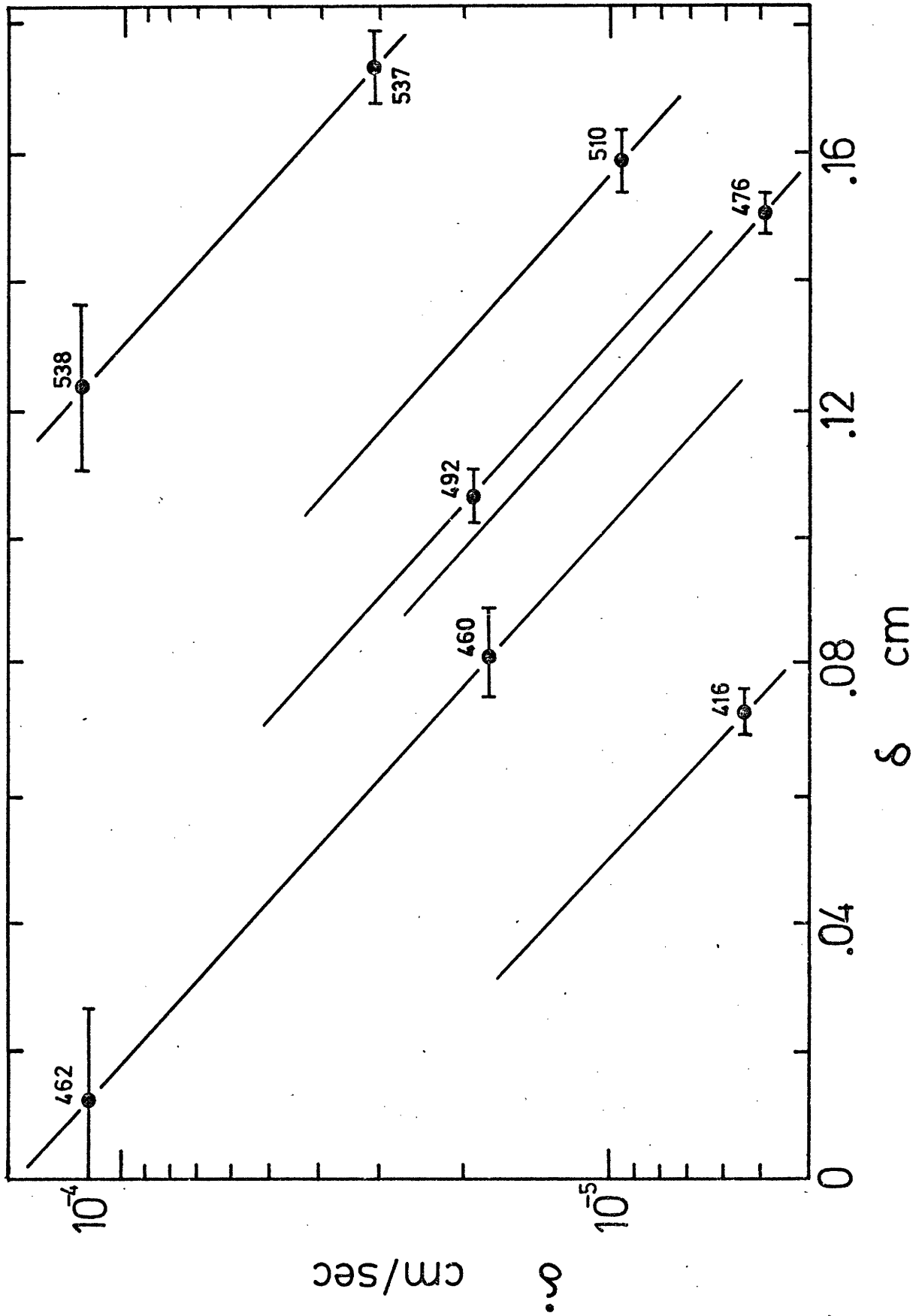


FIG 1

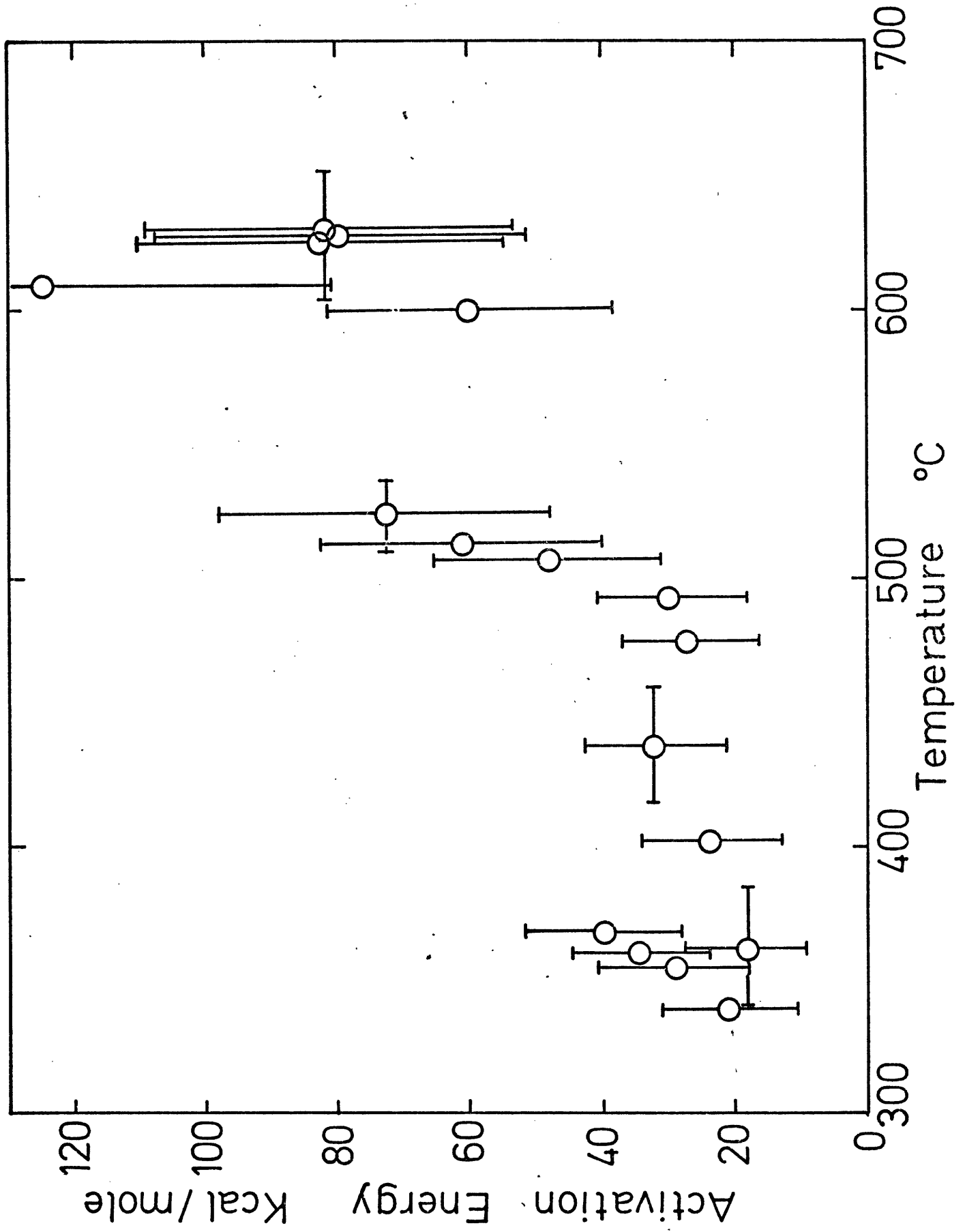


Fig. 2





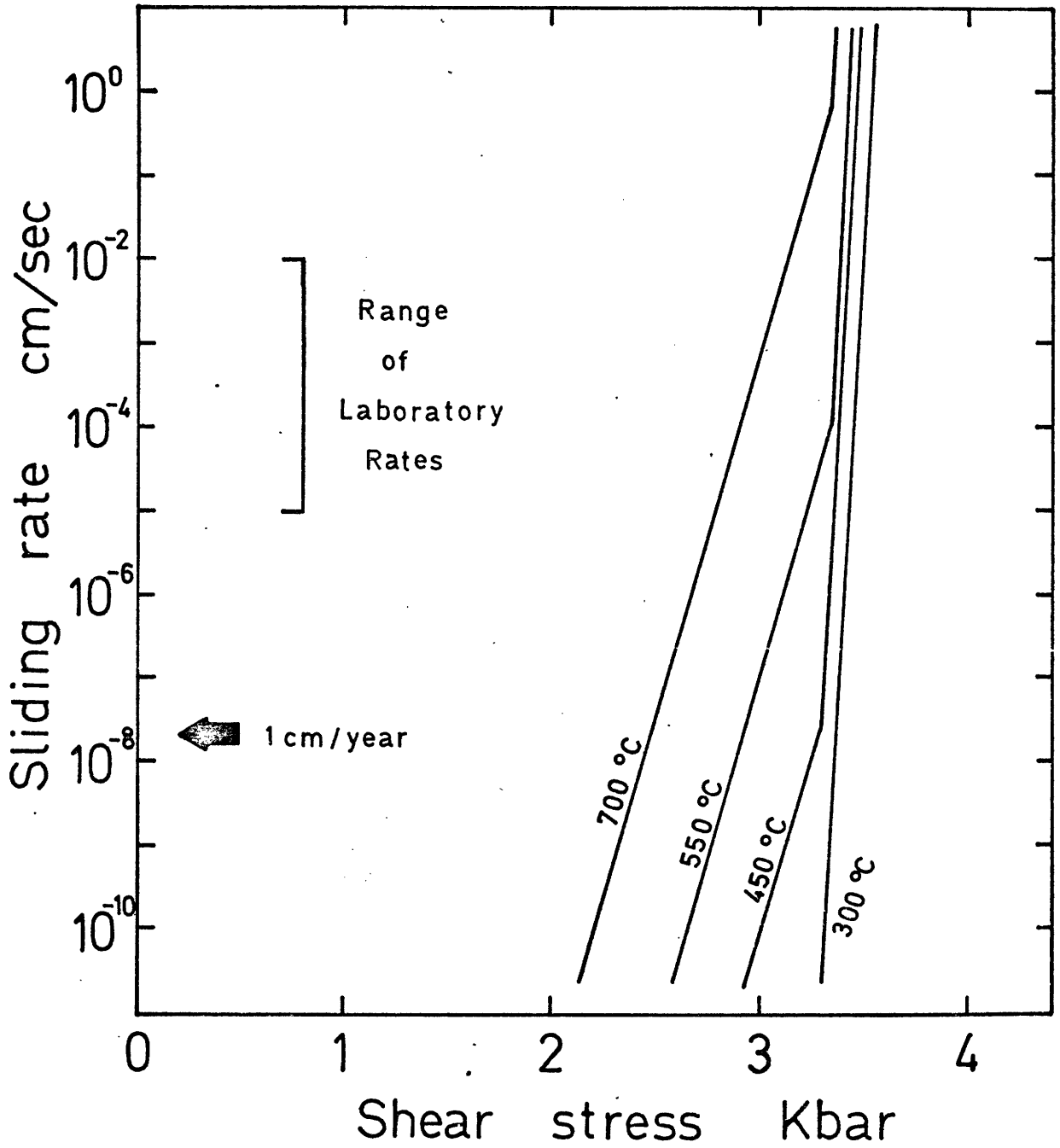


FIG 21.

## CHAPTER V

### ESTIMATION OF FRICTIONAL STRESS ON THE SAN ANDREAS FAULT FROM LABORATORY MEASUREMENTS

#### ABSTRACT

The average frictional shear stress for the San Andreas fault estimated from high temperature friction measurements is almost an order of magnitude higher than the limits placed by heat flow measurements. This difference cannot be explained simply by the fractured character of rocks in the fault zone, by the high temperatures at depth, or by the presence of serpentine. It could be explained by low strength alteration materials in the fault zone or by pore pressures considerably in excess of hydrostatic. These possibilities can be tested by direct sampling of the fault at depth. The low geological rates and the large scale of the natural fault compared to the laboratory sample also may be important differences, but present data are insufficient for their evaluation.

#### INTRODUCTION

Recent studies of heat flow on several portions of the San Andreas fault (Henyey and Wasserburg, 1971) have revealed that no significant anomaly occurs. Brune and others (1969) argued that this lack of anomaly puts an upper limit on the average frictional stress of about 250 bars. Such low stress does not seem to be compatible with laboratory observations of rock strength (for example, Griggs et al., 1960) or friction strength (Stesky et al., 1974) at the temperatures and pressures

appropriate for the earth's crust. Indeed, laboratory measurements of friction predict that the heat flow anomaly on the San Andreas fault should be several times larger than that actually measured (Stesky and Brace, 1973). How can these differences be explained? In this paper, I will examine this question in the light of our present understanding of friction in rocks. Several alternate explanations can be suggested to account for the difference in stress estimate, a number of which can be tested by laboratory and field observations.

#### CONSTRAINTS OF HEAT FLOW DATA

Henyeu measured the heat flow produced near major strike-slip faults in the San Andreas fault system of California (Henyeu and Wasserburg, 1971). He found a mean value of  $1.65 \mu\text{cal}/\text{cm}^2/\text{sec}$  and profiles made across several faults showed a maximum anomaly of  $0.5 \mu\text{cal}/\text{cm}^2/\text{sec}$ , located at the faults. Correction of the data for extraneous effects reduced the anomaly to about  $0.3 \mu\text{cal}/\text{cm}^2/\text{sec}$ .

Brune and others (1969) calculated several models of the distribution of shear stress with depth on a vertical strike-slip fault which would be required to produce the observed heat flow anomaly by frictional heating. Assuming a steady-state creep rate of 5 cm/year, they estimated that for all models, an average stress of about 100 bars is required for the upper 20 km of the fault. Heating from greater depth has negligible effect on the surface heat flow anomaly and so the stresses much below 20 km are indeterminate by this technique (Brune et al., 1969). This analysis assumed that all the mechanical work is converted to heat in the form of friction. On the other hand, if part of the energy is released as seismic radiation, the average strength of the fault would be higher. Brune and others (1969) estimated that for a maximum apparent seismic

stress of about 100 bars and a maximum stress drop of 100 bars, the upper limit on the fault strength is about 250 bars.

#### EXPERIMENTAL OBSERVATIONS

Measurement of the frictional strength of faulted rock at high temperature and pressure is now possible (Brace and Byerlee, 1970) and data exist for a number of rocks at pressures from 2 to 6 kbars and temperatures to 700°C (Stesky et al., 1974). These rocks include Westerly granite, San Marcos gabbro, Mt. Albert peridotite, Twin Sisters dunite, Snowy Mountain anorthosite, and partly serpentinized Spruce Pine dunite. Faults were formed in cylinders of rock at 500 bars pressure and 25°C by axial loading in a triaxial deformation apparatus. The pressure and temperature were then raised to the desired conditions and the cylinder reloaded until sliding occurred. Measurements of axial force, confining pressure, and fault angle were then used to calculate the shear stress for sliding. In a few high temperature runs, water at high pressure was present in the rock sample; for most, however, the samples were nominally dry and vented to the atmosphere. Complete descriptions of the experimental technique and measurements were given earlier (Stesky et al., 1974).

The frictional stress,  $\tau$ , varies with temperature and pressure. The data for one rock, Westerly granite, are shown in Figure 1, with contours of  $\tau$ . There is some scatter in the measurements, due in part to variations in fault angle. Also shown is the approximate boundary between stick-slip, at low temperatures and high pressures, and stable sliding, at high temperatures (Brace and Byerlee, 1970). There seems to be little change in frictional strength across the boundary; so stable sliding does not represent weakening of the fault. On the contrary, Engelder (1974)

suggested that the friction stress during stable sliding may be slightly higher than during stick-slip.

Up to about 500°C, the friction stress in Westerly granite was relatively unaffected by temperature. It decreased 2 or 3% per 100° increase. Above 500°C,  $\tau$  decreased more rapidly with temperature at a given pressure, on the order of 20 % per 100°. This change in behavior is related in part to the increased ductility of quartz in the granite above 500°C (Chapter IV). Below 500°C, the deformation seems largely to be brittle. San Marcos gabbro behaved somewhat similarly, although the transition in temperature sensitivity was at a lower temperature, near 300°C. No information exists on the deformation mechanisms of the gabbro.

Our data for other rock types are more limited, although we can compare all of the rocks at the same confining pressure. Figure 2 shows the variation of friction stress with temperature for a number of rocks at 4 kbars pressure and a constant shortening rate of  $10^{-5}$  sec<sup>-1</sup>. Included also are measurements of two serpentinites, studied by Raleigh and Paterson (1965), and granite sand at 3.1 kbars pressure and large strain (Byerlee and Brace, 1969).

For the rocks that we studied, the friction stress varied somewhat widely with rock type, although much less than for fracture strength (Handin, 1966). Most rocks had a higher temperature dependence below 500°C than the granite. The serpentinites do not seem to be significantly weaker than the other rocks, at least below the temperature at which dehydration occurs (300° to 500°C). The crushed granite sand, a possible analogue for gouge, is similarly quite strong and at higher pressures approaches the strength of intact rock.

## CALCULATION OF SHEAR STRESSES ON SAN ANDREAS FAULT

To estimate the stresses, a dynamic model of the fault is required. We assume that the San Andreas is a vertical strike-slip fault and that the vertical principal compressive stress can be estimated as a function of depth. Then there are two special cases of stress state. In case I, the vertical, or intermediate, stress is equal to the minimum horizontal stress, taking compression positive. This case is equivalent to the laboratory triaxial test. In case II, the vertical stress is equal to the maximum horizontal stress. For faulting, these two cases are the limits of stress within which a vertical fault would be formed. For friction, the stresses may exceed these limits, but only by an amount necessary for a fault of a new orientation to form. However, for many rocks, below a few kilometers depth, fracture and friction strengths may be similar, so these cases may be considered as approaching the limits for friction also.

The two stress states can be plotted as circles on a Mohr diagram (Figure 3), from which the shear stress for sliding can be read. We assume that the fault angle is  $30^{\circ}$ , that the effective vertical stress is given by the lithostatic minus the hydrostatic pressure, and that the temperature is given by the Basin-and-Range geotherm (shown stippled in Figure 1). These temperatures are likely to be on the high side (Heney and Wasserburg, 1971), but will give us minimum values of stress. The results for gabbro are shown in Figure 4. Gabbro was chosen since it fell within the band of friction strengths of rocks measured in our laboratory (Figure 2). The error bars are related both to scatter in the data and to inaccuracies in extrapolating to normal stresses lower than in our experiments. Also shown are the results of similar calculations for a number of other rock types, to be discussed later.

Based on our measurements, then, the frictional stress on the San Andreas fault should fall somewhere between the curves I and II in Figure 4. Without further assumption as to stress state, the choice cannot be narrowed further. Some support for case I in the vicinity of the Transverse Ranges is suggested by thrust faulting associated with the San Andreas system; for thrust faults the vertical stress is the least principal compression (Figure 3).

The average frictional stress over a 20 km depth predicted by our studies would range from 750 bars for case II to 2000 bars for case I. These values are clearly higher than the 250 bars maximum stress calculated by Brune and others (1969) from heat flow studies. Following Brune and others (1969), we can calculate the heat flow anomaly for our model. The shear stress is approximated as a linear function of depth and the heat-flow equation for a planar source is used (equation 4a of Henyey and Wasserburg, 1971). For a sliding velocity of 5 cm/year, the heat flow anomaly would be between 1.7 and 6.7  $\mu\text{cal}/\text{cm}^2/\text{sec}$ . These values are 5 to 20 times greater than observed.

In this calculation we have assumed that all the mechanical energy is converted to heat. But there are likely to be other energy sinks, for example, seismic radiation and new surface area. Are they sufficiently large to account for the low heat flow? Assuming an average shear stress,  $\tau$ , of 1 kbar, a fault depth,  $D$ , of 20 km, and a sliding velocity,  $\dot{\delta}$ , of 5 cm/year, the mechanical energy released per unit fault length is given by  $E = \tau \dot{\delta} D$ , or about  $10^{16}$  ergs/year/cm length. The seismic energy,  $E_s$ , released is likely to be comparable to that released by the San Francisco earthquake ( $M \sim 8.3$ ) occurring every hundred years ( $E_s \sim 10^{23.7}$  ergs/year). For a fault length of about 1000 km, the seismic energy released is about

$5 \times 10^{15}$  ergs/year/cm length. Brune and others (1969) estimated that the energy lost due to seismic radiation corresponded to a shear stress difference of about 150 bars. Thus it seems likely that only a portion of the mechanical energy is removed by seismic waves. In any case, many areas of the San Andreas are creeping aseismically, so that the seismic energy produced is negligible.

The creation of new surfaces by fracture in the fault zone requires energy in the form of surface energy. Brace and Walsh (1962) measured the fracture surface energy for a number of minerals, a typical value being about  $1000 \text{ ergs/cm}^2$ . Using this value, it is easy to show that for a shear stress of 1 kbar, a fault depth of 20 km, and a total offset of 300 km (Hill and Hobson, 1968), the total energy released is  $6 \times 10^{22}$  ergs/cm fault length and, if all this energy is used to make new surface, all rock within 2000 km of the fault would be reduced to 1  $\mu\text{m}$ -sized grains! Clearly, new surface is a negligible sink for mechanical energy.

Thus the majority of the frictional energy expended in our fault model would be released as heat and would produce the heat flow anomaly. That no anomaly has been measured on the San Andreas fault suggests that our model must be reconsidered. The difference may be due in some way to the materials we have chosen for our experiments or the conditions we have used for the 20 km deep seismic zone.

One possibility is that the actual materials in the fault zone are quite different from the rocks we have studied. The fine-grained crushed rock of the fault zone is susceptible to hydrothermal alteration producing clays, carbonates, serpentine, chlorite, and other hydrous minerals. Frictional data seem to be available for only a few such materials (Figure 4). Serpentine seems to be as strong as fresh silicate rocks (Handin,

1964); the calculated shear stresses are bounded by those of the gabbro. Clays and carbonates are somewhat weaker (Mauer, 1965; Donath et al., 1972) and predict fault strengths approaching that estimated by Brune and others (1969). Clearly, additional work is needed, particularly on actual fault zone materials.

Another important factor may be pore pressure. In our calculations we assumed that pore pressure was hydrostatic; as the pore pressure approaches lithostatic, the shear stress to cause sliding drops. Figure 5 shows the effect that varying the pore pressure has on the fault strength at 15 km depth. For a hydrostatic pore pressure the stress is 3.5 and 1 kbars for case I and II, respectively. For a pore pressure equal to 90% of lithostatic, the stresses drop to about 500 and 100 bars, respectively. The average frictional stress would be between 60 and 350 bars. High pore water pressure has been measured in a number of drill holes near the San Andreas fault (Berry, 1973). The high pressures are associated with the Franciscan complex and are near lithostatic in places. Berry suggested that the pore pressure decreases to near hydrostatic at the fault, but there seems little data to settle the question conclusively.

For aqueous pore fluids there may be other effects as well, such as pressure solution and stress corrosion. Field evidence shows that pressure solution may be important for faults in quartzose rocks (Elliot, 1973), but we have little knowledge of the strengths implied by the process. Byerlee (1967) found that water produced a weakening of about 400 bars in his laboratory faults at 25°C. In a few experiments at higher temperature, we found that water had little effect on the friction stress, within the scatter of the measurements (Stesky et al., 1974). Whether water is more important at the lower rates in nature or in other rock types is not known; clearly, this is an area for much further research.

Sliding rate, another important factor, may be quite different in the laboratory than in the earth. Experiments have shown that two types of rate effects exist, depending on the sliding behavior (Dieterich, 1972; Chapter II). Decreasing the rate causes the stick-slip stress to increase but the stable sliding stress to decrease. Thus, in earthquake areas, the fault may strengthen with time between events. Fault creep, on the other hand, may occur at much lower stresses than stable sliding does in the laboratory. But experiments suggest that at temperatures below 400°C the rate effect is small. The stress changes by only a few percent for three orders of magnitude change in rate (Chapters II and IV).

The final difference between the laboratory and the earth is that of scale. Natural faults are larger, thicker, and more irregular than their laboratory counterparts. In addition, they pass through rocks of different properties, rather than the homogeneous rock used in experimental work. We may never be able to truly simulate natural faults in detail, but a few factors may be evaluated.

The thickness of gouge may cause a significant difference between field and experiment. Granular materials like crushed rock or sand are quite strong, under confining pressure, after large strain, at least at room temperature (Figure 2). The crushed granite sample with a shear zone about 1 cm wide sustained nearly the same shear stress as a 0.5 mm wide fault in granite rock. At lower pressure, the crushed rock was somewhat weaker than the faulted rock, suggesting that gouge thickness may be more important at shallow depths. On the other hand, field studies suggest that even for wide fault zones, the deformation may be confined to narrow regions within the broad zone (Engelder, 1974).

Fault area may also be an important factor. Pratt and others (1974) found that joint strength decreased by 50% for two orders of magnitude increase in joint area. The cause of this decrease is poorly understood but may be related to variations in true contact area. It is not known whether a similar size effect occurs also with gouge-filled faults.

#### CONCLUSION

The average frictional shear stress for the San Andreas fault, estimated from laboratory experiments, is almost an order of magnitude higher than the limit placed by heat flow measurements. This difference cannot be explained simply by the fractured character of the rocks in the fault zone, or the high temperatures; we show that fractured rocks sustain high shear stresses at the pressure and temperature conditions assumed for the upper 20 km of the fault zone. Several possible explanations, such as the effects of rate, scale, and chemical activity of water, await further experimental work for their evaluation. Two possibilities could be tested by drilling into the fault zone. One is that the fault zone is composed of weak alteration materials such as clays and carbonates. If this proves to be the case, a powerful constraint may be placed on the physical models of the earthquake; stick-slip or brittle fracture would seem to be ruled out. The other possibility is that the pore pressure is high, perhaps close to lithostatic pressure; such high pressure could lower the friction stress to levels compatible with the limits imposed by heat flow and at the same time permit sudden stress drops through fracture or stick-slip.

#### ACKNOWLEDGMENTS

The experimental studies were supported by the U.S. Geological Survey under Contract No. 14-08-0001-13229.

## REFERENCES

- Berry, F.A.F., 1973. High fluid potentials in California Coast Ranges and their tectonic significance. *Bull. Am. Assoc. Pet. Geol.*, 57 (7): 1219-1248.
- Brace, W.F. and Byerlee, J.D., 1970. California earthquakes: Why only shallow focus? *Science*, 168: 1573-1575.
- Brace, W.F. and Walsh, J.B., 1962. Some direct measurements of the surface energy of quartz and orthoclase. *Am. Min.*, 47: 1111-1122.
- Brune, J.N., Henyey, T.L. and Roy, R.F., 1969. Heat flow, stress, and rate of slip along the San Andreas Fault, California. *J. Geophys. Res.*, 74(15): 3821-3827.
- Byerlee, J.D., 1967. Frictional characteristics of granite under high confining pressure. *J. Geophys. Res.*, 72(14): 3639-3648.
- Byerlee, J.D. and Brace, W.F., 1969. High-pressure mechanical instability in rocks. *Science*, 164: 713-715.
- Dieterich, J.H., 1972. Time-dependent friction in rocks. *J. Geophys. Res.*, 77 (20): 3690-3697.
- Donath, F.A., Fruth, L.S., Jr., and Olsson, W.A., 1972. Experimental study of frictional properties of faults. In: *New Horizons in Rock Mechanics*, 14th Symp. Rock Mech., University Park, Penn.: 189-222.
- Elliot, D. 1973. The motion of thrust sheets. *Am. Geophys. Union, Trans.*, 54(4): 462 (abstract).
- Engelder, J.T., 1974. Coefficients of friction for sandstone sliding on quartz gouge. In: *Advances in Rock Mechanics*, Vol. II, Part A, *Natl. Acad. Sci.*, Washington, D.C.: 499-504.
- Griggs, D.T., Turner, F.J., and Heard, H.C., 1960. Deformation of rocks at 500° to 800°C. In: D.T. Griggs and J. Handin (Editors), Rock Deformation, *Geol. Soc. Am., Mem.*, 79: 39-104.

- Handin, J., 1964. Strength at high confining pressure and temperature of serpentinite from Mayaguez, Puerto Rico. In: A Study of Serpentinite, Natl. Acad. Sci. -- Natl. Res. Council Publ., 1188: 126-131.
- Handin, J., 1966. Strength and ductility. In: S.P. Clark, Jr. (Editor), Handbook of Physical Constants. Geol. Soc. Am., Mem., 97: 223-290.
- Henye, T.L. and Wasserburg, G.J., 1971. Heat flow near major strike-slip faults in California. J. Geophys. Res., 76(32): 7924-7946.
- Hill, M.L. and Hobson, W.R., 1968. Possible post-Cretaceous slip on the San Andreas fault zone. In: W.R. Dickinson and A. Grantz (Editors), Proc. Conf. on Geological Problems of the San Andreas Fault System. Stanford Univ. Publ., Stanford, Calif., 9: 123-
- Mauer, W.C., 1965. Shear failure of rock under compression. J. Soc. Petrol. Eng., 5(2): 167-
- Pratt, H.R., Black, A.D., and Brace, W.F., 1974. Friction and deformation of jointed quartz diorite. In: Advances in Rock Mechanics, Vol. II, Part A, Natl. Acad. Sci., Washington, D.C.: 306-310.
- Raleigh, C.B. and Paterson, M.S., 1965. Experimental deformation of serpentinite and its tectonic implications. J. Geophys. Res., 70(16): 3965-3985.
- Stesky, R.M. and Brace, W.F., 1973. Estimation of frictional stress on the San Andreas fault from laboratory measurements. In: R.L. Kovach and A. Nur (Editors). Proc. Conf. on Tectonic Problems of the San Andreas Fault System. Geol. Sci., XIII, Stanford Univ., Stanford, Calif.: 206-214.
- Stesky, R.M., Brace, W.F., Riley, D.K., and Robin, P.-Y.F., 1974. Friction in faulted rock at high temperature and pressure. Tectonophysics, 23: 177-203.

## FIGURE CAPTIONS

- Figure 1. Shear stress during sliding on a fault in granite as a function of effective confining pressure and temperature. Contours of 3, 4, and 5 kbar shear stress are shown, as well as the stick slip--stable sliding boundary (short dashes). The Basin-and-Range geotherm, assuming hydrostatic pore pressure, falls between the dotted lines; this geotherm was used to construct Figure 4.
- Figure 2. Stress difference for sliding on a fault in various rocks and granite sand at 4 kbar confining pressure as a function of temperature. Ant. and Liz. refer to antigorite-bearing and lizardite-bearing serpentinites of Raleigh and Paterson (1965).
- Figure 3. Two special stress states, I and II, for a vertical wrench fault and known vertical principal stress.
- Figure 4. Shear stress on a vertical wrench fault for cases I and II of Figure 3, along the geotherm shown in Figure 1. Shear stress for serpentinite (Raleigh and Paterson, 1965) and for slate and shale (Mauer, 1965) are also shown.
- Figure 5. The effect of pore pressure,  $P_p$ , on the frictional stress for cases I and II, assuming the effective pressure law:
- $$\tau = f(\sigma_n - P_p),$$
- where  $\tau$  and  $\sigma_n$  are the shear and normal stresses and  $f$  is some function. The vertical dashed line marks approximately the case of hydrostatic pore pressure.

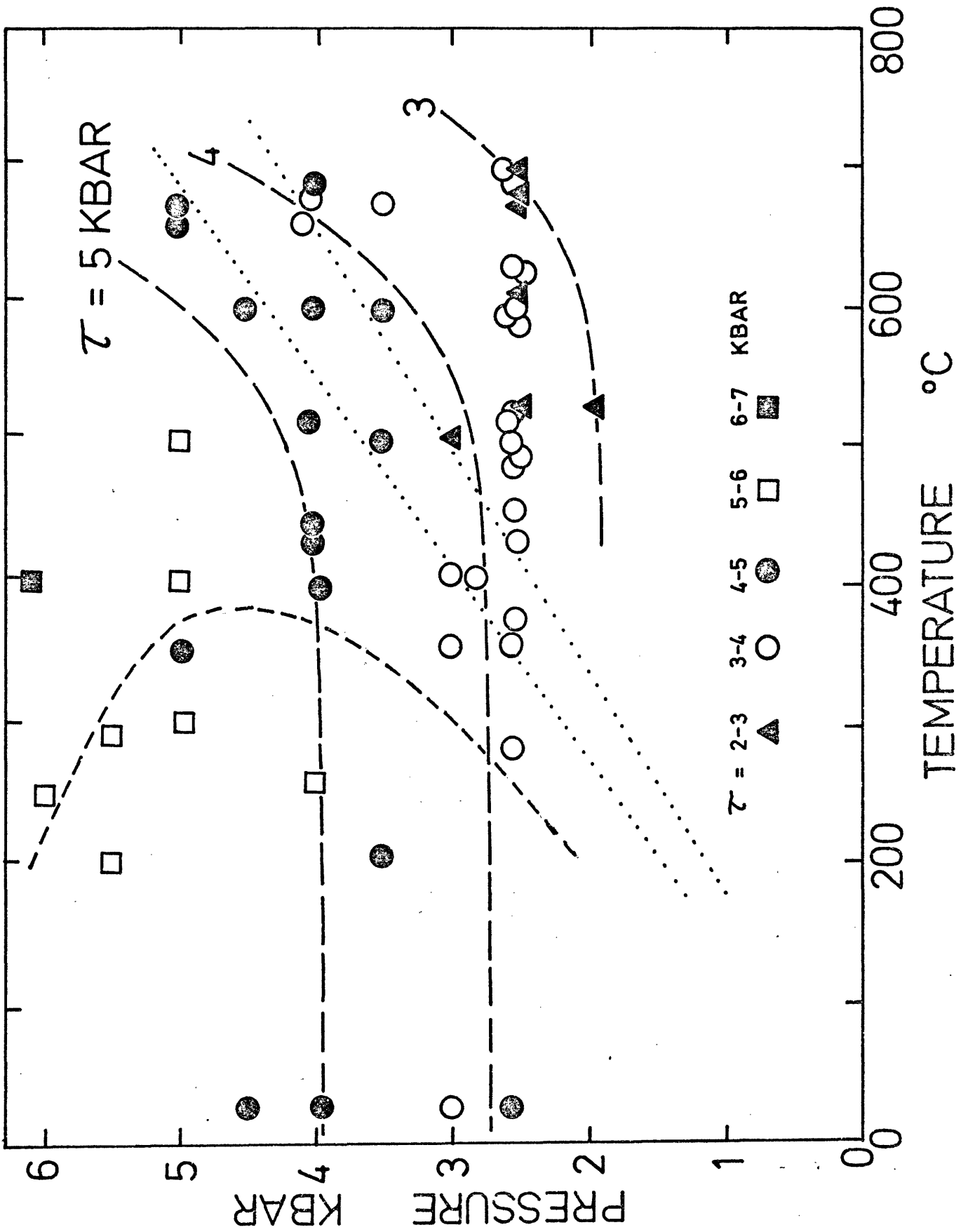


FIG 1

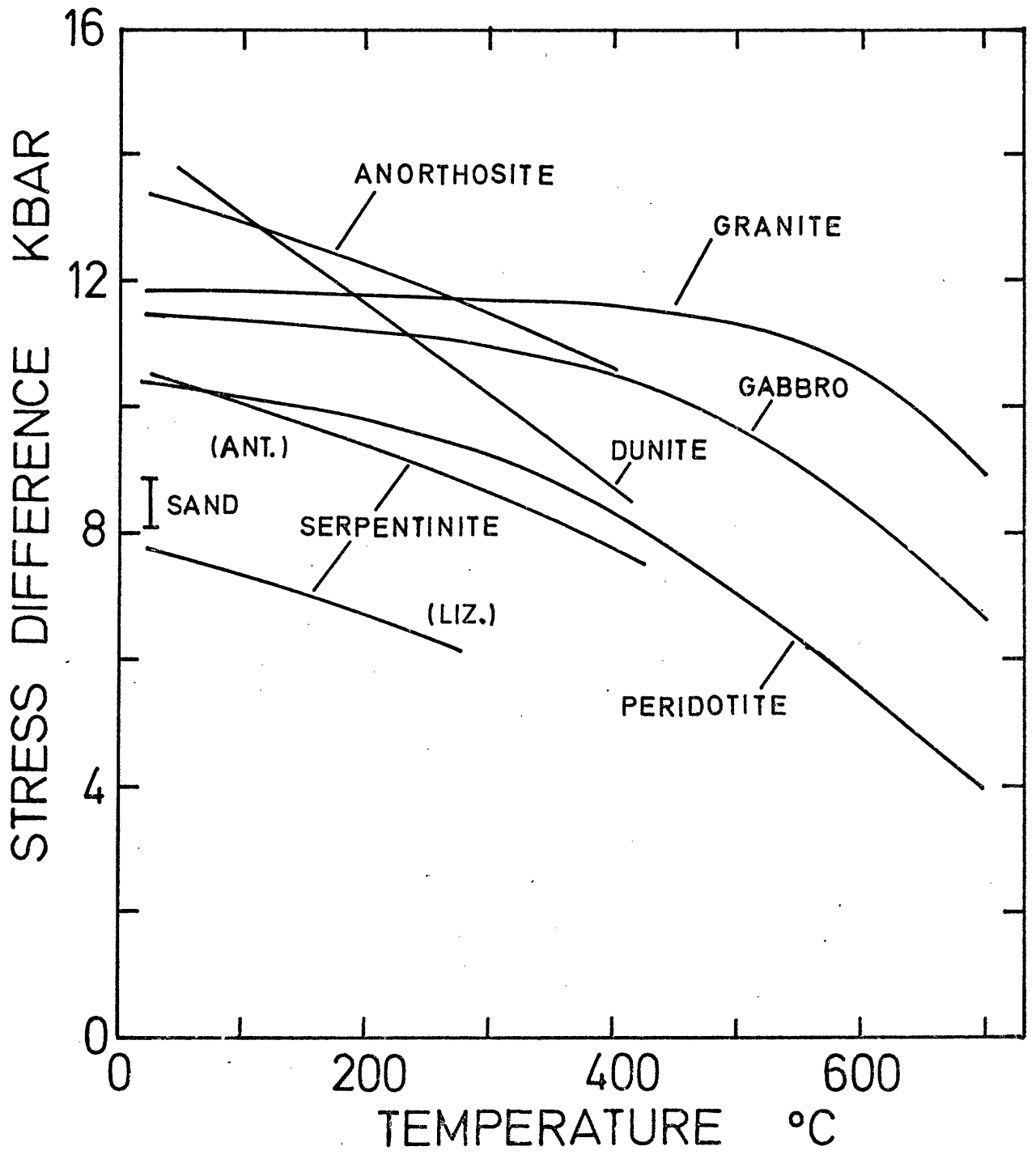


FIG 2

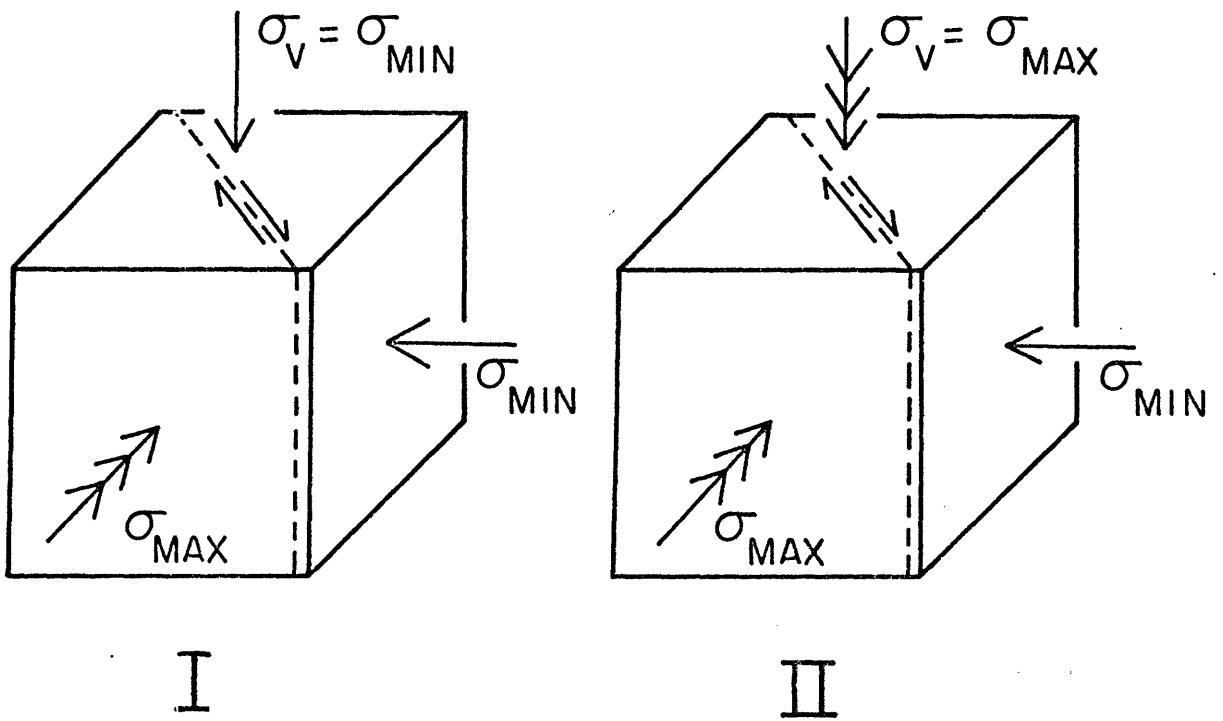
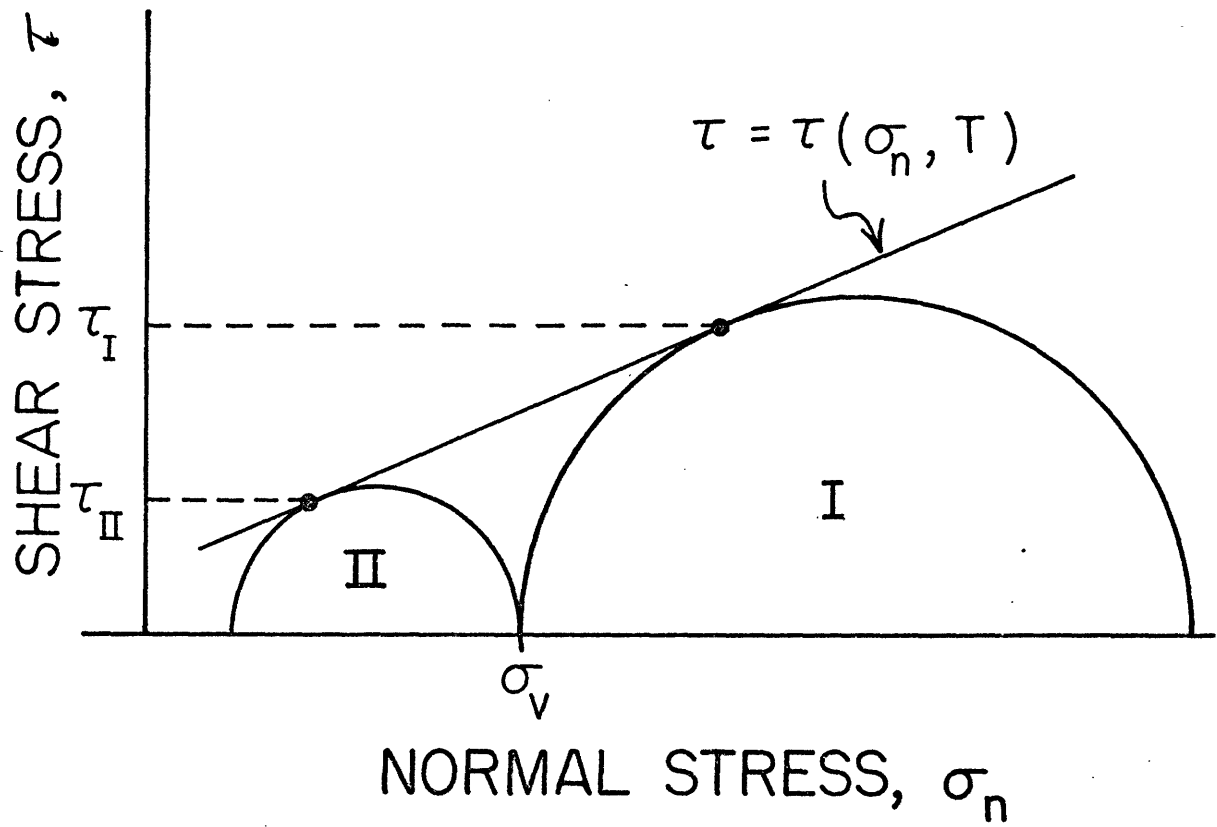


FIG 3

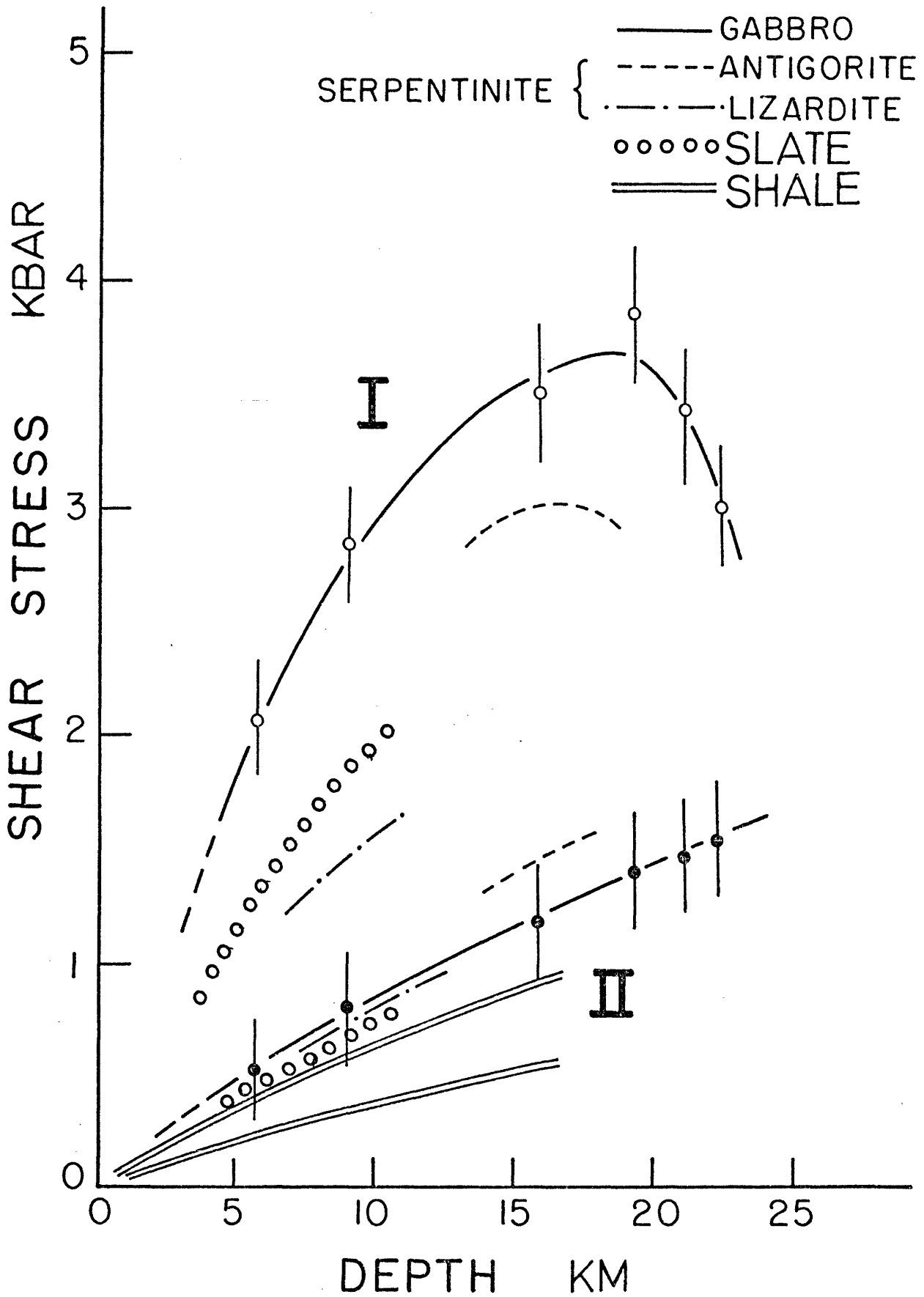


FIG. 4

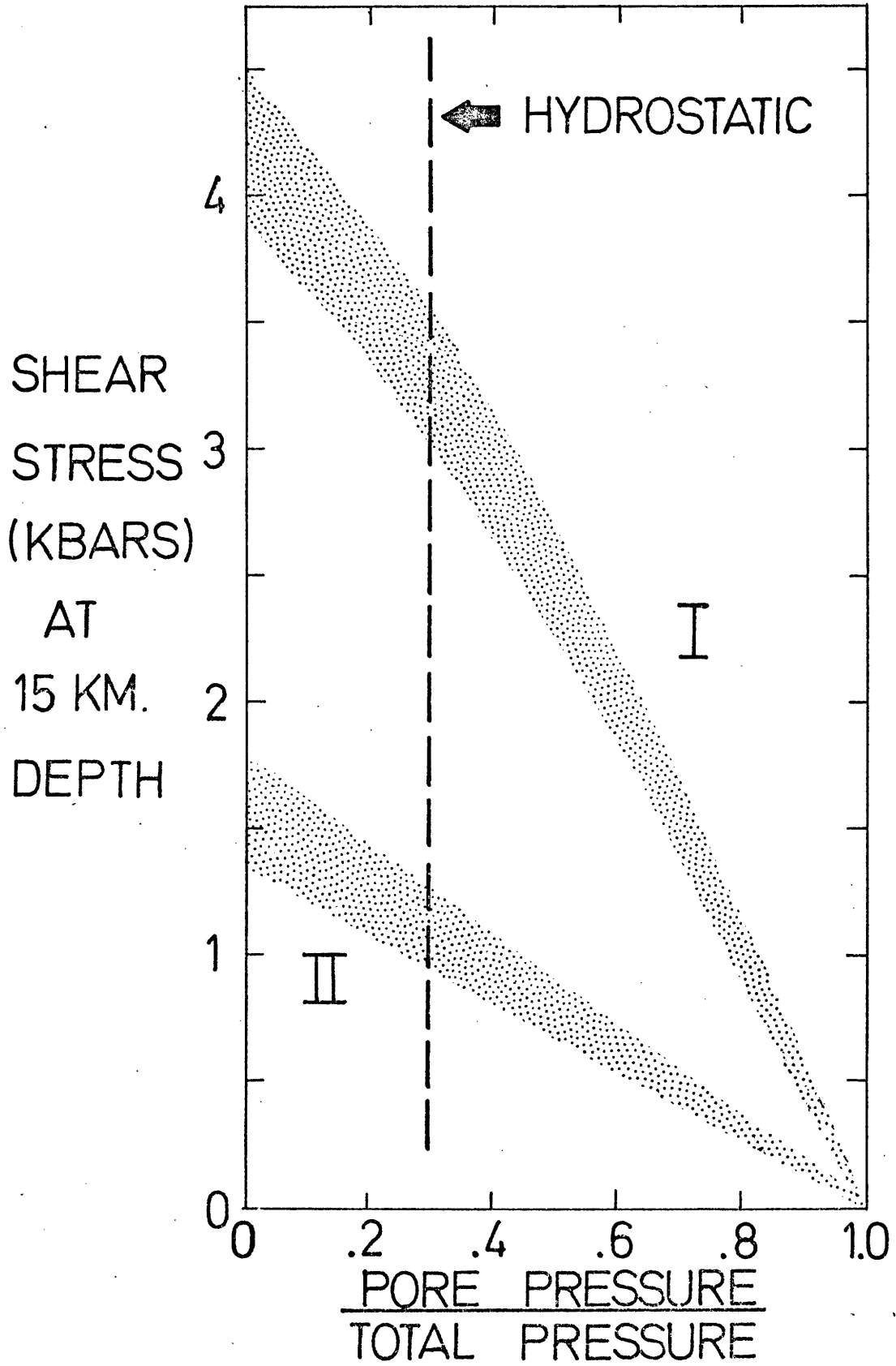


FIG 5

## SUMMARY

This thesis is the result of a study of how faulted rock behaves under stress at high temperature and pressure and what processes determine this behavior. The study was prompted by the realization that very little information exists on the mechanical properties of faults under these conditions. Yet such data are crucial if we are to understand natural faults. Since temperature increases with depth in the earth, studies of fault behavior at room temperature may have no relevance to natural faults at depth. Further, experience has shown that the processes that occur at very low rates in the earth can be studied in the laboratory by using high temperature, which speeds up the processes. Thus laboratory measurements at high temperature can be extrapolated to the much lower rates in nature.

The problem was examined in several ways. First I measured the stress needed to cause sliding at different temperatures, pressures, and sliding rates. I used several different rocks so that I could see how changes in rock type affect the measurements. Further, in two experiments made at high temperature, rocks containing water were used to see whether presence of water has a marked effect.

Then, once the mechanical characteristics of the faults were established, I attempted to learn for one rock, a granite, what processes were occurring in the fault zone and how they produced the observed fault behavior. To discover the processes, I used a combination of (1) mechanical

tests designed to detect the presence of brittle cracking and to determine the activation energy for sliding, and (2) petrographic examination of the deformed fault material.

When the processes can be fully understood, the properties of faults in the earth can be predicted. Although our understanding is still imperfect, I applied our existing knowledge to a geological problem: the strength of the San Andreas fault.

I sought the answers to several key questions. First, in what ways and under what conditions can sliding occur along a fault? Earlier work showed that sliding can occur in two ways: (1) in a jerky manner, called stick-slip, where sliding occurs in a series of sudden, rapid, and audible slips, and (2) in a smooth, steady manner, called stable sliding. Apparently, stick-slip is prevalent at low temperatures and high pressures, while stable sliding occurs at high temperatures. Because stick-slip may be a possible earthquake mechanism, I wanted to better define the conditions under which it occurs. Using measurements made by W.F. Brace and D.K. Riley, I found that stick-slip occurs in many different rocks, including granite, gabbro, dunite, quartzite, and anorthosite, and under nearly the same conditions in each: pressures of 2 to 4 kbar and temperatures up to 200 - 300°C. One rock, the quartzite, was unusual because stick-slip occurred up to 450°C; on the other hand, another rock, a peridotite, did not slide by stick-slip motion even at room temperature.

A second key question area was: What is the strength of faulted rock? Is it different for the two kinds of sliding motion? How is it affected by temperature, pressure, and sliding rate? I found that, remarkably, the stress to cause sliding in faulted rock is little affected by rock type, temperature, sliding rate, and presence of water over the range of

conditions found in the upper 20 km of the earth's crust. Pressure, on the other hand, affects the strength quite dramatically: the strength at 4 kbars is nearly double that at 2 kbars. Thus, the strength of faults in the earth should increase rapidly with depth, because of the greater pressures, and should not depend strongly on the local geology, in many cases. Internal pore fluid pressure also should have a marked effect on the strength. Further, the stress for sliding depends little on the type of sliding motion; thus smooth, steady sliding does not necessarily imply a weak fault.

But to understand these results I had to probe deeper, to learn about the processes occurring in the fault zone during sliding. Why is it, for example, that two types of motion occur? One possibility is that smooth sliding at high temperature results from plastic flow of the fault material, since minerals tend to deform plastically at high temperature. But, then, why is the sliding stress so little affected by temperature and rate, much less so than is the stress for fracture or flow of solid rock? To answer some of these questions I concentrated my effort on one rock, Westerly granite, deformed at 2.5 kbars pressure. It is composed of several different minerals, two feldspars (microcline and oligoclase), quartz, and two micas (biotite and muscovite). Each deforms differently under different conditions. But up to about 500°C the dominant process seems to be brittle cracking of the fault material. Smooth, stable sliding, then, is not the result of plastic flow at high temperatures. The micas deform plastically, but do so at all temperatures, even at temperatures where stick-slip motion occurs. Thus, some other, more subtle, process must explain the difference in sliding motion.

Above  $500^{\circ}\text{C}$  the quartz, too, becomes plastic and causes the sliding stress to decrease more rapidly with increasing temperature and decreasing sliding rate. But still the changes in sliding stress are much smaller than observed for the strength of solid rock. To explain this difference I postulated that the porosity of the fault zone plays a role in determining its strength. A highly porous material is much weaker than a material with low porosity. Decreasing the sliding rate or increasing the temperature may allow the fault to become more compacted and hence stronger than if the porosity did not change. Thus the effect of sliding rate and temperature on the sliding stress is offset to some extent by the concurrent change in porosity. Note, too, that the effect of porosity helps to explain why many different rocks have nearly the same fault strength. Weak minerals will tend to compact to lower porosity than strong minerals, so that the difference in strength of the two porous materials is less than that of the minerals themselves.

While many questions have been answered, much work remains to be done. The over-riding question is still: What causes stick-slip sliding? Why does a  $50^{\circ}$  decrease in temperature cause a stable sliding fault to become unstable? A possible answer is again the role of porosity. If a fault zone, initially compacted, rapidly dilates, or increases in porosity, as sliding begins, then the fault could become very weak and hence slip rapidly. But what prevents this rapid increase in porosity at high temperature? Perhaps a few percent of mica or serpentine or other plastic mineral. Variations in porosity of the fault material may play a role in many aspects of fault behavior. But these ideas need to be tested experimentally. Very little attention has been paid to fault zone porosity in laboratory experiments. I anticipate that the results will be worth the effort.

Another important area for further work involves determining the role of mineral behavior during frictional sliding. I found that fault properties were markedly different depending on whether quartz (forming only 30% of the rock) deformed brittly or plastically. What happens if quartz is present in other proportions, or is the only mineral present? Quartzite slides with stick-slip motion up to very high temperatures, much higher than that for granite with 30% quartz. In fact, the transition to stable sliding in quartzite may occur only when the quartz becomes plastic. No weak minerals, such as mica, are present in the quartzite, suggesting again the importance of mineral behavior.

"It is useful to be assured that the heavings of the earth are not the work of angry deities. These phenomena have causes of their own."

Seneca (4 B.C.-A.D. 65)

## APPENDIX A

## SUMMARY OF FRICTION STRESS MEASUREMENTS

Tables I to IV summarize our measurements of the frictional strength and behavior of Westerly granite, San Marcos gabbro, Mt. Albert peridotite, Snowy Mountain anorthosite, Pigeon Cove granite, Rutland quartzite, and Twin Sisters dunite (see Table I, Chapter I, for description of these rocks). Except where otherwise noted, the piston-displacement rate,  $\delta$ , was approximately  $10^{-4}$  cm/sec.

The runs are arranged in order of increasing pressure, P. For runs involving several measurements of the same sample, the letter A, B, or C at the end of the sample designation indicates the order of the measurements. The temperatures, T, are averages estimated over the fault area. The differential stress,  $\sigma_D$ , was taken to be the peak stress, in the case of stick slip, or the steady sliding stress, in the case of stable sliding. The reproducibility of the frictional stress in duplicate experiments was about  $\pm 10\%$ . Often in stable sliding runs, particularly in runs involving several sliding measurements at different pressures and temperatures, the stress increased to a maximum, then decreased slightly to a residual constant value (see, for example, Chapter I, Figure 4). Such initial peaks were typically about 5% higher than the steady sliding stress. These differences were well within the scatter of the data and we made no special attempt at reaching final, steady sliding stress.

The fault displacement,  $\delta$ , was determined from the change in length of the sample after unloading. The maximum area change calculated from the displacement rarely exceeded about 8%. For the incremental runs, the displacement tabulated with the first data point in the series includes that estimated for the initial fracturing.

We also indicate the type of sliding motion. The characteristics of stick-slip (STK), stable sliding (STA), and transitional sliding (STA/STK) were discussed in Chapter I. For the sawcut and fracture series, the type of motion is explicitly stated. For the fault series, stable sliding was obtained in all but a few runs; only the exceptions are therefore indicated in the tables.

TABLE I

Sawcut series: Westerly Granite ( $\theta = 30^\circ$ )

Sample	Motion	P (kbar)	T ( $^\circ\text{C}$ )	$\sigma_D$ (kbar)	$\delta$ (mm)	Comments
H5	STA	1.00	303	3.2	2.1	$\dot{\delta} = 10^{-3}$ and $10^{-5}$ cm/sec
H16	STK	1.91	140	4.6	1.0	
H9A	STA	1.99	191	5.5	1.2	
H7A	STA	1.99	302	5.3	1.4	
H1	STA	2.08	468	2.7	2.8	$\dot{\delta} = 10^{-3}$ cm/sec
R2	STK	2.09	25	6.1	2.6	
R3	STK	2.09	25	6.3	2.3	
H2	STA	2.09	306	4.6	2.4	$\dot{\delta} = 10^{-3}$ cm/sec
H7B	STA	3.05	305	7.9	0.8	
R1	STK	3.14	25	7.9	3.1	
H9B	STK	4.00	197	9.1	1.0	
H4	STK	4.00	293	8.5	1.5	
H6	STA	4.02	440	4.8	1.4	

TABLE II

Fracture series

Sample	Motion	P (kbar)	T ( $^\circ\text{C}$ )	Sliding $\sigma_D$ (kbar)	$\delta$ (mm)	Fracture $\sigma_D$ (kbar)	$\theta$ (deg)	Comments
<u>Westerly granite</u>								
A27	STA	2.20	335	6.9	2.7	11.5	29	
A30	STA	2.50	302	7.5	3.2	11.9	30	
A38	STA	2.51	151	4.2	3.8	13.2	26	
A26	STA	3.00	340	8.3	2.7	12.9	31	
A48	STK	3.10	24	8.4	4.6	15.2	28	
A20	-	4.00	24	-	2.1	16.6	31	
A25	-	4.00	152	-	2.3	16.4	28	
A21	-	4.00	260	-	2.4	15.9	28	
A22	STA	4.00	305	12.2	1.9	15.3	32	
A11	STA	4.00	470	9.5	2.1	13.0	28	
A13	STA	4.01	355	11.8	1.5	14.5	30	
A12	STA	4.01	630	3.9	2.0	10.4	31	
A29	STA	5.00	355	13.1	1.7	15.7	32	
<u>San Marcos gabbro</u>								
A14	STA	3.00	300	8.2	2.3	10.2	30	
A19	?	4.00	24	-	1.3	13.2	31	
A47	STA/STK	4.00	24	11.7	2.0	13.8	32	Small, in- audible stress drops

TABLE II (continued)

## Fracture series

Sample	Motion	P (kbar)	T (°C)	Sliding $\sigma_D$ (kbar)	$\delta$ (mm)	Fracture $\sigma_D$ (kbar)	$\theta$ (deg)	Comments
<u>San Marcos gabbro (cont.)</u>								
A17	STA	4.00	203	10.0	1.7	12.2	29	
A16	STA	4.00	405	9.0	2.0	10.5	32	
A44	STA/STK	4.01	152	10.1	3.7	12.3	32	
A18	STA	4.02	100	11.2	1.8	13.0	30	
A15	STA	4.02	300	10.0	1.8	11.8	30	
<u>Twin Sisters dunite</u>								
A43	STA	3.53	106	>11.7	3.0	14.6	30	
A23	STK	4.00	24	14.6	3.3	14.8	32	
A39	STA	4.01	365	9.2	2.9	9.2	30	
A42	STA	4.02	192	11.7	2.5	15.2	33	
<u>Mount Albert peridotite</u>								
A24	STA	4.00	24	11.7	2.1	11.7	32	

TABLE III

## Fault series

Sample	P (kbar)	T (°C)	Sliding $\sigma_D$ (kbar)	$\delta$ (mm)	$\theta$ (deg)	Comments
<u>Westerly granite</u>						
S46A	1.00	25	4.5	1.4	27	
S46D	1.00	25	4.5	0.2	27	
S47A	1.00	25	4.9	2.1	27	
S47D	1.00	25	5.5	2.0	27	
S52D	1.00	25	6.0	0.5	27	
S46C	1.00	100	4.4	0.4	27	
S47C	1.00	100	5.3	1.0	27	
S46B	1.00	200	4.4	0.5	27	
S47B	1.00	200	5.2	1.0	27	
S50A	1.01	25	4.4	1.3	25	
S50D	1.01	25	4.8	0.3	25	
S50C	1.01	115	4.6	0.3	25	
S50B	1.02	220	4.5	0.3	25	
S45B	1.50	200	7.1	0.8	27	
H15	1.92	527	6.7	1.3	25	
S54A	1.99	570	6.8	1.7	28	
S54B	1.99	640	6.8	0.5	28	
S51A	2.00	225	7.2	2.3	25	

TABLE III (continued)

## Fault series

Sample	P (kbar)	T (°C)	Sliding $\sigma_D$ (kbar)	$\delta$ (mm)	$\theta$ (deg)	Comments
Westerly granite (continued)						
S52A	2.00	230	7.4	1.4	27	
S51B	2.00	300	7.5	0.6	25	
S52B	2.00	300	7.8	0.4	27	
S52C	2.00	400	7.8	0.3	27	
S58B	2.00	675	6.9	0.6	25	
S59	2.00	675	6.6	2.1	30	
S56B	2.01	357	7.2	0.3	24	
S57A	2.01	403	7.1	1.6	26	
S56A	2.01	430	6.8	1.8	24	
S57B	2.01	520	7.1	0.4	26	
S53A	2.02	370	7.9	1.5	29	
S55A	2.02	340	7.4	1.7	24	
S55B	2.02	440	7.5	0.6	24	
S58A	2.02	510	7.4	1.7	25	
S53B	2.02	515	8.2	0.4	29	
S53C	2.02	610	8.1	0.4	29	
S45A	2.50	325	9.2	2.4	27	
S40	2.50	380	8.9	2.7	24	
S28	2.51	303	10.7	1.9	(27)	Complex fault
S34	2.51	375	10.5	1.9	30	
S35	2.51	400	8.3	2.3	30	
S43	2.51	480	8.9	3.1	29	
S33	2.51	590	8.1	2.2	28	
S29	2.52	305	8.6	2.2	25	
S41	2.52	350	8.2	3.1	29	
S31A	2.52	626	7.9	1.0	29	
S49	2.52	630	7.8	3.0	25	
S27	2.52	695	7.6	2.2	25	
S5A	2.53	490	8.9	1.5	24	
S1A	2.53	505	8.7	1.1	28	
S25	2.53	522	7.6	3.0	27	
S17	2.53	525	8.8	1.8	26	
S31B	2.53	547	9.0	1.1	29	
S4A	2.53	630	8.8	1.1	27	
S32	2.53	650	7.3	1.4	23	
S4B	2.53	690	8.1	0.3	27	
S30	2.54	415	8.5	2.7	25	
S20	2.54	455	8.7	2.0	27	
S5C	2.54	495	9.2	0.1	24	
S2A	2.54	520	8.7	1.2	28	
S3	2.54	590	9.1	2.0	27	
S6A	2.54	610	8.1	1.6	23	
S4C	2.54	630	8.9	0.5	27	
S9A	2.54	685	7.8	1.6	25	

TABLE III (continued)

## Fault series

Sample	P (kbar)	T (°C)	Sliding $\sigma_D$ (kbar)	$\delta$ (mm)	$\theta$ (deg)	Comments
<u>Westerly granite (continued)</u>						
S15	2.55	282	9.0	2.6	26	
S14B	2.55	355	10.1	0.8	25	$\dot{\delta} = 10^{-3}$ cm/sec
S5B	2.55	600	8.6	0.2	24	
S16	2.56	375	8.0	2.1	28	
S6B	2.56	700	7.4	0.4	23	
S9C	2.57	680	7.7	0.4	25	
S10B	2.57	700	8.4	0.3	27	
S14A	2.61	23	11.0	2.1	25	$\dot{\delta} = 10^{-3}$ cm/sec; STK
A1	2.84	407	7.0	1.4	30	
A8	2.99	407	7.9	2.0	28	
H22	3.00	354	7.8	1.7	?	
A10	3.00	508	5.4?	1.8	29	Possible jacket leak
S24B	3.06	23	9.8	1.1	26	STK
H25	3.52	205	11.3	2.2	?	STA/STK
S9B	3.54	675	9.8	0.3	25	
S1B	3.55	505	10.9	0.2	28	
S7A	3.55	600	10.3	1.3	28	
S22A	3.96	405	11.7	1.6	25	
S22B	3.97	23	12.7	1.5	25	STK
H11	4.00	260	12.3	3.7	30	$\dot{\delta} = 10^{-3}$ cm/sec; STK
S37	4.02	631	12.3	2.4	31	
S38	4.03	431	12.3	2.4	25	
S2B	4.03	520	12.3	0.3	28	
S18	4.04	445	11.5	1.6	25	
H10	4.05	439	12.2	1.5	29	
S8	4.07	605	12.1	1.8	27	
S10A	4.07	690	11.8	1.9	27	
S13B	4.09	685	9.5	0.4	25	
S12A	4.10	660	10.7	1.8	25	
S24A	4.56	23	11.1	1.9	26	STK
S7B	4.57	605	12.0	0.4	28	
H21	4.95	302	14.4	1.3	?	
H21'	5.02	354	13.4	2.0	?	STK
H26	5.02	507	13.1	2.0	?	STA?
S12B	5.04	660	11.8	0.2	25	
H19	5.05	403	14.4	3.2	?	
S13A	5.05	675	11.4	1.6	25	
A45	5.50	204	14.2	2.0	30	STK
A46	5.50	298	14.0	0.8	26	
A37	6.00	252	16.3	0.6	26	STA/STK?
H20	6.11	405	14.9	1.6	?	

TABLE III (continued)

## Fault series

Sample	P (kbar)	T (°C)	Sliding $\sigma_D$ (kbar)	$\delta$ (mm)	$\theta$ (deg)	Comments
<u>San Marcos gabbro</u>						
HT12A	1.17	25	4.6		30	
HT30	2.00	103	6.8	2.7	29	
HT24	2.50	152	6.9	2.5	?	
HT23	2.50	251	7.1	2.3	?	
S2A	2.50	270	7.2	1.5	28	
S6A	2.50	525	5.5	1.0	29	
S2B	2.50	655	5.1	0.8	28	
S3D	2.50	665	4.0	0.6	32	
S5D	2.50	680	6.6	0.4	27	
S2C	2.51	265	7.2	0.3	28	
S5A	2.51	320	7.4	1.1	27	
S5C	2.51	320	7.7	0.4	27	
S9A	2.51	605	6.1	0.9	27	
S3A	2.51	660	5.0	1.2	32	
S20F	2.51	665	4.4	0.6	30	
S1	2.52	265	7.6	2.5	28	
S20B	2.52	660	5.0	0.2	30	
S21	2.52	250	7.0	1.3	28	
S14E	2.53	680	4.1	0.4	28	
S22	2.54	520	7.1	1.0	25	
S16A	2.54	680	5.1	1.0	27	
S19E	2.54	680	4.6	0.4	29	
S16G	2.55	700	3.7	0.1	27	
S16C	2.56	685	4.7	0.2	27	
S8D	2.58	555	5.7	0.2	30	
S9D	2.58	615	6.5	0.6	27	
S16E	2.58	695	3.8	0.2	27	
S11	2.59	707	6.6	3.4	28	
S17C	2.60	650	6.0	0.6	26	
S14A	2.60	660	6.0	1.0	28	
HT28	3.00	103	8.6	2.4	28	
S5B	3.50	320	9.7	0.5	27	
HT27	3.50	356	8.6	2.6	29	
S16B	3.52	690	6.5	0.3	27	
S9B	3.54	605	8.3	0.3	27	
S16F	3.54	700	5.1	0.2	27	
S8C	3.58	540	7.8	0.3	30	
S14D	3.58	670	5.8	0.3	29	
S4D	3.91	665	5.6	0.3	29	
HT14	4.00	140	11.0	2.7	27	
HT12B	4.00	398	11.0	1.5	30	
S8A	4.03	545	8.8	1.3	30	
S17A	4.03	640	9.2	1.4	26	
S20C	4.03	660	7.2	0.3	30	
HT17	4.04	512	9.3	2.8	31	
S20E	4.04	660	6.4	6.2	30	

$\dot{\delta} = 10^{-3}$  cm/sec;  
 STK  
 $\dot{\delta} = 10^{-3}$  cm/sec

TABLE III (continued)

## Fault series

Sample	P (kbars)	T (°C)	Sliding $\sigma_D$ (kbar)	$\delta$ (mm)	$\theta$ (deg)	Comments
<u>San Marcos gabbro (continued)</u>						
S19A	4.06	650	8.0	1.1	29	
S20A	4.06	655	7.6	0.8	30	
S14B	4.06	665	7.8	0.3	29	
S19D	4.07	665	7.3	0.2	29	
S10	4.08	595	9.5	1.2	28	
S4A	4.08	660	6.7	1.2	29	
HT18	4.13	100	12.0	2.0	29	STK
HT29	4.50	304	9.9	1.7	30	
S4B	4.95	660	7.4	0.4	29	
S6C	4.98	545	8.9	0.2	29	
HT13	5.00	197	11.7	4.3	25	$\delta = 10^{-3}$ cm/sec; STK
S17B	5.01	645	10.6	0.2	26	
S3C	5.02	650	7.4	0.4	32	
S19B	5.02	655	8.7	0.3	29	
S16D	5.02	695	7.3	0.4	27	
S9C	5.03	600	10.8	0.4	27	
S14C	5.03	665	8.6	0.4	29	
S8B	5.05	540	10.3	0.3	30	
S4C	5.93	660	7.8	0.4	29	
S20D	6.02	660	8.7	0.2	30	
S19C	6.03	660	9.6	0.2	29	
<u>Mount Albert peridotite</u>						
S3	2.52	502	5.3	1.8	33	
S4	2.56	630	6.5	2.8	32	
A9	3.97	150	10.9	1.8	30	
A6	4.00	213	9.7	1.4	30	
S1B	4.02	202	9.1	0.5	33	
A1C	4.02	440	8.1	0.3	33	
S2C	4.02	530	6.7	0.5	32	
S1A	4.04	23	10.5	1.3	33	
S2A	4.04	88	9.3	1.1	32	
S1D	4.04	670	4.6	0.6	33	
S2B	4.05	305	8.0	0.3	32	
<u>Pigeon Cove granite</u>						
A3	2.94	253	11.8	1.3	25	
A2	3.00	528	9.5	1.0	22	
A4	3.04	102	11.7	1.7	26	STK
<u>Rutland quartzite</u>						
A32	3.00	22	13.9	1.4	(30)	STK; complex fault
A36	3.00	640	9.9	1.0	(30)	Complex fault
A33	3.04	440	11.9	1.4	(27)	STK; complex fault

TABLE III (concluded)

## Fault series

Sample	P (kbar)	T (°C)	Sliding $\sigma_D$ (kbar)	$\delta$ (mm)	$\theta$ (deg)	Comments
<u>Snowy Mountain anorthosite</u>						
A5	3.50	508	9.5	1.9	29	STK
A31	4.00	22	13.4	2.7	31	
A35	4.00	256	11.9	1.6	28	
A34	4.00	352	11.1	1.7	28	

TABLE IV

## Pore pressure study: Westerly granite

Sample	Motion	$P_c$ (kbar)	$P_p$ (kbar)	T (°C)	$\sigma_D$ (kbar)	$\delta$ (mm)	$\theta$ (deg)	Conditions of fault formation
HOL-2	STK	3.01	0	23	9.4	5.2	?	Dry, $P_c = 3.04$ kbar, $T = 23^\circ\text{C}$
HOL-1	STK	3.05	0	23	9.3	3.1	?	Dry, $P_c = 3.01$ kbar, $T = 23^\circ\text{C}$
HOL-3	STK	3.22	0.20	140	9.0	2.5	28	$P_c = 0.72$ kbar, $P_p = 0.22$ kbar, $T = 140^\circ\text{C}$
HOL-4	STA	3.25	0.21	265	9.5	1.5	30	$P_c = 0.55$ kbar, $P_p = 0.04$ kbar, $T = 23^\circ\text{C}$

## APPENDIX B

## JACKET CONSTRAINTS

Comparison of friction measurements at 25°C made with the copper-graphite and the polyurethane jackets suggested that there was little difference in sliding strength and type of motion for pressures greater than 2 kbars (Chapter I). The assumption was made that the polyurethane provided little constraint so that runs made with this type of jacketing could be used as standard. Because the present study relied on the copper-graphite jacket combination having little effect on the friction measurements, it seemed worthwhile to examine more quantitatively the question of jacket effects.

Several kinds of jacket effects are expected:

- (1) support of the confining pressure
- (2) constraint on the lateral expansion of the rock
- (3) support of axial load.

To analyze these effects we require data on the strength of copper and graphite. Measurements have been made of the strength of copper up to 300°C and 2 kbars pressure, by Handin and Hager (1958; tabulated by Handin, 1966); they are plotted in Figure B1. An upper limit to the strength of copper seems to be about 2 kbar. Robin (personal communication, 1975) studied the compressive strength of the graphite used in the friction experiments at 25°C and pressures to 6.5 kbars. His unpublished data are reproduced in Figure B2. Included in this figure is one measurement, made

by the author, of graphite strength at 325°C and 3 kbars pressure to about 4% axial strain. The stresses were calculated from the measured axial load and the initial cross-sectional area. Barrelling and conical failure occurred at large strains, so the stress data are less reliable above 10% or so strain. There seems to be little systematic difference in compressive strength of graphite with pressure (above 2 kbars) and temperature (to 325°C). A representative value is about 1 kbar, used in the following analysis. No measurements were made of the tensile strength; Ely (1965) found that it was typically one-third of the compressive strength, or about 350 bars.

The dimensions of the jackets are as follows:

copper sleeve: outer diameter, 1.91 cm; inner diameter, 1.85 cm

graphite sleeve: outer diameter, 1.85 cm; inner diameter, 1.59 cm.

(1) Support of confining pressure

This is the problem of the collapse of a hollow cylinder. If we assume that the jacket materials are elastic until yielding, we can use the solution for the radial,  $\sigma_r$ , and tangential,  $\sigma_\theta$ , stresses (Jaeger and Cook, 1969):

$$\sigma_{r_1} = 0 \quad , \quad \sigma_{\theta_1} = \frac{2PR_2^2}{R_2^2 - R_1^2} \quad \text{(inner wall)}$$

$$\sigma_{r_2} = P \quad , \quad \sigma_{\theta_2} = \frac{P(R_2^2 + R_1^2)}{R_2^2 - R_1^2} \quad \text{(outer wall)}$$

where P is the confining pressure,  $R_1$  and  $R_2$  are the radii of the inner and outer wall, respectively. Under confining pressure the axial stress,  $\sigma_z$ , in both cases is P. Failure of the cylinder will occur when  $\sigma_\theta - \sigma_r$  equals the yield strength,  $\sigma_y$ , of the material. Since  $\sigma_\theta - \sigma_r$  is greatest

at the inner wall, the formulas for  $\sigma_{\theta 1}$  and  $\sigma_{r1}$  will be used. Thus at failure,

$$\sigma_y = \frac{2PR_2^2}{R_2^2 - R_1^2}$$

For copper the collapsing pressure,  $P_c$ , is 70 bars, while for graphite  $P_c$  is 130 bars. The actual collapsing pressure is probably much less, since yielding of the graphite and copper begins at much lower stresses. In fact, a strain of a few percent is sufficient to collapse the jacket onto the rock. However, the jacket could support as much as 100 bars difference in pressure between the outer and inner walls, resulting in an overestimate of the confining pressure acting on the rock of as much as 100 bars.

(2) Constraint on lateral expansion of the rock

This problem can be analyzed in terms of the excess confining pressure provided by the jacket on the rock. This is equivalent to the internal pressure required to cause the jacket to yield. Again using the elastic solutions (Jaeger and Cook, 1969):

$$\sigma_y^T = - \frac{2P'R_1^2}{R_2^2 - R_1^2}$$

where  $\sigma_y^T$  is the tensile strength of the jacket material, and  $P'$  is the internal pressure.

For the copper jacket the bursting pressure,  $P_B$ , is about 70 bars, and for the graphite sleeve  $P_B$  is about 60 bars. Thus the maximum lateral constraint acting on the rock due to the jacket is equivalent to an excess confining pressure of about 70 bars. Again this value is probably on the high side and in any case will tend to offset the difference between the external and internal confining pressures caused by the jacket.

(3) Support of axial load.

Because of its finite cross-sectional area and strength, the jacket will support a certain fraction of the axial force. The force carried by the jacket is given by:

$$F = \sigma_y \pi (R_2^2 - R_1^2)$$

For the copper jacket  $F$  is about  $4 \times 10^8$  dynes, and for the graphite sleeve  $F$  is about  $7 \times 10^8$  dynes. Thus the jacket supports about 5% of the total load if the rock, with a cross-sectional area of  $2 \text{ cm}^2$ , is under 10 kbars axial stress. Again, because of yielding at low stress the fraction of load supported by the jacket is probably much less. This is particularly true in a friction experiment where very small strains (less than 1%) occur in the regions away from the fault. In the high shear regions around the edge of the fault, however, the full shear resistance of the jacket materials could be developed. Thus, the frictional stress in the rock could be overestimated by as much as 5%, although this error is well within the measurement uncertainty.

Thus the stresses supported by the jacket are small, but may not be negligible. The question of how the jacket affects the sliding motion is more complex. At high pressures, where the fraction of load carried by the jacket is small, the effect on the motion would be negligible. Apparently this is so above 2 kbars. At lower pressures the ductile jacket supports a much higher fraction of the load and its effect could be appreciable. Support for this idea is the finding of Byerlee and Brace (1968) that 3% of ductile serpentine in a dunite is sufficient to stabilize the sliding motion. However, a much more important factor may be the distribution of the ductile minerals; the serpentine in the dunite was distributed uniformly around the grain boundaries. In any case, our

jacket trials (Chapter I) did indicate that the sliding was somewhat stabilized by the jacket.

#### REFERENCES

- Byerlee, J.D. and Brace, W.F., 1968. Stick-slip, stable sliding, and earthquakes - effect of rock type, pressure, strain rate, and stiffness. *J. Geophys. Res.*, 73: 6031-6037.
- Ely, R.E., 1965. Strength of graphite tube specimens under combined stresses. *J. Am. Ceram. Soc.*, 48: 505-508.
- Handin, J., 1966. Strength and ductility. In: S.P. Clark, Jr. (Editor), Handbook of Physical Constants, *Geol. Soc. Am., Mem.*, 97: 223-290.
- Handin, J. and Hager, R.V., 1958. Experimental deformation of sedimentary rocks under confining pressure: tests at high temperature. *Am. Ass. Petrol. Geol. Bull.*, 42: 2892-2934.
- Jaeger, J.C. and Cook, N.G.W., 1969. Fundamentals of Rock Mechanics, Methuen, London, 513 pp.

#### FIGURE CAPTIONS

- Figure B1 Stress-strain relations in copper deformed under triaxial compression (solid lines) and extension (dashed lines) at various pressures and temperatures (from Handin, 1966).
- Figure B2 Stress-strain relations in graphite deformed under triaxial compression at room temperature and various pressures (solid lines) and at 325°C and 3 kbars (dashed line). All stress measurements were calculated using the initial cross-sectional area. The room temperature measurements are from unpublished data of P.-Y.F. Robin (personal communication, 1975) and the high temperature measurement is from an experiment made by the author.

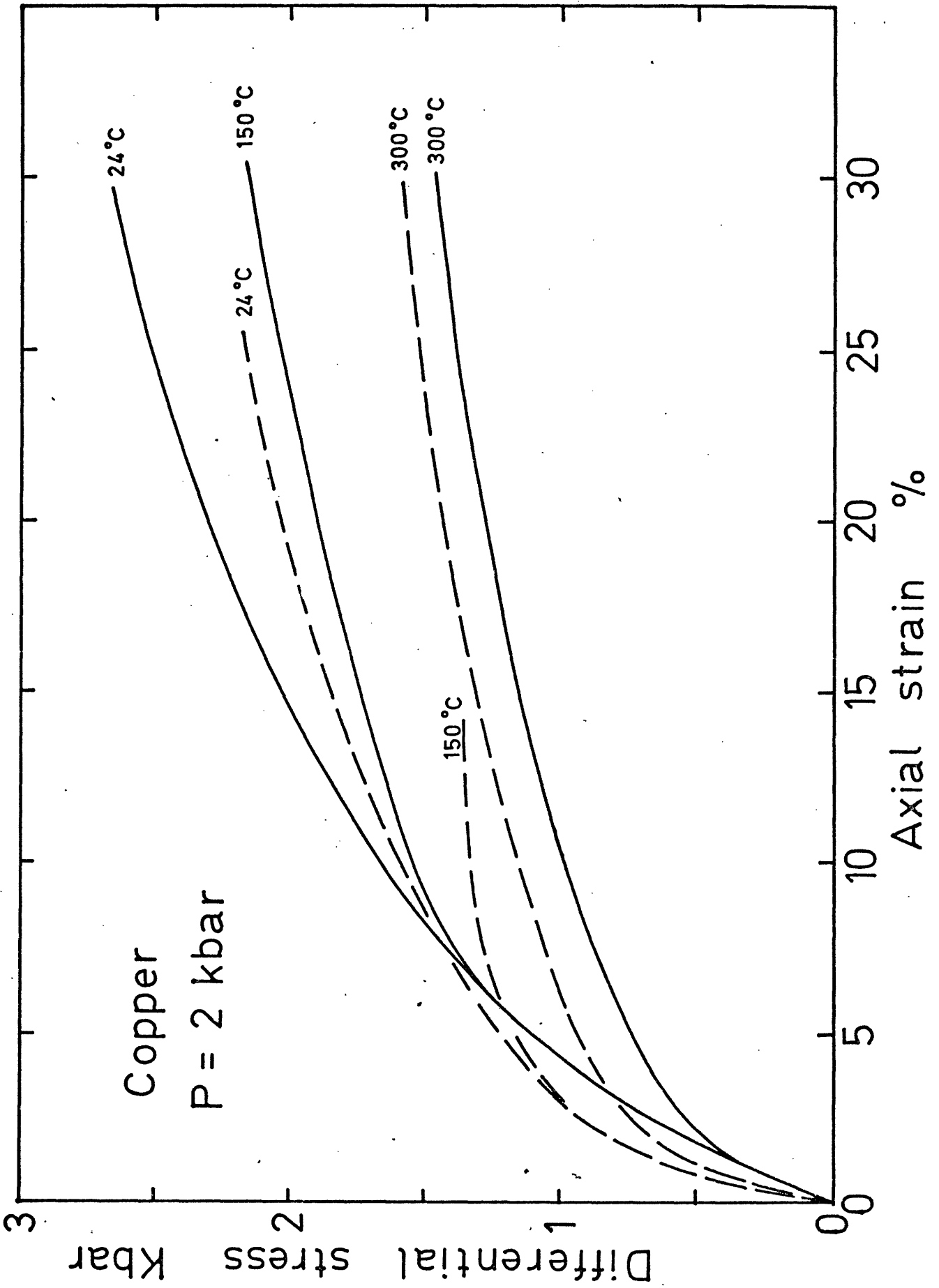


FIG B1

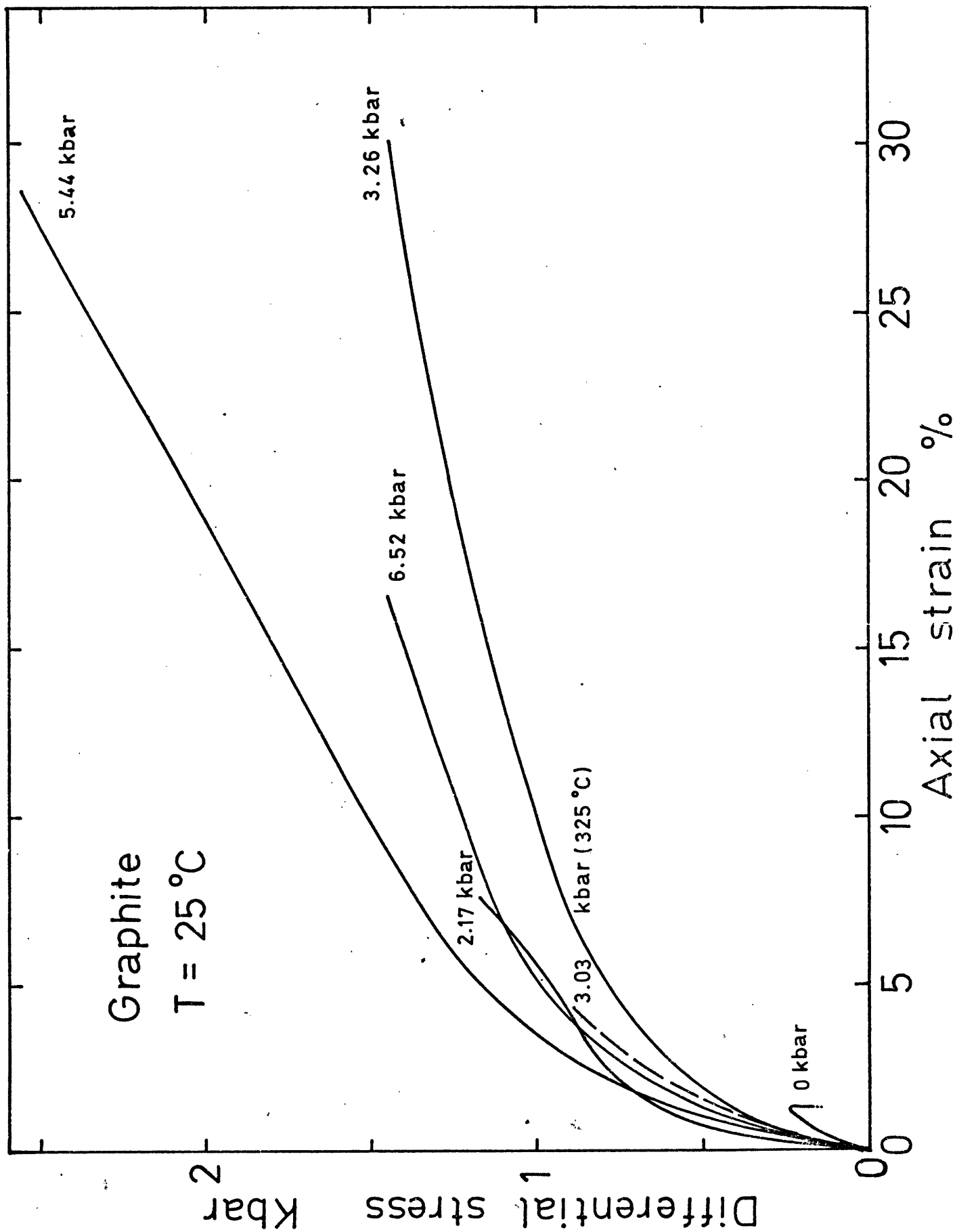


FIG B2

## BIOGRAPHY

I was born to Caroline and Michael Stesky on July 27, 1945, in Toronto, Ontario. I spent my childhood in Garnet, Ontario, Waterford, Ontario, and finally in Toronto. I attended the University of Toronto where I earned a Bachelor of Science in Geology and a Master of Science in Geology and Geophysics, and the Massachusetts Institute of Technology where I received a Doctor of Philosophy. My work has carried me to many places: geological mapping in northern Ontario and in the Rocky Mountains of British Columbia and Alberta, and marine geophysical surveying on the Grand Banks and the Mid-Atlantic Ridge, with trips to Halifax, Nova Scotia, the Azores, and Portugal. I married Christine Anne Simons on August 21, 1971; we are expecting our first child in September 1975. I am an Assistant Professor of Geology at Erindale College, University of Toronto.